Path-following Control for Power Generating Kites Using Economic Model Predictive Control Approach

by

Zhang Zhang
B.Eng., Hefei University of Technology, 2016

A Dissertation Submitted in Partial Fulfillment of the
Requirements for the Degree of

MASTER OF APPLIED SCIENCE

in the Department of Mechanical Engineering

© Zhang Zhang, 2019
University of Victoria

All rights reserved. This dissertation may not be reproduced in whole or in part, by photocopying or other means, without the permission of the author.

Path-following Control for Power Generating Kites Using Economic Model Predictive Control Approach

by

Zhang Zhang
B.Eng., Hefei University of Technology, 2016

Supervisory Committee

Dr. R. Supervisor Main, Supervisor
(Department of Same As Candidate)

Dr. M. Member One, Departmental Member
(Department of Same As Candidate)

Dr. Member Two, Departmental Member
(Department of Same As Candidate)

Dr. Outside Member, Outside Member
(Department of Not Same As Candidate)

Supervisory Committee

Dr. R. Supervisor Main, Supervisor
(Department of Same As Candidate)

Dr. M. Member One, Departmental Member
(Department of Same As Candidate)

Dr. Member Two, Departmental Member
(Department of Same As Candidate)

Dr. Outside Member, Outside Member
(Department of Not Same As Candidate)

ABSTRACT

Exploiting high altitude wind energy using power kites is an emerging topic in the field of renewable energy. The claimed advantages of power kites over traditional wind power technologies are the lower construction costs, less land occupation and more importantly, the possibility of efficiently harvesting wind energy at high altitudes, where more dense and steady wind power exists. One of the most challenging issues to bring the power kite concept to real industrialization is the controller design. While traditional wind turbines can be inherently stabilized, the airborne nature of kites causes a strong instability of the systems.

This thesis aims to develop a novel economic model predictive path-following control (EMPFC) framework to tackle the path-following control of power kites, as well as provide insightful stability analysis of the proposed control scheme.

Chapter 3 is focused on the stability analysis of EMPFC. We proceed with a sampled-data EMPC scheme for set-point stabilization problems. An extended definition of dissipativity is introduced for continuous-time systems, followed by giving

sufficient stability conditions. Then, the EMPFC scheme for output path-following problems is proposed. Sufficient conditions that guarantee the convergence of the system to the optimal operation on the reference path are derived. Finally, an example of a 2-DoF robot is given. The simulation results show that under the proposed EMPFC scheme, the robot can follow along the reference path in forward direction with enhanced economic performance, and finally converges to its optimal steady state.

In **Chapter 4**, the proposed EMPFC scheme is applied to a challenging nonlinear kite model. By introducing additional degrees of freedom in the zero-error manifold (i.e., the space where the output error is zero), a relaxation of the optimal operation is achieved. The effectiveness of the proposed control scheme is shown in two aspects. For a static reference path, the generated power is increased while the kite is stabilized in the neighborhood of the reference path. For a dynamic reference path, the economic performance can be further enhanced since parameters for the reference path are treated as additional optimization variables. The proposed EMPFC achieves the integration of path optimization and path-following, resulting in a better economic performance for the closed-loop system. Simulation results are given to show the effectiveness of the proposed control scheme.

Finally, **Chapter 5** concludes the thesis and future research topics are discussed.

Contents

List of Tables

List of Figures

ACKNOWLEDGEMENTS

First of all, I would like express my deepest gratitude to my supervisor, Dr. Yang Shi for all his guidance and encouragement during my Master's studies. He always shared with me many resourceful and inspiring ideas during individual meetings and group meetings. When I suffered from frustrations, it was him who was always there, and encouraged me with great enthusiasm, impressive kindness and patience. His passions and rigorous attitude towards research inspire me to handle every thing with a professional attitude. Without his consistent and illuminating instructions, this thesis could not have reached its present form.

Moreover, it is my honor and luck to know the present and former members in the Applied Control and Information Processing Lab at the University of Victoria. Kunwu Zhang helped finding me a house and guided me a lot in the daily life during the first several months since I arrived in Victoria. Qi Sun and Qian Zhang gave me many valuable suggestions on my studies and research. Chao Shen shared with me his in-depth understanding on AUV control. Jicheng Chen's open mind ,Bingxian Mu's selflessness and Changxin Liu's concentration on research all taught me a lot. Thanks to Tianyu Tan and Chonghan Ma, for being my closest friends. Moreover, I deeply cherish the time with Yuanye Chen, Xiang Sheng, Yuan Yang, Chen Ma, Huaiyuan Sheng, Zhuo Li, Henglai Wei, Tianxiang Lu, Xinxin Shang, Haoqiang Ji, Bo Cai, and Tingting Yu. All these beautiful days I had with you guys will be my precious memories.

At last, but the most importantly, I would like to thank my parents and all my families for their love and support. I love them all from the bottom of my heart.

Nomenclature

Abbreviations

AWE	airborne wind energy
AWES	airborne wind energy systems
DoF	degree of freedom
EMPC	economic model predictive control
EMPFC	economic model predictive path-following control
FHOCP	finite horizon optimal control problem
FGs	fly-generator systems
GGs	ground-generator systems
LEMPC	Lyapunov-based economic model predictive control
MPC	model predictive control
NMPC	nonlinear model predictive control
OCP	optimal control problem

Notations

(x_s, u_s)	the pair of optimal steady state
$x(\cdot, x(t_0)\|u(\cdot))$	the solution of a system $\dot{x} = f(x, u)$, starting at time t_0, from initial state $x(t_0)$, and driven by input signal $u(\cdot)$
$\mathbf{I}^{n\times n}$	n-dimension identity matrix
$\mathbf{0}^{m\times n}$	m-by-n zero matrix
$\|x\|$	2-norm of a vector x
$\|x\|_\infty$	infinity norm of a vector x
$\|x\|_Q$	weighted norm $\sqrt{x^T Q x}$, Q is positive semi-definite
$\|A\|_Q$	induced 2-norm of a matrix A
$\mathcal{PC}(\Omega)$	the set of piecewise continuous and right continuous functions on $\mathbb{R}$ with value taken from $\Omega \subset \mathbb{R}^n$
$int(\mathcal{S})$	the interior of a set $\mathcal{S}$
diag$(\cdot)$	the diagonal operation of several scalars

Chapter 1

Introduction

1.1 Airborne Wind Energy

Exploring new renewable energy technologies has become one of the most urgent and strategic issues that mankind is facing today. With the development of non-OECD (Organization for Economic Co-operation and Development) countries, the world energy consumption has increased about 52% from 1990 to 2012, and is predicted to grow by 48% from 2012 to 2040 [1] (cf. Figure 1.1). Unfortunately, almost 70% of the electric power is currently generated by fossil sources (e.g., oil, coal and nature gas), which contributes to the growth of energy-related CO_2 emission by 2.4% per year since 2000 [10, 11]. Such global energy situation has world-widely arose concerns about environmental pollution, climate change and energy crisis.

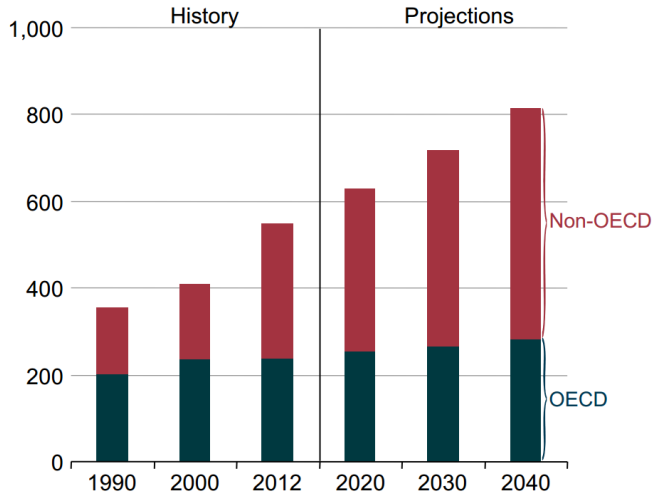

Figure 1.1: Total world energy consumption, 1990-2040 (quadrillion Btu) [1].

Developing renewable energy is a key point to tackle this issue. According to IEO2016 Reference Case [1], the renewable energy is the fastest-growing source of energy from 2012 to 2040, at an average increasing rate of 2.6% per year. In fact, the projected share of renewables for total energy consumption increases from 22% in 2012 to 30% in 2040, cf. Figure 1.2. Wind power is the second largest renewable energy source, apart from hydropower, with a global installed capacity increasing from 60 GW in 2005 to 350 GW in 2014 (at an average growth rate of 22% per year) [10]. Actually, if only 20% the wind energy that is profitable for the traditional wind technology based on wind turbines, can be captured, the global energy demand for all purposes will be satisfied [12]. However, traditional wind power technologies, based on wind turbines, has two major limitations in terms of energy production costs and land occupation. Specifically, wind turbines require heavy towers, foundations and huge blades, resulting in much higher energy production costs with respect to thermal plants. As for the land occupation, wind farms based on wind turbines 2.5 MW rated power have an average power density of 3.7 MW/km2 [13], about 260 times lower than that of large thermal plants. Thus, traditional wind energy generators, wind turbines, are not yet competitive with thermal generators, despite the increasing price of oil and gas.

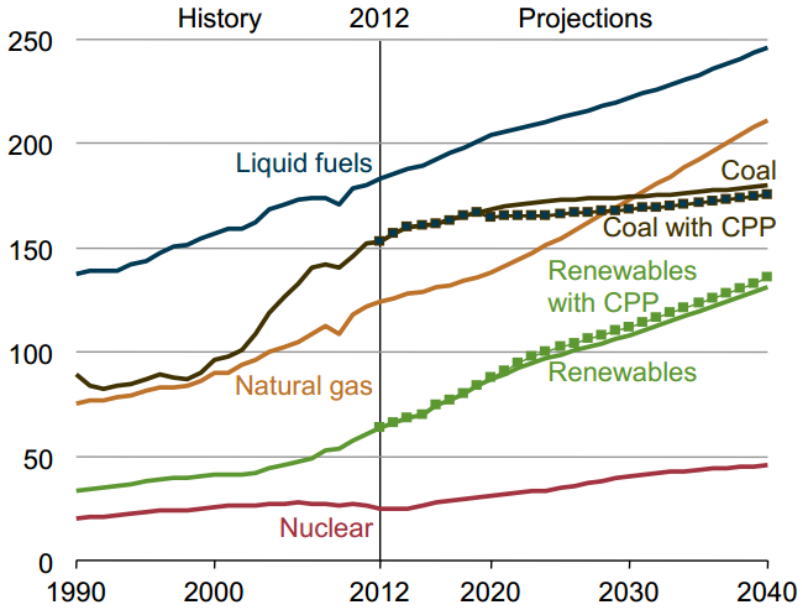

Figure 1.2: World energy consumption by different energy source, 1990-2040 (quadrillion Btu) [1].

To overcome these limitations of traditional wind energy technology, many re-

search groups and renewable energy companies nowadays are developing High Altitude Wind Energy technology since the wind power density increases with the height above the ground. In fact, at the altitude of 500-1000 m, the average wind power density is about three times higher than that at 100 m, and at the altitude of 10,000 m, it is 40 times higher [14]. This motivates novel technologies of wind energy generation which can be realized by capturing wind energy at high altitudes over the ground (200m-10km) where more dense and steady wind power exists. These technologies have been classified using an umbrella-name, Airborne Wind Energy (AWE) technology. Today, research institutions and commercial entities such as KiteGen (Italy), Makani Power (Google X, USA) and AmpyxPower (The Netherlands) contribute to an emerging development of AWE technology, cf. Figure 1.3. Next, we give a classification of various concepts of AWE systems.

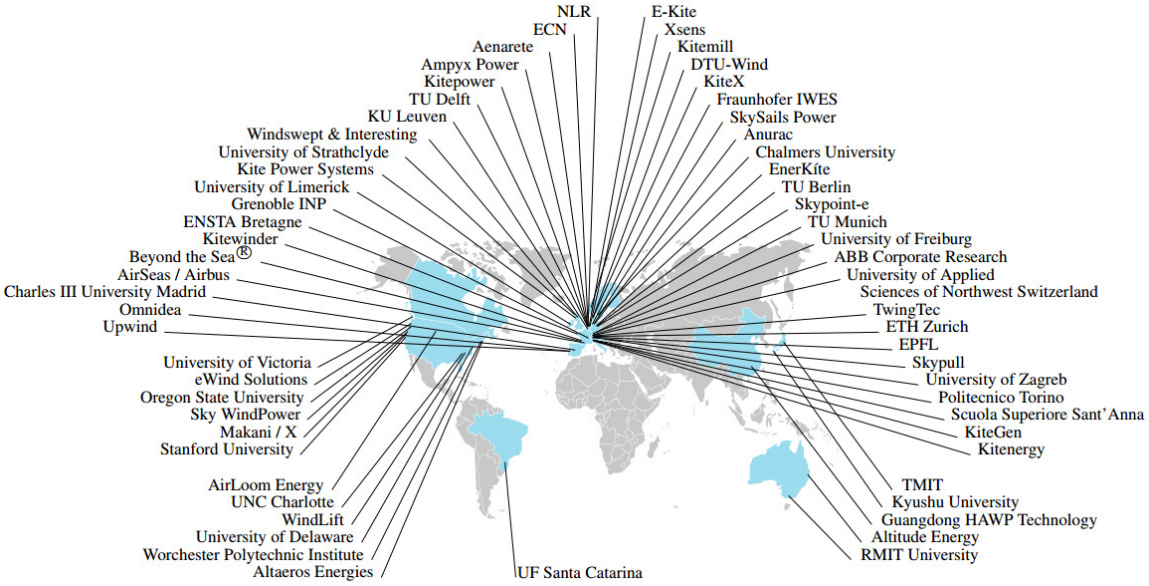

Figure 1.3: Airborne wind energy research and development activities in 2017 [2].

1.1.1 Classification of Airborne Wind Energy Systems

Different concepts of airborne wind energy systems (AWESs) have been well developed these years. Generally, they can be divided into two types: Ground-generator systems (GGs) and Fly-generator systems (FGs). As the name suggested, the power generation of GGs is done by a generator on ground station while in FGs such generation is done by on-board turbines (see Figure 1.4). A further classification can be made

between configurations adopting rigid wings [15–17], and configurations that employ flexible wings like power kites [9, 18–20]. Other AWE concepts based on lighter-than-air structures [21] and multi-wing structures [5, 22, 23] will also be introdunced in the following sections.

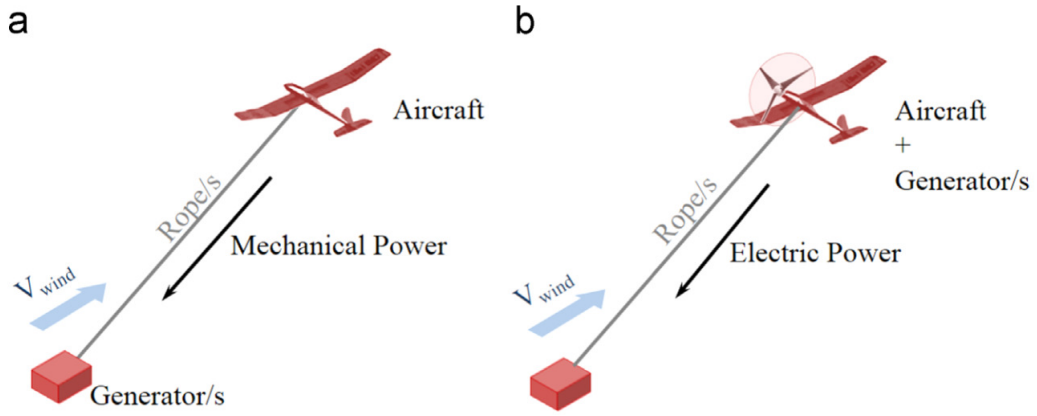

Figure 1.4: Comparison between GGs (left) and FGs (right) [3].

Ground-Gen AWE Systems

In GGs, the power generation is based on exploiting high tension in the cables to pull a generator on the ground. The power generation of most GGs are in so called pumping mode, which can be divided into two phases: traction (or reel-out) phase and retraction (or reel-in) phase. During the traction phase, the tethered aircrafts are in crosswind flight condition (flying roughly perpendicular to the wind speed direction) to access a high apparent wind speed, and thus the efficiency of harnessing wind power is greatly increased. Actually, it has been investigated that crosswind power generation can provide a power one or two orders of magnitude higher than non-crosswind generation [24]. A typical periodic path for traction phase is a figure-eight path, since by following this kind of path, the aircraft can maintain crosswind flight condition as well as avoid entangling of cables. Once the tether is completely reeled out, retraction phase begins. During the retraction phase, the generators act as motors to recoil the cables and we want to minimize the dissipative power by reducing tension on cables. This is realized by decreasing the angle-of-attack of airfoils and moving them to a position with high elevation angle where the tension on cables is significantly reduced. Therefore, only a fraction of the previously generated power is spent to rewind the tether. This way of two-phase power generation is called pumping

mode, which can be illustrated in Figure 1.5.

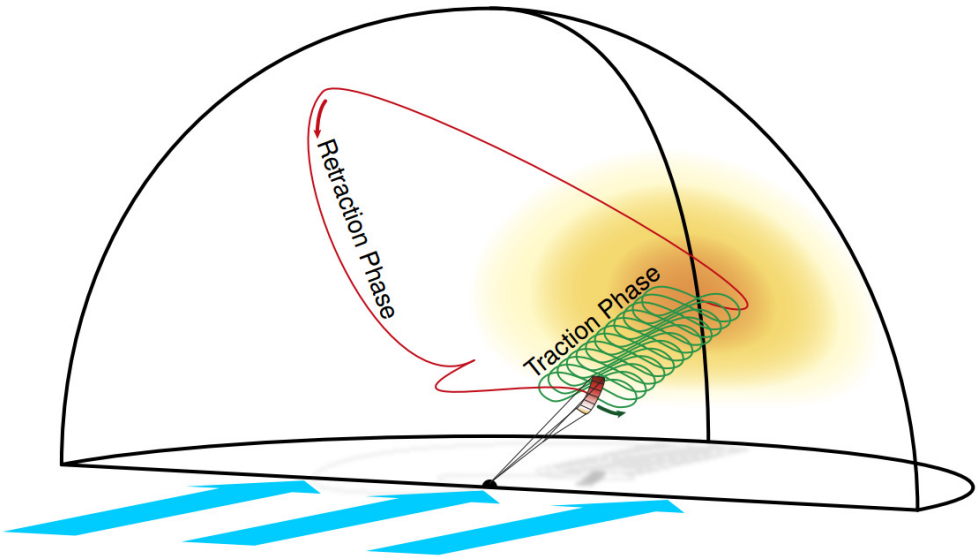

Figure 1.5: Illustration of pumping mode power generation [4]. The traction phase (green), flying a crosswind pattern, and the retraction phase (red), flying outside the power zone (orange). The wind direction is indicated by the arrows (blue).

Fly-Gen AWE Systems

In FGs, the power is generated by on-board turbines carried by airfoils flying in crosswind condition. These AWE systems are in so-called drag mode, since the on-board generators add additional drag force to produce electricity, see Figure 1.4a. The electricity is transmitted via conductive cables to the ground-based power grid. Compared to GGs, the advantage of FGs is its potential capability of autonomous take-off and landing using on-board propellers (generators) to provide thrust and lift force. One of most famous prototypes of Fly-Gen AWE Systems is made by Makani Power [25]. Their latest prototype, MAKANI-M600, has 26m wing span and 600KW rated power. It employs a carbon fiber wing with multiple on-board generators and propellers. In contrast to GGs, a constant tether is employed during the power generation phased and it is sustained by the incoming wind. When the tether has reached its operation length, the airfoil starts to fly in crosswind condition with circular path. The orientation of the airfoil is controlled by an on-board computer in order to follow the desired path.

Multi-wing Systems

In single wing configuration of AWE systems, while employing a longer tether to reach a higher altitude, the aerodynamic drag force on the cables may become significantly large in crosswind flight condition. Therefore, the motion of tethers imposes a limit on the efficiency of the overall system. To address this issue, concepts based on dual-wing configuration have been investigate in [5, 22] (on-board generation) and [23] (ground-based generation). The main idea of the dual-wing design is to separate the tether into two parts: the main tether and the secondary tethers. Since the two airfoils are connected to the main tether in a balanced manner, the main tether is almost static in the air and the extra drag force is significantly reduced, as visualized in Figure 1.6. For this reason the operating length of cables can be longer in dual-wing AWESs and the optimal flight altitude is relatively high.

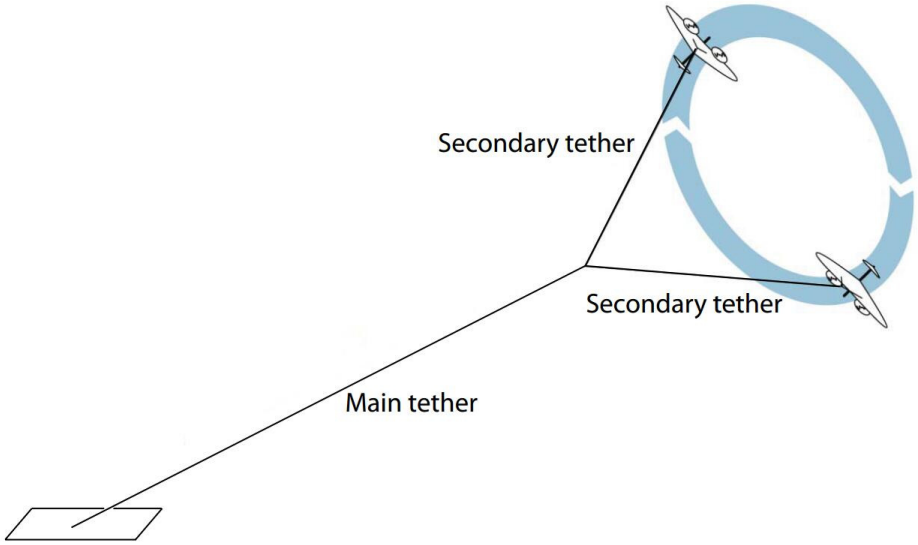

Figure 1.6: Schematic diagram of a dual-wing AWE system [5].

Another concept of multi-wing configuration adopts several wings attached on a single tether. In order to increase the total characteristic area and realize a large scale power generation, the wings are stacked evenly on the main tether, one after the other. This concept has been previously investigated by W. Ockels, using the idea of laddermill. The power generation can be in pumping or laddering mode [26]. In these configurations, the distance between wings should be appropriately chosen such that the total power generation is maximized. Inspired by these conceptions, a prototype with 500 kW rated power has been built by a Chinese company [6, 27], see Figure

1.7. This prototype employs several kite-guided umbrellas in a ladder system which makes the mechanical structure of wings even more simple and lighter. The umbrellas ascends in an open-state and huge pulling force is used for power generation. When the tether reaches its maximum length, the umbrellas descend in a closed-state.

Figure 1.7: An artistic vision (left) and an implemented prototype (right) of an umbrella-ladder system [6].

1.2 Pumping Kites with Fixed Ground Generators

1.2.1 Concept of Kite Generators in Pumping Mode

Among various concepts of AWE system, a popular one is based on using large power kites to extract wind power at high altitude (up to 1000m). In fact, many groups have built kite generator prototypes to test their practical power generation capability (e.g., KiteGen, KitePower, KITEnergy and Windlift). A kite generator system is mainly consists of three parts: a large power kite, high-strength cables and a ground-level generator, as shown in Figure 1.8. Similar to most of ground-based AWESs, the power generation for a kite generator is in so called lift mode [24] since the high tension in cables is mainly resulted from the lifting force of the kite in the crosswind flight condition. The cables can transmit traction force to the generator, as well as control the position and orientation of the kite. When the cables reach their maximum length

in the traction phase, retraction phase begins and only a portion of the generated power is consumed to pull the kite back to its initial position. We call this two-phase of power generation as pumping mode which has been widely investigated through literature (e.g. [8, 19, 20, 28, 29]).

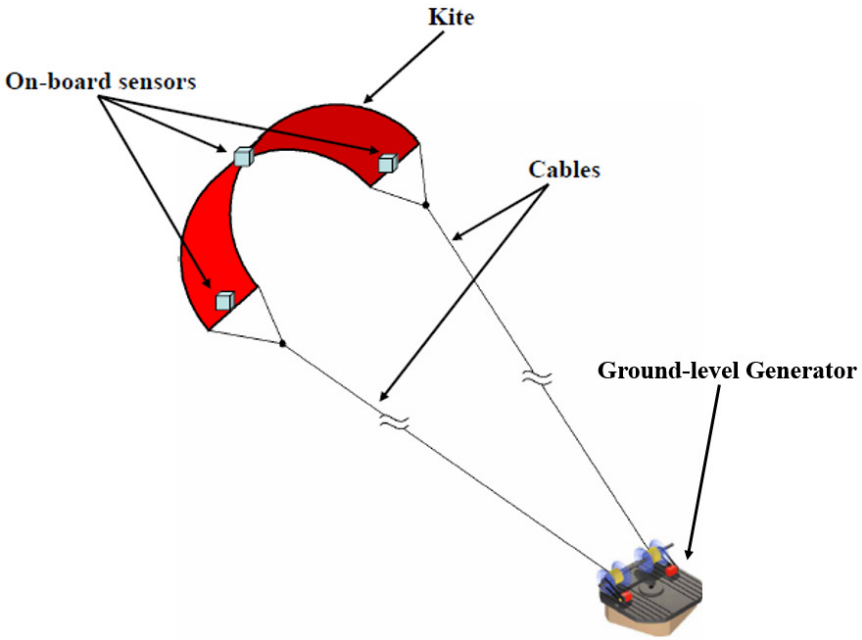

Figure 1.8: A typical configuration of a kite generator system. Illustration from [7].

In general, there are three advantages of kite generators compared to traditional wind turbines. First of all, they have the capability of harvesting wind energy at a high attitude where the wind power density is much larger. Since the generated power grows with the cube of apparent wind speed, the rated power of kite generators can be much larger with respect to those of wind towers placed in the same location. Moreover, the low operating altitude affects not only the performance but also the location where a wind turbine can be mounted. The steadier and stronger wind power at a high altitude allows kite generators to be installed in a much larger number of locations. The third advantage is the high efficiency of the area utilization, which can be illustrated by Figure 1.9. In traditional wind turbines, the 20% outer part of the rotor blades contribute to 80% of the power generation. This is because the apparent wind speed at the outer part of the blade is much larger than that at the inner part, and the generated power grows with the cube of apparent wind speed. In contrast, in a kite system, the tethered kite flying in crosswind conditions acts as the outer part of the blades and the less-productive inner blades are replaced by the tether. Hence,

there is no such bulky structure like heavy foundations, towers or huge blades which makes kite generators much lighter and cheaper to construct.

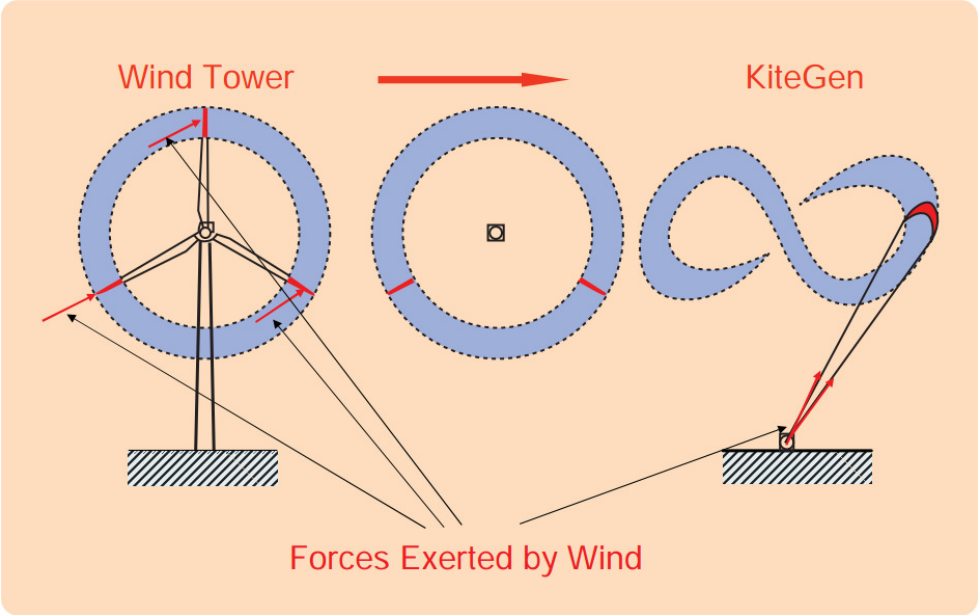

Figure 1.9: Comparison between kite generators and traditional wind turbines in power generation. Illustration from [8].

The control design of power kites is a challenging task. While traditional wind turbines can be inherently stabilized, the airborne nature of kites causes a strong instability of the systems. The tethered flight is a fast, unstable and perturbed process. For this reason, automatic control of the kite system flying in all wind and weather conditions is required. The applied controller should not only stabilize the kite in a pre-designed flight pattern but also optimize the generated power in a transient phase (e.g., under varying wind speed and wind turbulence).

1.2.2 Literature Review of Controlling Kites

As mentioned before, the idea of using kites for high altitude wind power generation can be traced back to Loyd's seminar paper [24] in which he analyzed the maximum energy can be theoretically generated by power kites (neglecting the drag force of cables). However, the related research was then almost abandoned. Until 2001, Moritz Diehl firstly proposed a nonlinear point-mass model of kites on the basis of Newton's law of motion [30]. Under the assumption that the apparent wind speed vector is always contained in kite's symmetry plane, which is reasonable when the

kite is flying in crosswind condition, the direction of the aerodynamic forces can be determined by the apparent wind speed, kite's roll angle ψ (the only input variable) and the angle of attack. Then, a more accurate kite model is developed by considering aerodynamic force and gravity of cables [9]. In [23, 31], a Lagrangian model of kites is formulated considering the effect due to the elasticity and the internal friction of the cables.

Considering these nonlinear kite models and the objective of maximizing the generated power under constraints, Nonlinear Model Predictive Control (NMPC) can be such a candidate control strategy. In NMPC, the control input at each sampling time is obtained by solving a finite horizon optimal control problem (FHOCP), where the measured state vector is used as the initial condition for each optimization problem and the prediction of system behavior can be obtained by using the available nonlinear model. In the existing works of kite controller design, both standard (tracking) NMPC [32–34] and economic MPC (EMPC) [8, 9, 35] have been successfully applied to the aforementioned kite models. In [32], several optimized reference trajectories are precomputed which are parameterized by different wind speeds. Then, the NMPC scheme is employed to track such optimized reference obits. In [8, 9, 35], however, no precomputed trajectory is needed and the corresponding EMPC scheme is designed by using pure economic cost function associated with the generated power. Using additional technical constraints, the kite is forced to go along the desired trajectories (figure-eight orbits). The trajectories obtained from the EMPC scheme intuitively have better economic performance than those from a standard NMPC scheme, because they are not limited to be periodic. However, in these works using EMPC, there is no closed-form expression of the reference path. Therefore, the shape of closed-loop trajectories can not be adjusted directly, and it is difficult to analyze the stability. Besides, when the wind speed changes, the kite can not be always stabilized in a reasonable area (i.e., may be too close to the border of the wind window), resulting in the stall of the kite.

In fact, most optimization-based control schemes like Model Predictive Control may be not practical for the kite project, since they require solving complex nonlinear optimization problems in real time and measuring the kite's position, speed, the nominal wind speed at the kite's altitude, and the forces acting on the tethers. Particularly, it is difficult to acquire the wind speed at the kite's altitude with only a few measurement points, since the wind field changes over distance and time. To tackle these problems, simple feedback strategies with simplified kite models need to

be developed. In this direction, a simplified model was originally studied based on concepts of turning angle (see e.g., [18], [36]), but the model parameters were obtained from experiments. In [20], an explicit expression of these model parameters is derived and a more convincing linearized model is obtained. Such control-oriented models are particularly suitable for feedback control since they have the advantage of being single-input and single-output. These models have been proved to be quite accurate in crosswind conditions through experimental data [18].

Now, we give an overview of the controller design using these simplified kite models. In [18], a hierarchical control scheme is proposed, where the overall controller is separated into two layers of "guidance" and "control". In the outer loop controller, the reference heading angle is obtained according to the desired flight patterns in order to acquire high apparent wind speeds and forces. Unfortunately, the inner control loop is quite sophisticated and it requires the measure of apparent wind speeds at the kite's position. In [20], a simple guidance strategy is presented to obtain the reference turning angle and the control command can be easily computed under the feedback control law. The advantage of this hierarchical control scheme is that it can control the kite fly along figure-eight orbits in the presence of certain wind turbulence using only the measurements of the kite's position. Then, such a linearized model and a similar control strategy are employed to the kite retraction phase [29, 37] where a fully autonomous flight of kites for the whole power generation phase is realized. In addition, a real-time optimization algorithm is proposed [38] to compute the optimal average position of the flight orbits by using traction forces as feedback variables. This algorithm can be used as an extension of any existing controllers, providing a reference average position of the reference flight path to maximize the average traction force.

In summary, among the above-mentioned works based on simplified kite models, the power optimization is considered in [38] by using traction forces as feedback variables, but others [20, 29, 36, 37] are focused on the stabilization of the desired flight pattern (i.e., figure-eight paths). Numerical and experimental results are presented to validate corresponding control schemes, respectively in [20, 29, 36–38]. However, none of these works considers a closed-form expression of the reference paths and no theoretical proofs for the stability are given. Thus, we can not directly adjust the shape of closed-loop trajectories under these control schemes. Furthermore, some internal information of systems is lost since only dynamics of turning angle is considered in the simplified model.

Some other interesting control strategies aiming to fulfill other requirements, are introduced here. First of all, since some feedback variables such as the apparent wind speeds are not easy to measure, so-called robustified optimal control problem is formulated [31, 39]. By solving periodic Lyapunov differential equations, an intrinsically open loop stable trajectory is found such that the kite generates as much power as possible. Thus, there is no need to employ any feedback in these schemes. Secondly, as mentioned before, it is generally hard to obtain an accurate kite model when kites are flying in different flight conditions. To tackle the model uncertainty of kites, non-model-based approaches have been also proposed [40], which is based on the concept of direct-inverse control [41]. In this work, an inverse model of the kite is directly computed from measured input-output data, and thus avoiding the need to derive an accurate kite model.

Another challenging issue for power kites to really foster its industrial development is autonomous takeoff and landing. Currently, even no related approach has been proposed, at least from public literature. Alternatively, we can find the solution in rigid aircrafts for autonomous takeoff [42], where a model-based, hierarchical feedback controller is designed. This work aims to stabilize the aircraft during the takeoff and to achieve figure-eight flight patterns parallel to the ground. For autonomous landing, further efforts should be made not only on control aspect, but also on the development of new aircraft configurations and concepts specifically designed for this purpose. However, these issues such as the mechanical design of the kite systems are beyond the scope of this thesis.

1.3 Objectives and Challenges

1.3.1 Objectives

In this thesis, we aim to formulate output path-following control problems for kites with economic consideration (generated power). In this work, there are three requirements of the controller design for a kite generator system:

- The kite can be stabilized on the reference paths in the presence of wind turbulence.
- The kite system has the optimal transient performance with respect to certain economic criteria. Moreover, when the kite flys along the reference paths, the

forward speed is optimal with respect to the economic criteria.

- The state and input constraints of the kite system are satisfied. For example, the kite should be avoided to fly close to the border of the wind window (where the stall of kite mostly happens) or near the ground.

For the first requirement, we want to prove the closed-loop trajectory is asymptotic convergent to the reference path for the nominal kite system and the robustness of the controller can be shown by simulation results. In the second requirement, the transient economic performance represents the economic performance when the system is disturbed and deviates from the reference path. Besides, since the reference path is usually defined in the output space, additional degrees of freedom such as kite's forward speed and its orientations are allowed along the reference path. Thus, the economic performance can be further improved even if the system has no deviation from the reference path in output space. This objective motivates our choice of so-called Economic Predictive Path-following Control to be a candidate control scheme, which is discussed in detail later. Finally, the third requirement of constraints can be satisfied under the scheme of MPC.

1.3.2 Challenges

In general, crosswind flight of tethered kites is a fast, strongly nonlinear, unstable and constrained process. Controlling such process is a very challenging task. More specifically, designing a controller fulfilling aforementioned requirements for kite generators is challenging due to the following reasons:

- In order to reduce the weight of the kite, there are limited actuators on the kite. In fact, there are only two control inputs (kite's roll angle and the reeling speed of cables) in the kite model we employed. Thus, the limited inputs make the kite an under-actuated system. For this under-actuated system, some internal states can not be controlled which makes the stability and robustness of the system hard to be guaranteed. More importantly, due to the limited inputs, the system behavior is somehow confined. This intrinsically-existed constraint requires us to design a suitable output reference path.

- The varying wind speed can be treated as an unknown external input. This external input influences the system behavior considerably. Specifically, it affects

the apparent wind speed, orientations of the kite and the traction forces on the cables. Hence, the speed of kites on the reference path can not be determined.

- The kite model is a fast and strongly nonlinear dynamics, which makes optimization-based controllers difficult to be implemented.

1.4 Motivations and Contributions

1.4.1 Motivations

Output Path-following vs. Trajectory Tracking

In [32–34], NMPC scheme has been formulated to solve trajectory tracking problems of kite systems. However, as we mentioned before, the forward speed of kites on the reference path can not be pre-computed due to the varying wind speed. When the wind turbulence is large or the wind speed varies in a wide range, the kite may not be able to be stablized on a reference trajetory with a pre-specified timing law. Even if it could be stabilized, the generated power is disspative since the glider ratio of the kite may be decreased in order to track the inconsistent kite's speed. Thus, trajectory tracking is not appropriate in this case. In contrast, path-following is more flexible than trajectory tracking, since its objective is driving the system to reach and follow a geometric path, without a pre-specified timing law. Here is a brief description of path-following problems using θ to describe the path evolution. Given a system

$$\begin{aligned} \dot{x} &= f(x,u) \\ y &= h(x,u) \quad t \geq 0, \end{aligned}$$

with state $x \in R^{n_x}$, input $u \in R^{n_u}$, output $y \in R^{n_y}$ and a predefined reference path

$$\mathcal{P} = \{\bar{p} \in \mathbb{R}^{n_y} | \bar{p} = p(\theta), \theta \in [0, \infty)\}.$$

The objective of the path-following problem is to drive the system to the zero-path-error manifold

$$e_P(t) := y(t) - p(\theta(t)) = 0 \quad t \geq 0,$$

where $\theta : [0, \infty) \to [0, \infty)$ is a timing law to be specified which gives an additional degree of freedom for the zero-path-error manifold.

Moreover, the intention of defining the reference path in output space is to allow additional degrees of freedom such as the kite's orientations along the reference path. Thus, the economic performance can be further improved on the zero-path-error manifold. In other words, we want to design a controller to regulate the time-varying error dynamics at the origin of output space, meanwhile optimize other internal states to further enhance the economic performance.

Why Economic Model Predictive Path-following Control?

- **Path Convergence:** The kite system is asymptotically convergent to the reference path.
- **Economic Performance:** When stabilizing kites on a given output reference path, economic performance can be further enhanced in two aspects. First of all, when the system is disturbed and deviates from the reference path, the transient economic performance can be enhanced while the closed-loop trajectory is still asymptotically convergent to the reference path. In other words, the system is driven to the reference path optimally with respect to certain economic criteria under the designed control law. Secondly, after the kite is stabilized along the output reference path, the economic performance can be further improved due to additional degrees of freedom such as kite's orientations.
- **Constraint Satisfaction:** The kite system is subject to state and input constraints.
- **Varying Wind Speed:** Due to the varying wind speed, the speed assignment along the reference path can not be predefined which motivates our choice of path-following control.

In summary, considering aforementioned objectives and requirements, so-called Economic Model Predictive Path-following Control (EMPFC) is a possible solution and the main idea is to solve the path-following problem from an EMPC perspective.

1.4.2 Contributions

- **Stability analysis of EMPFC.** To access the stability and feasibility of EMPFC, optimal steady state set for the output path-following problems is defined. The existence of the optimal steady state set implies that the economic cost function is chosen such that the optimal steady state is at the origin of the error space and the corresponding steady state set is not empty. New definition of dissipativity for the output path-following problems is given. Sufficient conditions that guarantee the convergence of the system to the optimal operation on the reference path are derived. In addition, an example of a 2-DoF robot shows that, the proposed EMPFC scheme achieves better economic performance while the system can follow along the reference path in forward direction and finally converge to its optimal steady state.

- **Sampled-data EMPC for set-point stabilization problems**. Most existing literature on EMPC is in a discrete-time manner [43–46]. We extent the assumption of dissipativity to continuous-time systems. With this "continuous dissipativity" and other stability conditions, the stability of sampled-data EMPC for set-point stabilization problems is guaranteed.

- **Kite controller design during traction phase using EMPFC.** The proposed EMPFC scheme is successfully applied to a challenging nonlinear kite model. On the one hand, it achieves the trade-off between the convergence and the economic performance. On the other hand, due to the relaxation of the optimal operation, it adapts to a wide range of wind speed and considerable wind turbulence. The effectiveness of the proposed control scheme is shown in two aspects. For a static reference path, the generated power is increased while the kite is stabilized in the neighborhood of the reference path. For a dynamic reference path, the economic performance can be further enhanced since parameters for the reference path are treated as additional optimization variables. Thus, the proposed EMPFC scheme achieves the integration of path optimization and path-following, resulting in a better economic performance for the closed-loop system. Numerical experiments have been done to testify the effectiveness of the proposed control scheme.

Chapter 2

Kite Model Descriptions

Developing an accurate kite model is a very challenging task since its soft natural leads to an easy deformation. The deformation of inflatable flexible wings affects the orientation of the aerodynamic lift and drag forces, and thus affecting the motion of the kite.

To overcome this challenge, various kite modeling methods have been proposed in the literature. One realistic way to model the global dynamics and deformation of kites is using a finite element model [47]. In a finite element model, the structure and the physical material properties of kites are intrinsically included, hence the system parameters can be directly obtained. Another simpler approach is using a rigid body model [48–50]. In these models, the moments of inertial of kites or tethers are included, hence deformations can be investigated. For example, Houska [49] superimposes bending of the arced shape of the kite as an additional state by introducing a second order differential equation. Together with the three degrees of freedom (DoFs) of the body, the three DoFs of the tether model and the two DoFs from the control mechanism, he formulates a 9-DoF kite model.

The above-mentioned models can describe the dynamics of kites realistically to some extend. However, from a control perspective, an overly complicated model is not necessarily required. A simple model helps us to understand the basic laws that govern the movement of the kite, in order to do preliminary analysis of trajectory optimizations and system performances. Moreover, it allows us to implement computationally demanding controllers such as optimization-based controllers.

In this chapter, we introduce a point-mass kite model [9] where the motion is influenced by controlling the roll angle and the angle of attack, and thus the orientation of the lift and drag forces can be changed. Three different coordinate systems are

introduced and the detailed derivation of each force acting on the kite is given. In addition, the applied wind shear model is introduced.

2.1 A Point-mass Kite Model

One simple way to model a kite is using a point-mass kite model. In 2001, Moritz Diehl firstly proposed a nonlinear point-mass model of kites on the basis of Newton's law of motion [30]. Under the assumption that the effective wind speed vector is always contained in kite's symmetry plane, which is reasonable when kite is flying in crosswind condition, the direction of the aerodynamic forces can be determined by the effective wind speed, roll angle of the kite ψ (also the only input variable) and the angle of attack α. Based on this model, a more accurate kite model was developed considering aerodynamic forces and gravity of cables [9]. Furthermore, the elasticity and the internal friction of cables were additionally considered to model the kite [23, 31]. These point-mass models may not be very accurate since they neglect the flexibility and moments of inertial of kites. Nevertheless, they are appropriate to be used for controller design and system performance evaluation.

In this section, we introduce a point-mass kite model [9] considering the effect of cables (gravity and aerodynamic forces). To begin with, three coordinate systems are introduced in order to easily describe the motion and the orientation of the tethered kite moving on a spherical plane. These coordinate systems are listed as follows:

- Global Coordinate (G): An inertial Cartesian coordinate system is defined by (x, y, z) whose origin is located at the ground station of the kite system. A basis of this coordinate system is $(\vec{e}_x, \vec{e}_y, \vec{e}_z)$ where $\vec{e}_x$ is aligned with the nominal wind speed and $\vec{p}$ is the position of the kite center of mass, as shown in Figure 2.1.

- Local Coordinate (L): The local coordinate system is a non-inertial spherical coordinate system defined by (θ, ϕ, r) whose origin is located at the kite center of mass. A basis of this coordinate system is $(\vec{e}_\theta, \vec{e}_\phi, \vec{e}_r)$ (shown in Figure 2.1, red frame).

- Body Coordinate (B): The body coordinate system is a non-inertial Cartesian coordinate system to describe the orientation of the kite. A basis of this coordinate system is $(\vec{x}_b, \vec{y}_b, \vec{z}_b)$ where $\vec{x}_b$ coincides with the kite longitudinal axis pointing forward, $\vec{y}_b$ coincides with the kite transversal axis pointing from the

left to the right wing tip (looking from behind), together with the third unit vector $\vec{z}_b$ completes a right-handed coordinate system.

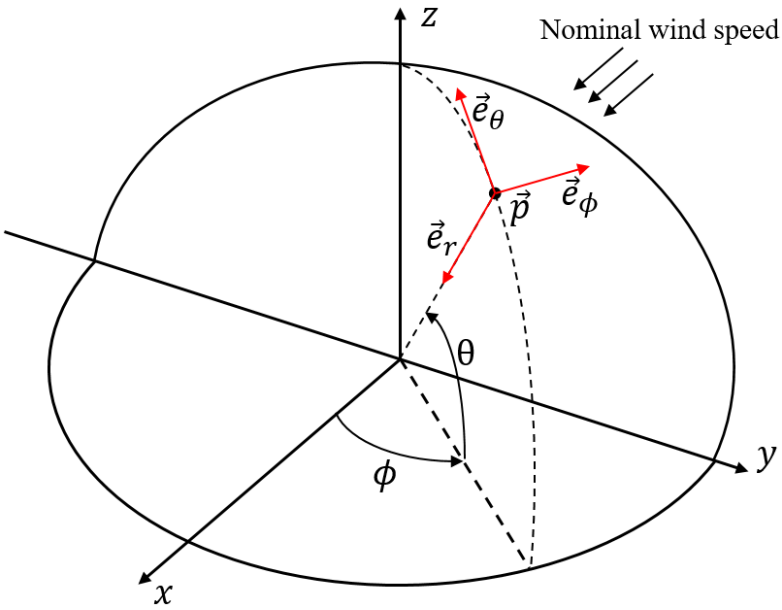

Figure 2.1: Illustration of the kite coordinate systems.

2.1.1 Newton's Law of Motion in Spherical Coordinates

The rotation matrix from the local coordinate to the global coordinate is given by

$$R_{LG} = \begin{pmatrix} -\sin(\theta)\cos(\phi) & -\sin(\phi) & -\cos(\theta)\cos(\phi) \\ -\sin(\theta)\sin(\phi) & \cos(\phi) & -\cos(\theta)\sin(\phi) \\ \cos(\theta) & 0 & -\sin(\theta) \end{pmatrix} = (\vec{e_\theta}, \vec{e_\phi}, \vec{e_r}). \tag{2.1}$$

The position of the point-mass of the kite can be expressed by local coordinates (θ, ϕ, r)

$$\vec{p}_{\{G\}} = \begin{pmatrix} x \\ y \\ z \end{pmatrix} = r \begin{pmatrix} \cos(\theta)\cos(\phi) \\ \cos(\theta)\sin(\phi) \\ \sin(\theta) \end{pmatrix}. \tag{2.2}$$

From the Newton's law of motion, we obtained

$$\ddot{\vec{p}} = \frac{d^2\vec{p}}{dt^2} = \frac{\vec{F}}{m},$$

where $\vec{F} \in \mathbb{R}^3$ is the total force acting on the kite and m is the mass of the kite.

From (2.1) and (2.2), the partial derivatives of $\vec{p}$ with respect to θ, ϕ, r can be expressed in the basis of local coordinate

$$\frac{\partial \vec{p}}{\partial \theta} = r\vec{e}_\theta, \quad \frac{\partial \vec{p}}{\partial \phi} = r\cos(\theta)\vec{e}_\phi, \quad \frac{\partial \vec{p}}{\partial r} = -\vec{e}_r.$$

Hence, $\dot{\vec{p}}$ can be obtained in local coordinate

$$\dot{\vec{p}}_{\{L\}} = \frac{\partial \vec{p}}{\partial \theta}\dot{\theta} + \frac{\partial \vec{p}}{\partial \phi}\dot{\phi} + \frac{\partial \vec{p}}{\partial r}\dot{r} = \begin{pmatrix} r\dot{\theta} \\ r\dot{\phi}\cos(\theta) \\ -\dot{r} \end{pmatrix}. \tag{2.3}$$

Similarly, second partial derivatives of $\vec{p}$ are given by

$$\frac{\partial^2 \vec{p}}{\partial \theta^2} = r\vec{e}_r, \quad \frac{\partial^2 \vec{p}}{\partial \phi^2} = r\sin(\theta)\cos(\theta)\vec{e}_\theta + r\cos^2(\theta)\vec{e}_r, \quad \frac{\partial^2 \vec{p}}{\partial r^2} = 0,$$

and

$$\frac{\partial^2 \vec{p}}{\partial \theta \partial \phi} = -r\sin(\theta)\vec{e}_\phi, \quad \frac{\partial^2 \vec{p}}{\partial \theta \partial r} = \vec{e}_\theta, \quad \frac{\partial^2 \vec{p}}{\partial \phi \partial r} = \cos(\theta)\vec{e}_\phi.$$

Then, we have $\ddot{\vec{p}}$ in local coordinate:

$$\begin{aligned}
\ddot{\vec{p}}_{\{L\}} =& \frac{d}{dt}\left(\frac{\partial \vec{p}}{\partial \theta}\dot{\theta} + \frac{\partial \vec{p}}{\partial \phi}\dot{\phi} + \frac{\partial \vec{p}}{\partial r}\dot{r}\right) \\
=& \frac{\partial^2 \vec{p}}{\partial \theta^2}\dot{\theta}^2 + \frac{\partial^2 \vec{p}}{\partial \phi^2}\dot{\phi}^2 + \frac{\partial^2 \vec{p}}{\partial r^2}\dot{r}^2 + 2\frac{\partial^2 \vec{p}}{\partial \theta \partial \phi}\dot{\theta}\dot{\phi} + 2\frac{\partial^2 \vec{p}}{\partial \theta \partial r}\dot{\theta}\dot{r} + 2\frac{\partial^2 \vec{p}}{\partial \phi \partial r}\dot{\phi}\dot{r} \\
&+ \frac{\partial \vec{p}}{\partial \theta}\ddot{\theta} + \frac{\partial \vec{p}}{\partial \phi}\ddot{\phi} + \frac{\partial \vec{p}}{\partial r}\ddot{r} \\
=& \begin{pmatrix} r\ddot{\theta} + r\dot{\phi}^2\sin(\theta)\cos(\theta) + 2\dot{r}\dot{\theta} \\ r\ddot{\phi}\cos(\theta) - 2r\dot{\theta}\dot{\phi}\sin(\theta) + 2\dot{r}\dot{\phi}\cos(\theta) \\ -\ddot{r} + r\dot{\theta}^2 + r\dot{\phi}^2\cos^2(\theta) \end{pmatrix} = \frac{\vec{F}_{\{L\}}}{m},
\end{aligned} \tag{2.4}$$

where $\vec{F}_{\{L\}}$ denotes the overall force acting on the kite in the local coordinate system.

2.1.2 Overall Gravity Force

There are two parts of gravity forces affecting the behavior of the kite system and we evaluate them at the kite center of the mass. The first one is the weight of kite which can be obtained directly. The second one is the contribution of the weight of cables $F_{c,grav}$, which can be computed by using the equivalent torque equation around the point where the cables are attached to the ground generator. Assuming the gravity of each cable is applied at half of its length, we have

$$F_{c,grav} r\cos(\theta) = 2 \times \frac{1}{2} r\cos(\theta) \frac{\rho_c \pi d_c^2 r}{4} g,$$

where ρ_c is the density of cables, d_c is the diameter of each cable and g is the gravitational acceleration. Then, we can obtain the magnitude of the overall gravity force and by using the rotation matrix (2.1), the overall gravity force $\vec{F}_{grav}$ is given in local coordinate as follows

$$\vec{F}_{grav\{L\}} = \begin{pmatrix} -\left(m + \frac{\rho_c \pi d_c^2 r}{4}\right) g\cos(\theta) \\ 0 \\ \left(m + \frac{\rho_c \pi d_c^2 r}{4}\right) g\sin(\theta) \end{pmatrix}. \tag{2.5}$$

2.1.3 Aerodynamic Force of the Kite

The aerodynamic force of the kite $\vec{F}_{aer}$ depends on the apparent wind speed vector $\vec{v}_a$ and the roll angle ψ of the kite. The apparent wind speed is the relative velocity of the wind with respect to the kite and can be expressed by:

$$\vec{v}_a = \vec{v}_w - \dot{\vec{p}},$$

where $\vec{v}_w$ is the absolute wind speed and the kite speed $\dot{\vec{p}}$ can be obtained in (2.3).

Similarly to the aforementioned body coordinate system, now we define the wind coordinate system $(\vec{x}_w, \vec{y}_w, \vec{z}_w)$ for the convenience of describing the aerodynamic forces. Briefly speaking, it is an non-inertial coordinate system with origin located at the kite's center of mass, with basis vector $\vec{x}_w$ pointing towards the apparent wind speed, $\vec{z}_w$ contained in the kite symmetry plane and pointing towards the top side of the kite, and $\vec{y}_w$ completing the right-handed coordinate system (see [9] for a more

detailed illustration). Basis vector $\vec{x}_w$ can be obtained in the local coordinate:

$$\vec{x}_w = \frac{\vec{v}_{a\{L\}}}{\left\|\vec{v}_{a\{L\}}\right\|}. \tag{2.6}$$

Assuming that the kite's trailing edge is always pulled by the tail into the direction of the apparent wind vector, i.e., basis vector $\vec{x}_w$ and $\vec{z}_w$ are always contained in the kite symmetry plane. Note that this assumption also indicates that vector $\vec{y}_w$ coincides with $\vec{y}_b$ pointing from the left to the right wing tip (looking from behind).

In [30], by introducing three requirements that $\vec{y}_w$ is perpendicular to $\vec{x}_w$, that its projection on the $\vec{e}_r$ equals $\sin(\psi)$ and that the kite is always in the same orientation with respect to cables, $\vec{y}_w$ can be uniquely determined. Following along this line, we can derive $\vec{y}_w$ in our setup:

$$\vec{y}_w = \vec{e}_w(\cos(\psi)\sin(\eta)) - (\vec{e}_r \times \vec{e}_w)\cos(\psi)\cos(\eta) + \vec{e}_r \cdot \sin(\psi), \tag{2.7}$$

where $\vec{e}_w$ is the unit vector of apparent wind speed vector projecting onto the tangent plane spanned by $\vec{e}_\theta$ and $\vec{e}_\phi$:

$$\vec{e}_w = \frac{\vec{v}_a - \vec{e}_r(\vec{e}_r \cdot \vec{v}_a)}{\|\vec{v}_a - \vec{e}_r(\vec{e}_r \cdot \vec{v}_a)\|},$$

and

$$\eta = \arcsin\left(\tan(\Delta\alpha)\tan(\psi)\right), \quad \Delta\alpha = \arcsin\left(\frac{-\vec{e}_r \cdot \vec{v}_a}{\|\vec{v}_a\|}\right).$$

Here $\Delta\alpha$ is the angle between the apparent wind speed and the tangent plane at the kite's position. Roll angle of kite ψ is the control input which influences the kite motion by changing the direction of aerodynamic force $\vec{F}_{aer\{L\}}$. The magnitudes of lift and drag force of the kite are respectively given by:

$$F_L = \frac{1}{2}\rho A C_L \left\|\vec{v}_a\right\|^2, \qquad F_D = \frac{1}{2}\rho A C_D \left\|\vec{v}_a\right\|^2, \tag{2.8}$$

where ρ is the air density, A is the characteristic area of the kite, C_L and C_D are the kite lift and drag coefficients, respectively. Note that we assume C_L and C_D to be constant, since the kite angle of attack α is almost a constant during the traction phase (around 13°). During the traction phase, an appropriate regulating mechanism and the massive aerodynamic force help to keep α in a low value thus the kite glider

ratio $\frac{C_L}{C_D}$ is large and huge traction force is generated.

By combing (2.6),(2.7) and (2.8), we obtain the aerodynamic force of the kite $\vec{F}_{aer\{L\}}$ as follows:

$$\vec{F}_{aer\{L\}} = F_D\vec{x}_w + F_L\vec{z}_w, \tag{2.9}$$

where the wind basis vector $\vec{z}_w = \vec{x}_w \times \vec{y}_w$.

2.1.4 Aerodynamic Force of Cables

Aerodynamic force of cables generally decreases the apparent wind speed and slows the kite down. The effect of this force reduces the efficiency of the system and cannot be neglected especially with long tethers. According to [9, 23], this drag force can be estimated by integrating the angular momentum along the cables. Since the apparent wind speed at each line segment is mainly determined by the motion of the kite and cables, we assume it is proportional to the distance from the ground generator. Then we obtain the overall angular momentum $\vec{M}_c$ of two cables:

$$\begin{aligned}\vec{M}_c =& 2\int_0^r (s\vec{e}_r) \times \frac{1}{2}\rho C_{D,c} d_c \cos(\Delta\alpha) \left(\frac{s|\vec{v}_a|}{r}\right)^2 \vec{x}_w \, ds \\ =& 2r\vec{e}_r \times \frac{1}{8}\rho C_{D,c} d_c \cos(\Delta\alpha)|\vec{v}_a|^2\vec{x}_w \\ =& r\vec{e}_r \times \vec{F}_{aer,c} \ ,\end{aligned}$$

where ρ is the air density, $C_{D,c}$ is the drag force coefficient of cables and $\vec{F}_{aer,c}$ is the estimated cable drag force. Note that the effective area of two cables equals $2rd_c\cos(\Delta\alpha)$ which is the projection of the cable front area on the plane perpendicular to the apparent wind vector (see Figure 2.2).

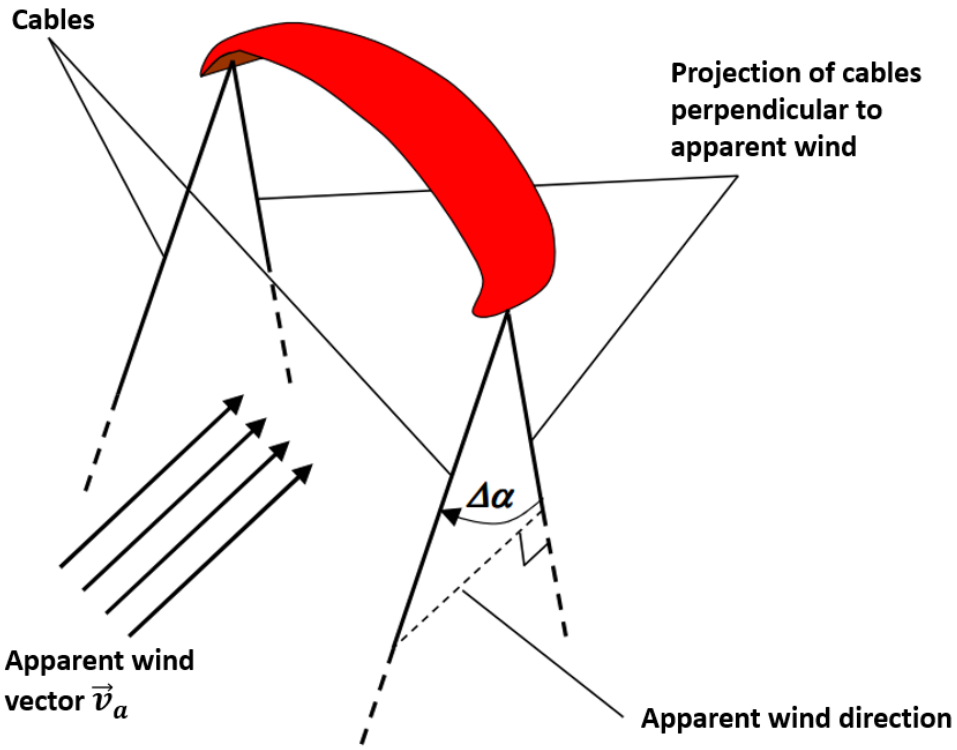

Figure 2.2: Illustration of effective front area of cables [9].

Then, the estimated cable drag force can be expressed by

$$\vec{F}_{aer,c\{L\}} = \frac{1}{4}\rho C_{D,c} r d_c \cos(\Delta\alpha)|\vec{v}_a|^2 \vec{x}_w. \tag{2.10}$$

In (2.10), the magnitude of $\vec{F}_{aer,c\{L\}}$ grows linearly with cables length r. Thus the aerodynamic force of cables can not be neglected for the kite system with long tethers (e.g. 500-1000m).

2.1.5 Wind Shear Model

Employing a realistic wind speed profile along z-axis is crucial in numerical experiments. First of all, the absolute wind speed $\vec{v}_w$ greatly affects the system behavior, such as the generated power, the force acting on cables and the closed-loop trajectory. Secondly, one of the main advantages of kite generators over conventional wind turbines is its capability to access a more constant and denser wind power. Thus, a realistic wind model helps us to evaluate the economic performance of kite systems accurately and makes the obtained results more convincing.

There has been many wind models proposed in the past years. In this thesis, we employ the wind shear model in the form of logarithmic function [51] to describe the nominal wind speed along x-axis $v_x(z)$:

$$v_x(z) = v_0 \frac{\ln\left(\frac{z}{z_0}\right)}{\ln\left(\frac{z_r}{z_0}\right)}$$

where z_r and v_0 are the reference height and the corresponding reference wind speed, respectively. z_0 is the surface roughness length [52] which is used to characterize the roughness factor of the considered terrain. Actually, for a given wind speed data set, these parameters can be computed using least square approximation.

Then, the absolute wind speed vector is given in the ground coordinate system:

$$\vec{v}_{w\{G\}} = \begin{pmatrix} v_x(z) \\ 0 \\ 0 \end{pmatrix} + \vec{v}_t, \tag{2.11}$$

where $\vec{v}_t$ is the unknown wind turbulence in the ground coordinate system, which may have components in all directions. In chapter 4, we will give a more detailed description of the applied wind model.

2.1.6 Overall Kite Model

The total force acting on the kite $\vec{F}_{\{L\}}$ in (2.4) is given by

$$\vec{F}_{\{L\}} = \vec{F}_{grav\{L\}} + \vec{F}_{aer\{L\}} + \vec{F}_{aer,c\{L\}} + \begin{pmatrix} 0 \\ 0 \\ F_{trac} \end{pmatrix}, \tag{2.12}$$

where F_{trac} is the traction force on cables.

By introducing the reference reeling out speed $\dot{r}_{ref}(t)$, the traction force F_{trac} can be regarded as a control input such that $\lim_{t\to\infty} \dot{r}(t) - \dot{r}_{ref}(t) = 0$.

Consider the first-order system:

$$\ddot{r} - \ddot{r}_{ref} = -\frac{\vec{F}_{\{L\}r}}{m} - \ddot{r}_{ref},$$

where $\vec{F}_{\{L\}r}$ denotes the third component of vector $\vec{F}_{\{L\}}$ in the local coordinate.

During the traction phase, $\dot{r}_{ref}$ is chosen to be constant or changes very slow, and thus $\ddot{r}_{ref}$ can be treated as small disturbance and $\dot{r} - \dot{r}_{ref}$ converges to zero if

$$-\frac{\vec{F}_{\{L\}r}}{m} = K(\dot{r} - \dot{r}_{ref}), \quad K \leq 0,$$

where k is the feedback gain. Then we have

$$F_{trac} = -(\vec{F}_{grav\{L\}r} + \vec{F}_{aer\{L\}r} + \vec{F}_{aer,c\{L\}r}) - mK(\dot{r} - \dot{r}_{ref}). \tag{2.13}$$

By combining equation (2.4)-(2.13), we can obtain the overall kite model:

$$\begin{aligned}\dot{x}(t) = &\begin{pmatrix} \dot{\theta} \\ \dot{\phi} \\ \dot{r} \\ \frac{\vec{F}_{\{L\}\theta}}{rm} - \dot{\phi}^2 \sin(\theta)\cos(\theta) - 2\frac{\dot{r}}{r}\dot{\theta} \\ \frac{\vec{F}_{\{L\}\phi}}{rm\cos(\theta)} + 2\dot{\theta}\dot{\phi}\tan(\theta) - 2\frac{\dot{r}}{r}\dot{\phi} \\ -\frac{\vec{F}_{\{L\}r}}{m} + r\dot{\theta}^2 + r\dot{\phi}^2\cos^2(\theta) \end{pmatrix} \\ = &f(x(t), u(t), \vec{v}_w(t), \dot{r}_{ref}(t)),\end{aligned}$$

where $x = [\theta \;\; \phi \;\; r \;\; \dot{\theta} \;\; \dot{\phi} \;\; \dot{r}]$ is the state vector and $u = \psi$ is the control input, $\vec{F}_{\{L\}\theta}$ and $\vec{F}_{\{L\}\phi}$ are the second and third component of the overall force $\vec{F}_{\{L\}}$, respectively.

Chapter 3

Economic Model Predictive Path-following Control

In this chapter we give the formualtion and the stability analysis of the proposed control scheme: economic model predictive path-following control (EMPFC). To begin with, we consider the case of sampled-data EMPC for set-point stabilization problems which is an extended version of traditional MPC (e.g., [53] and [54]) using a general economic cost. Sufficient conditions of stability are given. In Section 3.2 we study the output path-following problems considering economic performance. The proposed EMPFC scheme achieves better economic performance with guaranteed convergence to the optimal operation on the output reference path. At the end of the chapter, an example of a fully actuated robot is given to demonstrate the effectiveness of the proposed control scheme.

3.1 EMPC for Set-point Stabilization Problems

In [43], the stability of EMPC for nonlinear discrete-time system is proved under the assumption of strong duality of the steady-state problem. In [44], the assumption of strong duality is relaxed by using dissipativity. In fact, it has been shown that dissipativity is a sufficient condition for characterizing the optimality of steady-state operation. Hence, it plays an important role in establishing stability of EMPC. In essence, this assumption guarantees that the optimal operation with respect to the give economic cost is at the optimal steady state.

In this section, we firstly give an extended definition of dissipativity for continuous-

time systems. Then, we show that this definition of "continuous dissipativity" is applicable in a simple linear system. Finally, sufficient convergence conditions of sampled-data EMPC for set-point stabilization problems are given.

3.1.1 Dissipativity for Continuous-time System

To begin with, we consider a continuous time, constrained system

$$\dot{x}(t) = f(x(t), u(t)) \tag{3.1}$$

where states x are restricted to the simply connected and closed set $\mathcal{X} \subseteq \mathbb{R}^{n_x}$. The input signal is a piecewise continuous function with values in the compact set $\mathcal{U} \subset \mathbb{R}^{n_u}$, i.e. input signal $u(\cdot) \in \mathcal{PC}(\mathcal{U})$ (ensure the system has an absolutely continuous solution).

The optimal steady state is defined by

$$(x_s, u_s) = \arg\min\{\ell(x, u) | x \in \mathcal{X}, u \in \mathcal{U}, f(x, u) = 0\}$$

where $\ell(x, u)$ is a general economic cost. For the simplicity, we assume the optimal steady state (x_s, u_s) to be unique.

Definition 1 (Dissipativity for continuous time system)**.**
For all $x \in \mathcal{X}$ and $u \in \mathcal{U}$, if there exists a differentiable function (storage function) $S : \mathbb{R}^{n_x} \to \mathbb{R}$ such that

$$\frac{\partial S}{\partial x} f(x, u) \leq \ell(x, u) - \ell(x_s, u_s), \tag{3.2}$$

then system(3.1) *is dissipative with respect to the stage cost function $\ell(\cdot, \cdot)$.*
If moreover a positive definite continuous function $\rho : \mathcal{X} \to \mathbb{R}_{\geq 0}$ exists such that

$$\frac{\partial S}{\partial x} f(x, u) \leq \ell(x, u) - \ell(x_s, u_s) - \rho(x), \tag{3.3}$$

then system(3.1) *is said to be strictly dissipative.*

Remark 1. *The dissipation inequality* (3.2) *ensures that the increasing rate of the storage function $\frac{\partial S}{\partial x} f(x, u)$ cannot exceed the supply rate $\ell(x, u) - \ell(x_s, u_s)$. It is easy to show that strict dissipativity is a sufficient and necessary condition for the rotated*

stage cost function $L(x,u) := \ell(x,u) - \frac{\partial S}{\partial x} f(x,u) - \ell(x_s,u_s)$ *to be positive definite on* $\mathcal{X} \times \mathcal{U}$ *with respect to* (x_s,u_s)*. This rotated stage cost function will be used to construct an auxiliary cost function later.*

Next, we show that this assumption of "continuous dissipativity" is indeed applicable by the following example.

Example 1. Consider the following continuous-time linear system:

$$\dot{x} = (1-\alpha)(-x+u)$$

where $\alpha \in [0,1)$ is a parameter to be determined later. Consider the non-convex cost function

$$\ell(x,u) = (x+\frac{u}{3})(2u-x) + (x-u)^4.$$

Regardless α, the system admits equilibrium points on $x=u$, hence

$$\ell(x,u)|_{x=u} = \frac{4}{3}u^2.$$

So, the optimal steady-state is $(x_s,u_s)=(0,0)$, and $\ell(x_s,u_s)=0$. However, point $(0,0)$ is not a global minimum of $\ell(x,u)$. In fact, $\ell(\cdot,\cdot)$ has two global minima of $(x,u) = \pm(21\frac{\sqrt{6}}{64}, 7\frac{\sqrt{6}}{192})$ and $(0,0)$ is a saddle-point which can be visualized in Figure 3.1. Obviously, $\ell(x,u)$ is not positive definite with respect to (x_s,u_s).

Next, we show that $S(x) = kx^2$ is a candidate storage function for dissipativity. From (3.2), strict dissipativity holds if there exists k and $\varepsilon \geq 0$ such that

$$\begin{aligned}
& (x+\frac{u}{3})(2u-x) + (x-u)^4 - 2kx(1-\alpha)(-x+u) \geq \varepsilon x^2 \\
\Leftarrow \quad & (x+\frac{u}{3})(2u-x) - 2kx(1-\alpha)(-x+u) \geq \varepsilon x^2 \\
\Leftrightarrow \quad & \begin{bmatrix} -1+2k(1-\alpha) & \frac{5}{6}-k(1-\alpha) \\ \frac{5}{6}-k(1-\alpha) & \frac{2}{3} \end{bmatrix} \quad is\ PD,
\end{aligned}$$

which can be satisfied when $\alpha = 0.3$, $k = 1.5$.

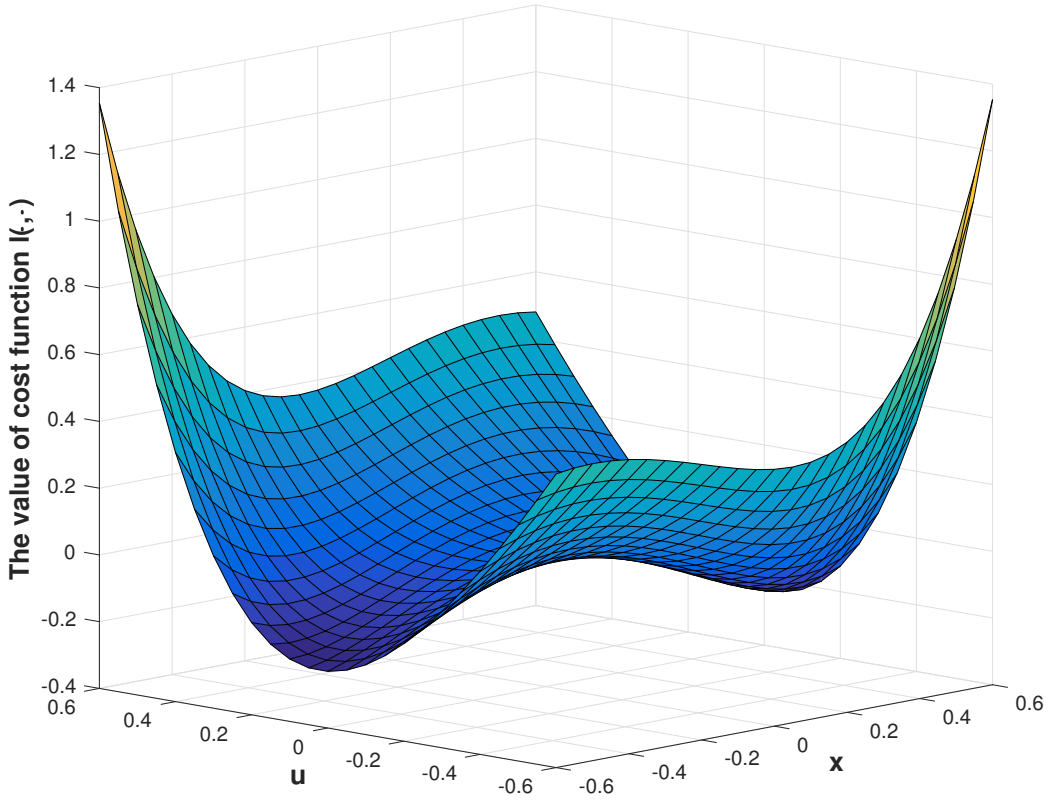

Figure 3.1: Non-positive definite cost function $\ell(\cdot,\cdot)$.

In fact, if we define the rotated stage cost function by

$$\begin{aligned} L(x,u) =& \ell(x,u) - \ell(x_s,u_s) - \frac{\partial S}{\partial x}\dot{x} \\ =& (x+\frac{u}{3})(2u-x) + (x-u)^4 - 2kx(1-\alpha)(-x+u), \end{aligned}$$

the strict dissipativity ensures that this rotated stage cost function is positive definite, cf. Figure 3.2.

Hence, we conclude that indeed some systems are strictly dissipative with respect to some $\ell(\cdot)$, even though $\ell(\cdot)$ is not positive definite.

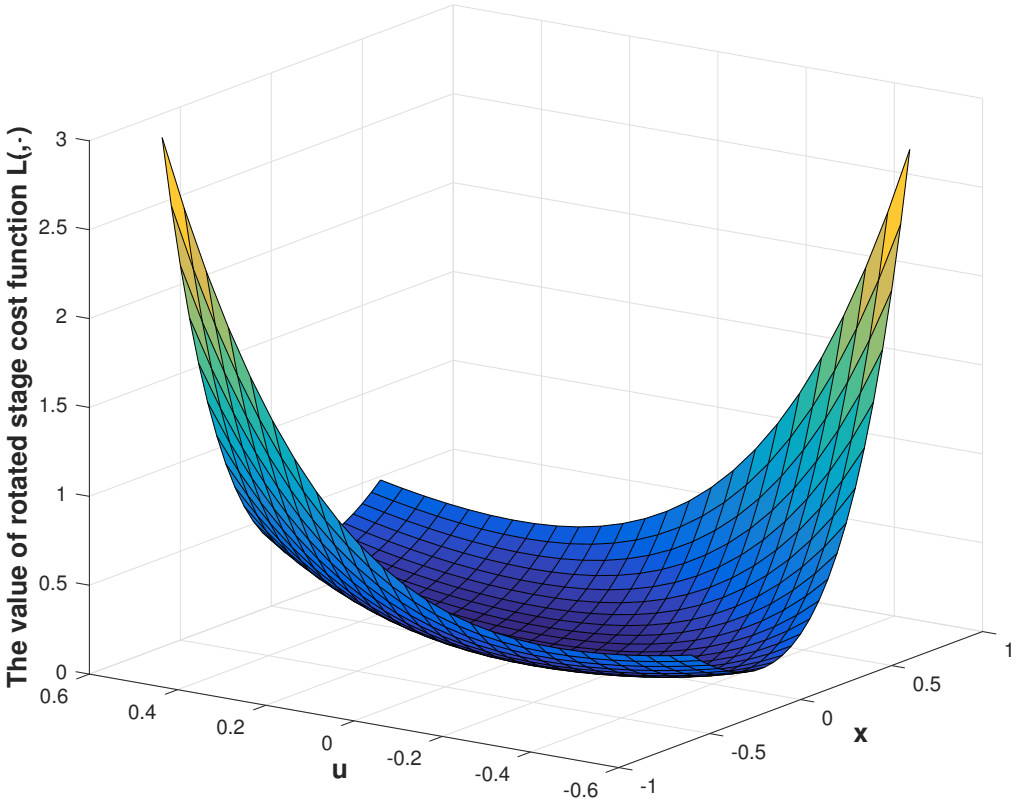

Figure 3.2: Positive definite rotated stage cost function $L(\cdot, \cdot)$, when $\alpha = 0.3$, $k = 1.5$.

3.1.2 Apply Dissipativity to Stability Analysis

First of all, we introduce the overall formulation of the proposed sampled-data EMPC scheme. Here, the sampled-data setting for continuous-time systems is similar to the ones studied in [53], [54]. The stage cost function we applied here is a general economic stage cost.

With a constant sampling period δ, at each sampling time $t_k = t_0 + k \cdot \delta$, $k \in \mathbb{Z}^+$, the

following open-loop optimal control problem (OCP) is solved repeatedly

$$\min_{\overline{u}(\cdot)\in\mathcal{PC}(\mathcal{U})} \quad J(x(t_k),\overline{x}(\cdot),\overline{u}(\cdot)) = \int_{t_k}^{t_k+T_p} \ell(\overline{x}(\tau),\overline{u}(\tau))d\tau + V_f(\overline{x}(t_k+T_p)) \tag{3.4a}$$

$$s.t. \quad \dot{\overline{x}}(\tau) = f(\overline{x}(\tau),\overline{u}(\tau)) \tag{3.4b}$$

$$\overline{x}(t_k) = x(t_k) \tag{3.4c}$$

$$\overline{x}(\tau) \in \mathcal{X} \tag{3.4d}$$

$$\overline{u}(\tau) \in \mathcal{U} \tag{3.4e}$$

$$\overline{x}(t_k+T_p) \in \mathcal{X}_f. \tag{3.4f}$$

Here, $\bar{x}$ and $\bar{u}$ indicate the predicted values which are not necessarily same as the system real evolutions. $\ell : \mathcal{X}\times\mathcal{U} \to \mathbb{R}$ is a general economic cost function. $V_f : \mathcal{X}_f \to \mathbb{R}$ and the set $\mathcal{X}_f$ is the terminal cost function and the terminal region, respectively, which are used to guarantee the feasibility and stability. $T_p = N \cdot \delta$ is the prediction horizon, where N is a positive integer. At each sampling time t_k, we do the prediction of the system behavior over the horizon $[t_k, t_k+T_p]$, and the optimal solution of the optimization problem (3.4) is denoted by $\bar{u}^*(\cdot, x(t_k))$ over the time span $[t_k, t_k+T_p]$. Then, the following input profile is applied to the system (3.1)

$$u_k^*(t) = \overline{u}^*(t, x(t_k)), \quad t \in [t_k, t_k+\delta], \tag{3.5}$$

while the remaining part of the $\bar{u}^*(\cdot, x(t_k))$ is discarded. At next sampling time t_{k+1}, the new states vector is available and this procedure is repeated.

Additionally, we suppose the solution to system (3.1) from any initial states $x(t_0) \in \mathcal{X}$, driven by an piecewise continuous and right continuous input signal $u(\cdot) \in \mathcal{PC}(\mathcal{U})$ uniquely exists for any $t \geq t_0$, which is denoted by $x(t, x(t_0)|u(\cdot))$.

Next, we construct an auxiliary OCP and show that it is equivalent to the original OCP (3.4). The rotated stage cost and rotated terminal cost for the auxiliary problem are defined by

$$L(x,u) := \ell(x,u) - \frac{\partial S}{\partial x} f(x,u) - \ell(x_s,u_s) \tag{3.6}$$

$$\widetilde{V}_f(x) := V_f(x) + S(x) - V_f(x_s) - S(x_s) \tag{3.7}$$

Then, the auxiliary cost function is

$$\widetilde{J}(x(t_k), \overline{x}(\cdot), \overline{u}(\cdot)) = \int_{t_k}^{t_k+T_p} L(\overline{x}(\tau), \overline{u}(\tau))d\tau + \widetilde{V}_f(\overline{x}(t_k+T_p)). \tag{3.8}$$

By using (3.8) as the objective function, together with the constraints (3.4b)-(3.4f), the auxiliary OCP can be defined.

Now, we make assumptions as follows.

Assumption 1 (Input and state constraints): The input signal $u(\cdot)$ is piecewise continuous and right continuous with values in a compact set $\mathcal{U} \subset \mathbb{R}^{n_u}$ with $u_s \in \mathcal{U}$, i.e. $u(\cdot) \in \mathcal{PC}(\mathcal{U})$. The state constraint set $\mathcal{X} \subseteq \mathbb{R}^{n_x}$ is closed and simply connected with $x_s \in \mathcal{X}$.

Assumption 2 (System dynamics): Function $f : \mathcal{X} \times \mathcal{U} \to \mathbb{R}^{n_x}$ in system (3.1) is Lipschitz continuous on $\mathcal{X} \times \mathcal{U}$.

Assumption 3 (Continuity of system evolution): For any $x_0 \in \mathcal{X}_0$ and any input function $u(\cdot) \in \mathcal{PC}(\mathcal{U})$, the system (3.1) has an absolutely continuous solution.

Assumption 4 (Cost function): The stage cost function $\ell : \mathcal{X} \times \mathcal{U} \to \mathbb{R}$ is continuous. The terminal cost function $V_f : \mathcal{X}_f \to \mathbb{R}$ is continuously differentiable in x and the terminal region $\mathcal{X}_f \subset \mathcal{X}$ is closed.

Assumption 5 (Strictly dissipativity): A differentiable storage function $S : \mathbb{R}^{n_x} \to \mathbb{R}$ and a continuous positive definite function $\rho : \mathcal{X} \to \mathbb{R}_{\geq 0}$ exist such that

$$\frac{\partial S}{\partial x} f(x, u) \leq \ell(x, u) - \ell(x_s, u_s) - \rho(x - x_s), \tag{3.9}$$

for all $x \in \mathcal{X}$ and $u \in \mathcal{U}$.

Lemma 1: If the assumption of strict dissipativity (3.9) holds, then the rotated stage cost (3.6) is lower bounded by a class κ function $\beta(||x - x_s||)$ on $\mathcal{X} \times \mathcal{U}$ and $L(x_s, u_s) = 0$.

Proof. $L(x_s, u_s) = 0$ can be directly obtained. In strict dissipation inequality (3.3), the positive definite function $\rho : \mathcal{X} \to \mathbb{R}_{\geq 0}$ denotes that $\rho(x - x_s) \geq 0$ for all $x \in \mathcal{X} \backslash \{x_s\}$ and $\rho(0) = 0$. Hence, there exists a class κ function $\beta(\cdot)$ such that

$$\rho(x - x_s) \geq \beta(||x - x_s||), \quad \forall x \in \mathcal{X}.$$

From (3.6), we have

$$\begin{aligned} L(x,u) &= \ell(x,u) - \frac{\partial S}{\partial x} f(x,u) - \ell(x_s,u_s) \\ &\geq \rho(x - x_s) \geq \beta(||x - x_s||), \quad \forall (x,u) \in \mathcal{X} \times \mathcal{U}. \end{aligned}$$

Lemma 2: The auxiliary OCP using objective function (3.8) and the original OCP (3.4) share identical solutions.

Proof. The auxiliary cost function is

$$\begin{aligned} \widetilde{J}(x(t_k), \overline{x}(\cdot), \overline{u}(\cdot)) &= \int_{t_k}^{t_k+T_p} L(\overline{x}(\tau), \overline{u}(\tau)) d\tau + \widetilde{V}_f(\overline{x}(t_k + T_p)) \\ &= \int_{t_k}^{t_k+T_p} \ell(\overline{x}(\tau), \overline{u}(\tau)) d\tau - S(x(t_k + T_p)) + S(x(t_k)) - \ell(x_s, u_s) \cdot T_p \\ &\quad + V_f(\overline{x}(t_k + T_p)) + S(x(t_k + T_p)) - V_f(x_s) - S(x_s) \\ &= J(x(t_k), \overline{x}(\cdot), \overline{u}(\cdot)) + C, \end{aligned}$$

where C is a constant which equals to $S(x(t_k)) - \ell(x_s, u_s) \cdot T_p - V_f(x_s) - S(x_s)$. Due to the same constraints in the auxiliary OCP and the original OCP, they share identical solutions.

Lemma 3: Given a control input $u \in \mathcal{U}$, the pair $(\widetilde{V}_f(\cdot), L(\cdot,\cdot))$ satisfies

$$\frac{\partial \widetilde{V}_f}{\partial x} f(x,u) + L(x,u) \leq 0 \quad \forall x \in \mathcal{X}_f,$$

if and only if $(V_f(\cdot), \ell(\cdot,\cdot))$ satisfies the following condition

$$\frac{\partial V_f}{\partial x} f(x,u) + \ell(x,u) - \ell(x_s,u_s) \leq 0 \quad \forall x \in \mathcal{X}_f.$$

Proof. Using the definition of rotated stage cost (3.6) and rotated terminal cost (3.7), we have

$$\begin{aligned} & \frac{\partial V_f}{\partial x} f(x,u) + \ell(x,u) - \ell(x_s,u_s) \leq 0 \\ \Leftrightarrow \quad & (\frac{\partial V_f}{\partial x} + \frac{\partial S}{\partial x}) f(x,u) - \frac{\partial S}{\partial x} f(x,u) + \ell(x,u) - \ell(x_s,u_s) \leq 0 \\ \Leftrightarrow \quad & \frac{\partial \widetilde{V}_f}{\partial x} f(x,u) + L(x,u) \leq 0 \end{aligned}$$

Theorem 1 (Convergence of EMPC for regulation problems)**.**
Given system (3.1) *and sampling period* $\delta \geq 0$*, assume Assumptions* $1-5$ *hold. Moreover, a terminal region* $\mathcal{X}_f$*, a terminal penalty* V_f *and a region of attraction* $\mathcal{X}_0$ *exist such that the following conditions hold:*
i. The optimization problem (3.4) *is feasible for all* $x_0 \in \mathcal{X}_0$*.*
ii. For all $x(t) \in \mathcal{X}_f$*, there exists a scalar* $\delta^+ \geq \delta > 0$ *and a control signal* $u_f(\cdot) \in \mathcal{PC}(\mathcal{U})$ *such that for all* $\tau \in [t, t+\delta^+]$

$$\frac{\partial V_f}{\partial x} f(x(\tau, x(t)|u_f(\cdot)), u_f(\tau)) + \ell(x(\tau, x(t)|u_f(\cdot)), u_f(\tau)) - \ell(x_s, u_s) \leq 0, \tag{3.10}$$

and the trajectory always stays in terminal region, i.e., $x(\tau, x(t)|u_f(\cdot)) \in \mathcal{X}_f$*.*
Then, the optimization problem (3.1) *is feasible for all sampling time* $t_k = t_0 + k\delta$*,* $k \in \mathbb{N}$ *and the closed-loop system resulting from EMPC strategy is asymptotically stable in the sense that* $\lim_{t\to\infty} ||x(t) - x_s|| = 0$*.*

Proof. From lemma 3, we know that the stability condition (3.10) is equivalent to that of the auxiliary problem using rotated stage cost (3.6) and rotated terminal cost (3.7). Then, the second condition in Theorem 1 is equivalent to:
For all $x(t) \in \mathcal{X}_f$ there exists a scalar $\delta^+ \geq \delta > 0$ and a control signal $u_f(\cdot) \in \mathcal{PC}(\mathcal{U})$ such that for all $\tau \in [t, t+\delta^+]$

$$\frac{\partial \widetilde{V}_f}{\partial x} f(x(\tau, x(t)|u_f(\cdot)), u_f(\tau)) + L(x(\tau, x(t)|u_f(\cdot)), u_f(\tau)) \leq 0, \tag{3.11}$$

and the trajectory always stays in terminal region $\mathcal{X}_f$.
From Lemma 1, we know that Assumption 5 (strict dissipativity) ensures the rotated stage cost $L(\cdot,\cdot)$ is lower bounded by a class κ function $\beta(||x - x_s||)$ over $\mathcal{X} \times \mathcal{U}$. Together with Lemma 2 and condition (3.11), Theorem 1 is equivalent to the following rotated theorem:
Given system (3.1) *and sampling period* $\delta \geq 0$*, assume Assumptions* $1-4$ *hold. In addition, the rotated stage cost* $L(\cdot,\cdot)$ *is lower bounded by a class* κ *function* $\beta(||x - x_s||)$ *over* $\mathcal{X} \times \mathcal{U}$*. Moreover, a terminal region* $\mathcal{X}_f$*, a terminal penalty* V_f *and a region of attraction* $\mathcal{X}_0$ *exist such that the following conditions hold:*
i. Replacing (3.4a) *by the rotated stage cost function* (3.8)*, the corresponding auxiliary OCP is feasible for all* $x_0 \in \mathcal{X}_0$*.*
ii. For all $x(t) \in \mathcal{X}_f$*, there exists a scalar* $\delta^+ \geq \delta > 0$ *and a control signal* $u_f(\cdot) \in$

$\mathcal{PC}(\mathcal{U})$ *such that for all* $\tau \in [t, t+\delta^+]$

$$\frac{\partial \widetilde{V}_f}{\partial x} f(x(\tau, x(t)|u_f(\cdot)), u_f(\tau)) + L(x(\tau, x(t)|u_f(\cdot)), u_f(\tau)) \leq 0,$$

and the trajectory always stays in terminal region, i.e., $x(\tau, x(t)|u_f(\cdot)) \in \mathcal{X}_f$.
Then, the auxiliary optimization problem is feasible for all sampling time $t_k = t_0 + k\delta$, $k \in \mathbb{N}$, *and the closed-loop system is asymptotically stable in the sense that* $\lim_{t\to\infty} ||x(t) - x_s|| = 0$.

This rotated theorem, with the auxiliary OCP using (3.8), positive definite rotated stage cost (3.6) and condition (3.11), has been proven in existing literatures (e.g., [54]—Theorem 3, [55]—Theorem 2.1).

Remark 2. *Dissipation condition* (3.9) *can be verified by constructing the following optimization problem*

$$D = \max_{S(\cdot)} \min_{(x,u)\in\mathcal{X}\times\mathcal{U}} L(x, u). \tag{3.12}$$

If $D = 0$, *the system is dissipative. Furthermore, if* $L(x, u) = 0$ *holds if and only if* $(x, u) = (x_s, u_s)$, *the system is strictly dissipative. Normally, we choose a storage function* $S(x)$ *in linear or quadratic form. In the case of linear storage function, the dissipation condition* (3.2) *becomes strong duality condition which is widely used in the context of infinite horizon optimal control, cf. [56]. The procedure for checking dissipativity would be further demonstrated in the example of a fully actuated robot in Section* 3.2.4.

3.2 EMPC for Output Path-following Problems

In last section, we discuss EMPC for regulation problems which is an extended version of traditional MPC (e.g., [53] and [54]) in a sampled-data setting for continuous-time systems using economic cost. While most results of EMPC are in discrete-time (e.g., [43], [44] and [57]), we focus on continuous-time systems in order to have a more insightful discussion of path-following problems. In this section, we start with defining the output path-following problems with economic consideration. Then, we describe the formulation of the proposed EMPFC scheme followed by giving sufficient convergence conditions. Finally, an example of a fully actuated 2-DoF robot is given to illustrate the proposed control scheme. The simulation results show that under the proposed EMPFC scheme, the robot can follow along the reference path in forward

direction with enhanced economic performance, and finally converges to its optimal steady state.

3.2.1 The Path-Following Problems with Economic Enhancement

We consider the nonlinear system as follows

$$\begin{aligned} \dot{x}(t) &= f(x(t), u(t)) \\ y(t) &= h(x(t)), \end{aligned} \tag{3.13}$$

where $x \in \mathcal{X}$ and $u \in \mathcal{U}$ are states and inputs subject to state constraints and input constraints correspondingly.

The reference path is defined in output space

$$\mathcal{P} = \{\bar{p} \in \mathbb{R}^{n_y} | \bar{p} = p(\theta), \theta \in [\theta_0, \theta_m]\} \tag{3.14}$$

where the function $p : \mathbb{R} \to \mathbb{R}^{n_y}$ is continuously differentiable, and θ is the path evolution variable. The time evolution of $\theta(t)$ is not necessarily to be known a priori, and hence the forward speed on the reference path can be treated as an additional degree of freedom. Note that θ_m can be replaced by $+\infty$ when we consider a infinitely long or periodic reference path.

The forward speed on the reference path is determined by a virtual dynamics of θ. For simplicity, we use an integrator chain to describe the virtual path dynamics

$$\begin{aligned} \dot{z} &= g(z, v) = Az + Bv, \quad z(t_0) = z_0 \in \mathbb{R}^{\hat{r}+1} \\ \theta &= Cz \end{aligned} \tag{3.15}$$

where z is the path evolution vector representing each derivative of θ; $\hat{r}$ is the value of the largest component in vector relative degree of (3.13) (see [55] for a detailed definition); v is a virtual input controlling the forward motion on the reference path, and

$$A = \left[\begin{array}{c|c} \mathbf{0}^{\hat{r}\times 1} & \mathbf{I}^{\hat{r}\times\hat{r}} \\ \hline 0 & \mathbf{0}^{1\times\hat{r}} \end{array}\right], \quad B = [0, \cdots, 0, 1]^{\mathrm{T}} \in \mathbb{R}^{\hat{r}+1}$$
$$C = [1, 0, \cdots, 0] \in \mathbb{R}^{1\times(\hat{r}+1)}.$$

We use $\mathcal{Z}$ and $\mathcal{V}$ to denote the state constraints and input constraints of the virtual system, respectively. By combining the original system (3.13) with the virtual system (3.15), we obtain the augmented system

$$\begin{aligned} \dot{\xi} &= \begin{bmatrix} \dot{x} \\ \dot{z} \end{bmatrix} = \begin{bmatrix} f_(x,u) \\ g(z,v) \end{bmatrix} = f_\xi(\xi,\omega) \\ e &= h(x) - p(Cz) = \tilde{h}(\xi), \end{aligned} \tag{3.16}$$

where $\xi = (x^{\mathrm{T}}, z^{\mathrm{T}})^{\mathrm{T}} \in \mathbb{R}^{n_x+\hat{r}+1}$ and $\omega = (u^{\mathrm{T}}, v^{\mathrm{T}})^{\mathrm{T}} \in \mathbb{R}^{n_u+1}$ are the augmented states and inputs respectively. Furthermore, we define the constraints for the augmented system to be $\xi \in \Xi := \mathcal{X} \times \mathcal{Z}$ and $\omega \in \Omega := \mathcal{U} \times \mathcal{V}$. The constraint for the error vector can then be defined by $\mathcal{E} := \{\tilde{h}(\xi) | \xi \in \Xi\}$.

Then the output path-following problems (OPFP) with economic enhancement for constrained system (3.13) can be defined to design a controller such that the following requirements are satisfied.

1. ***Path Convergence:*** *The output error $e = h(x) - p(\theta)$ converges to zero, i.e., $\lim_{t\to\infty} ||e(t)|| = 0$.*
2. ***Forward Motion:*** *The system follows the path $\mathcal{P}$ in the direction of $\dot{\theta} \geq 0$.*
3. ***Constraint Satisfaction:*** *The system constraints $x \in \mathcal{X}$ and $u \in \mathcal{U}$ are always satisfied.*
4. ***Economic Enhancement:*** *The closed-loop trajectory is suboptimal with respect to a predefined economic cost while the above three requirements are satisfied.*

For this output PF problems with economic consideration, our first priority is to guarantee the path convergence. Then, among all solutions that are asymptotically convergent in the output space, we want to find the best solution regarding economic performance. Hence, in the fourth requirement, we only require the closed-loop trajectory to be suboptimal and the economic enhancement is regarded as the secondary task in this problem.

3.2.2 Economic Model Predictive Path-Following Control

Now, we present our EMPC scheme to tackle the PF problems with economic consideration. The formulation of our control scheme is very similar to the one used in [58],

but the stage cost function here is a general economic cost. Hence, the convergence analysis is different.

The cost function to be minimized at each sampling time is

$$\begin{aligned} J(\xi(t_k), \overline{e}(\cdot), \overline{\xi}(\cdot), \overline{\omega}(\cdot)) = &\int_{t_k}^{t_k+T_p} \ell(\overline{e}(\tau), \overline{\xi}(\tau), \overline{\omega}(\tau)) d\tau \\ &+ V_f(\overline{\xi}(t_k + T_p)), \end{aligned} \tag{3.17}$$

where $\ell : \mathcal{E} \times \Xi \times \Omega \to \mathbb{R}$ is a general economic stage cost, $V_f : \Xi_f \to \mathbb{R}$ is the terminal cost. In order to account for the economic performance in state space, augmented state vector ξ is considered in the economic cost $\ell(\cdot, \cdot, \cdot)$.

Consider a constant sampling period δ, at each sampling time $t_k = t_0 + k \cdot \delta$, $k \in \mathbb{Z}^+$, the following OCP is solved repeatedly

$$\min_{\overline{\omega}(\cdot) \in \mathcal{PC}(\Omega)} \quad J(\xi(t_k), \overline{e}(\cdot), \overline{\xi}(\cdot), \overline{\omega}(\cdot)) \tag{3.18a}$$

$$s.t. \quad \dot{\overline{\xi}}(\tau) = f_\xi(\overline{\xi}(\tau), \overline{\omega}(\tau)), \quad \overline{\xi}(t_k) = \xi(t_k) \tag{3.18b}$$

$$\overline{e}(\tau) = \tilde{h}(\overline{\xi}(\tau)) \tag{3.18c}$$

$$\overline{\xi}(\tau) \in \Xi \tag{3.18d}$$

$$\overline{\omega}(\tau) \in \Omega \tag{3.18e}$$

$$\overline{\xi}(t_k + T_p) \in \Xi_f \subset \Xi. \tag{3.18f}$$

At the first sampling time t_0, the initial condition for the virtual dynamics can be obtained by

$$\begin{aligned} \theta(t_0) &= \arg\min_{\theta \in [\theta_0, 0]} ||h(x(t_0)) - p(\theta)||, \\ \overline{z}(t_0) &= (\theta(t_0), 0, \cdots, 0)^{\mathrm{T}}. \end{aligned} \tag{3.19}$$

At the following sampling time $t_k = t_0 + k \cdot \delta$, $k \in \mathbb{Z}^+$, the initial states for the virtual dynamics $z(t_k)$ are exactly the predicted value at time t_k from the last open-loop OCP, since there is no model mismatch or disturbance in the virtual system (3.15). Then, the minimizer of (3.18) can be obtained, which is denoted by $\bar{\omega}^*(\cdot, \xi(t_k))$ over the prediction horizon $[t_k, t_k+T_p]$. Similar to Section 3.1.2, only the first sampling period $t \in [t_k, t_k + \delta]$ of $\bar{\omega}^*(\cdot, \xi(t_k))$ is applied to the system (3.13) and the virtual system (3.15). The remaining part of $\bar{\omega}^*(\cdot, \xi(t_k))$ is discarded.

In order to ensure the forward motion along $\mathcal{P}$, the states for the augmented system (3.16) are additionally constrained in

$$\Xi = \{\mathcal{X} \times [\theta_0, \theta_m] \times [0, +\infty) \times \mathbb{R}^{\hat{r}-1}\} \subset \mathbb{R}^{n_x+\hat{r}+1}. \tag{3.20}$$

We want to guarantee that the closed-loop trajectory converges to the reference path in the output space, besides we want the closed-loop trajectory bounded in the state space (not necessarily convergent) to achieve a better economic performance. Hence, in (3.17), the stage cost function ℓ is only assumed to be dissipative in the output space, while the terminal cost V_f and the terminal region Ξ_f are defined in state space to ensure a bounded closed-loop state trajectory. Compared to OCPs for regulation problems in Section 3.1.2, these OCPs (3.18) additionally involves optimal evolutions of the virtual system, i.e., the optimal speed assignment on the reference path. Note that the terminal cost V_f in (3.17) is not necessarily positive definite. However, to satisfy the stability conditions we present in next section, we usually choose a positive definite terminal cost.

3.2.3 Convergence Analysis

The augmented error system is defined by

$$\dot{\zeta} = \begin{bmatrix} \dot{e} \\ \dot{z} \end{bmatrix} = \begin{bmatrix} \frac{\partial h}{\partial x} f(x,u) - \frac{\partial p}{\partial z_1} \dot{z}_1 \\ g(z,v) \end{bmatrix} := f_\zeta(\xi, \omega), \tag{3.21}$$

where $\zeta = (e^{\mathrm{T}}, z^{\mathrm{T}})^{\mathrm{T}} \in \mathbb{R}^{n_y+\hat{r}+1}$, ξ and ω is defined in (3.16).

Obviously, the mapping from ξ to ζ can be defined by

$$\zeta = \begin{bmatrix} h(x) - p(Cz) \\ z \end{bmatrix} := \hat{h}(\xi). \tag{3.22}$$

The constraints mapping to the augmented error space can be obtained by

$$\Gamma = \{\hat{h}(\xi) | \xi \in \Xi\}, \tag{3.23}$$

where $\hat{h}(\cdot)$ is from (3.22).

Before introducing the optimal steady state for the output path-following problems, we define a set in ξ-space (steady state set). For a given pair $(\zeta, \omega) \in \Gamma \times \Omega$,

the steady state set is defined as follows:

$$\Xi_s(\zeta,\omega) := \{\xi|\hat{h}(\xi)=\zeta, f_\zeta(\xi,\omega)\equiv 0, \xi\in\Xi\}. \tag{3.24}$$

Here, $f_\zeta(\xi,\omega)\equiv 0$ ensures that $\forall\xi\in\Xi_s(\zeta,\omega)$, (ζ,ω) is an equilibrium in the augmented error space, i.e., for all $\xi(t)\in\Xi_s(\zeta,\omega)$, and $\tau\geq t$

$$f_\zeta(\xi(\tau,\xi(t)|\omega),\omega)=0.$$

It follows that (3.24) is a positive invariant set under the constant input signal ω. Note that in (3.24), ξ itself is not necessarily an equilibrium.

Suppose that the economic cost function in (3.17) is chosen such that the optimal steady state (ζ_s,ω_s) is at the origin of the error space and the corresponding steady state set $\Xi_s(\zeta_s,\omega_s)$ is not empty. Then, the following optimization problem

$$\begin{aligned}\min_{\xi,\omega}\quad & \ell(e,\xi,\omega)\\ s.t.\quad & \xi\in\Xi_s(\zeta,\omega)\\ & \tilde{h}(\xi)=0\\ & \omega\in\Omega,\end{aligned} \tag{3.25}$$

has the solution in the form of $(\zeta_s,\omega_s)=([\mathbf{0}^{1\times n_y},\theta_s,\mathbf{0}^{1\times\hat{r}}]^{\mathrm{T}},\omega_s)$, and $\xi_s\in\Xi_s^*(\zeta_s,\omega_s)\subseteq\Xi_s(\zeta_s,\omega_s)$. We assume the first part of the solution (ζ_s,ω_s) uniquely existed and $\Xi_s(\zeta_s,\omega_s)$ is not empty. For simplicity, the solution of (3.25) is expressed by

$$\Sigma^*(\zeta_s,\omega_s)=\{(\zeta,\omega,\xi)|\zeta=\zeta_s,\omega=\omega_s,\xi\in\Xi_s^*(\zeta_s,\omega_s)\}, \tag{3.26}$$

which defines the optimal steady state set of (3.16) with respect the stage cost function in (3.17). Note that the element in $\Sigma^*(\zeta_s,\omega_s)$ is not necessarily a global minimizer of ℓ over $\mathcal{E}\times\Xi\times\Omega$. In essence, $\Sigma^*(\zeta_s,\omega_s)$ indicates that (ζ_s,ω_s) is the optimal steady state in ζ-space, and the augmented state vector ξ is confined in a set (or manifold), i.e., $\xi\in\Xi_s^*(\zeta_s,\omega_s)$. According to (3.24)-(3.25), $\Sigma^*(\zeta_s,\omega_s)$ is a positive invariant set under ω_s which ensures the invariance of the optimality. Since we want to guarantee the convergence to the output reference path, the economic cost function is chosen such that $\Sigma^*(\zeta_s,\omega_s)$ is at the origin of the error space, i.e., on the reference path.

Remark 3. *The optimal operation defined by* (3.25)-(3.26) *means to find the op-*

timal path parameter θ_s and the corresponding ω_s that keeps the system staying at the optimal point on the reference path. This optimal operation is not necessarily an equilibrium in the state space but its projection in the output space is an equilibrium. Actually, the optimal operation of $\xi(\cdot)$ and $\omega(\cdot)$ can be functions of time if only the convergence to the output reference path is required. However, we assume a constant ω_s and define a steady state set $\Xi_s(\zeta_s, \omega_s)$ for simplicity of the stability analysis. Assuming without loss of generality $\theta_s = 0$, consequently $\zeta_s = 0$. In the following discussions, we assume the optimal steady state to be $\Sigma^*(0, \omega_s)$ and (3.25) *admits a unique solution for the pair $(0, \omega_s)$.*

Remark 4. *The optimal steady state set $\Sigma^*(\zeta_s, \omega_s)$ can be generalized from optimal steady state defined in state space (cf. [43, 44]). If the output vector is defined to be same as the state vector, the invariant set $\Sigma^*(\zeta_s, \omega_s)$ becomes the unique solution ξ_s in state space, and the output path-following problem becomes state space path-following problem.*

Since $\Sigma^*(0, \omega_s)$ is the solution of (3.25), substituting any element in $\Sigma^*(0, \omega_s)$ to the stage cost function, we obtain an unique optimal value

$$\begin{aligned}\ell_s(0, \omega_s) =& \ell(e, \xi, \omega)|_{(\zeta,\xi,\omega)\in\Sigma^*(0,\omega_s)} \\ =& \ell(0, \xi, \omega_s)|_{\xi\in\Xi_s^*(0,\omega_s)}.\end{aligned}$$

Definition 2 (Strict Dissipativity for output path-following problems)**.**
If there exist a continuously differentiable storage function $S : \Gamma \to \mathbb{R}$ and a positive definite continuous function $\rho : \Gamma \to \mathbb{R}_{\geq 0}$ such that

$$\frac{\partial S}{\partial \zeta} f_\zeta(\xi, \omega) \leq \ell(e, \xi, \omega) - \ell_s(0, \omega_s) - \rho(\zeta), \tag{3.27}$$

for all $\xi \in \Xi$ and $\omega \in \Omega$, then the augmented error system (3.21) *is strictly dissipative with respect to the supply rate function: $\ell(e, \xi, \omega) - \ell_s(0, \omega_s)$.*

For simplicity, we use the augmented state vector ξ to express the stage cost function

$$\tilde{\ell}(\xi, \omega) := \ell(\tilde{h}(\xi), \xi, \omega) = \ell(e, \xi, \omega), \tag{3.28}$$

in which $\tilde{\ell} : \Xi \times \Omega \to \mathbb{R}$ is reformulated from the economic cost ℓ.

Similarly to Section 3.1.2, we construct an auxiliary OCP from OCP (3.18). The

rotated stage cost and rotated terminal cost are defined to be

$$L(\xi,\omega) := \tilde{\ell}(\xi,\omega) - \frac{\partial S}{\partial \zeta} f_\zeta(\xi,\omega) - \ell_s(0,\omega_s) \tag{3.29}$$

$$\tilde{V}_f(\xi) := V_f(\xi) + S(\hat{h}(\xi)) - S(0). \tag{3.30}$$

Then, the auxiliary cost function is

$$\begin{aligned}\widetilde{J}(\xi(t_k),\overline{\xi}(\cdot),\overline{\omega}(\cdot)) = &\int_{t_k}^{t_k+T_p} L(\overline{\xi}(\tau),\overline{\omega}(\tau))d\tau \\ &+ \tilde{V}_f(\overline{\xi}(t_k+T_p)).\end{aligned} \tag{3.31}$$

The auxiliary OCP of (3.18) is obtained by

$$\min_{\overline{\omega}(\cdot)\in\mathcal{PC}(\Omega)} \widetilde{J}(\xi(t_k),\overline{\xi}(\cdot),\overline{\omega}(\cdot)) \tag{3.32a}$$

subject to

$$\dot{\overline{\xi}}(\tau) = f_\xi(\overline{\xi}(\tau),\overline{\omega}(\tau)), \quad \overline{\xi}(t_k) = \xi(t_k) \tag{3.32b}$$

$$\overline{\xi}(\tau) \in \Xi \tag{3.32c}$$

$$\overline{\omega}(\tau) \in \Omega \tag{3.32d}$$

$$\overline{\xi}(t_k+T_p) \in \Xi_f. \tag{3.32e}$$

Compared to OCP (3.18), the constraint (3.18c) is removed since it is inherently included when constructing (3.28)-(3.30). In fact, these constraints (3.32b)-(3.32e) in the auxiliary OCP can be replaced by (3.18b)-(3.18f) and vice versa.

Now, we give the following assumptions.

Assumption 6 (Input and state constraints): For the augmented error system (3.21), the input signal $\omega(\cdot)$ is piecewise continuous and right continuous with values in a compact set $\Omega \subset \mathbb{R}^{n_u+1}$, i.e., $\omega(\cdot) \in \mathcal{PC}(\Omega)$. The constraint $\Gamma \subseteq \mathbb{R}^{n_y+\hat{r}+1}$ is closed and simply connected.

Assumption 7 (System dynamics): Function $f : \mathcal{X} \times \mathcal{U} \to \mathbb{R}^{n_x}$ in system (3.13) is Lipschitz continuous on $\mathcal{X} \times \mathcal{U}$. The output mapping $h : \mathbb{R}^{n_x} \to \mathbb{R}^{n_y}$ in (3.13) is continuously differentiable.

Assumption 8 (Continuity of system evolution): For any initial $\zeta_0 \in \Gamma$ and any input function $\omega(\cdot) \in \mathcal{PC}(\Omega)$, the augmented error system (3.21) has an absolutely

continuous solution.

Assumption 9 (Cost function): The stage cost function $\ell : \mathcal{E} \times \Xi \times \Omega \to \mathbb{R}$ is continuous. The terminal cost function $V_f : \Xi_f \to \mathbb{R}$ is continuously differentiable and the terminal region Ξ_f is closed.

Assumption 10 (Admissible reference path): The reference path in (3.14) is contained in the interior of the state constraints $\mathcal{X}$ under output mapping $h : \mathbb{R}^{n_x} \to \mathbb{R}^{n_y}$ in (3.13), that is, $\mathcal{P} \subseteq int(h(\mathcal{X}))$. In addition, the function $\bar{p} : \mathbb{R} \to \mathbb{R}^{n_y}$ in (3.14) is continuously differentiable.

Assumption 11 (Strictly dissipativity): The assumption of strict dissipativity defined in Definition 2 is satisfied.

Lemma 4: If the assumption of strict dissipativity (3.27) holds, then the rotated stage cost (3.29) is lower bounded by a class κ function $\beta_\zeta(||\zeta||)$ over $\Xi \times \Omega$ and $L(\xi, \omega_s) = 0$, $\forall \xi \in \Xi_s^*(0, \omega_s)$.

Proof. From (3.26), (3.28) and (3.29), we have

$$\begin{aligned} L(\xi, \omega_s) &= \ell(0, \xi, \omega_s) - \frac{\partial S}{\partial \zeta} f_\zeta(\xi, \omega_s) - \ell_s(0, \omega_s) \\ &= 0, \quad \forall \xi \in \Xi_s^*(0, \omega_s) \end{aligned}$$

In strict dissipation inequality (3.27), the positive definite function $\rho : \Gamma \to \mathbb{R}_{\geq 0}$ denotes that there exists a class κ function $\beta_\zeta(\cdot)$ such that

$$\rho(\zeta) \geq \beta_\zeta(||\zeta||), \quad \forall \zeta \in \Gamma.$$

From (3.27)-(3.29), we have

$$\begin{aligned} L(\xi, \omega) &= \tilde{\ell}(\xi, \omega) - \frac{\partial S}{\partial \zeta} f_\zeta(\xi, \omega) - \ell_s(0, \omega_s) \\ &= \ell(e, \xi, \omega) - \frac{\partial S}{\partial \zeta} f_\zeta(\xi, \omega) - \ell_s(0, \omega_s) \\ &\geq \rho(\zeta) \geq \beta_\zeta(||\zeta||), \quad \forall (\xi, \omega) \in \Xi \times \Omega. \end{aligned}$$

Lemma 5: The auxiliary OCP (3.32) and OCP (3.18) share identical solutions.

Proof. The auxiliary cost function is

$$\begin{aligned}
&\widetilde{J}(\xi(t_k), \overline{\xi}(\cdot), \overline{\omega}(\cdot)) \\
=&\int_{t_k}^{t_k+T_p} L(\overline{\xi}(\tau), \overline{\omega}(\tau))d\tau + \tilde{V}_f(\overline{\xi}(t_k+T_p)) \\
=&\int_{t_k}^{t_k+T_p} \tilde{\ell}(\overline{\xi}(\tau), \overline{\omega}(\tau))d\tau - S(\zeta(t_k+T_p)) + S(\zeta(t_k)) - \ell_s(0,\omega_s)\cdot T_p \\
&+ V_f(\overline{\xi}(t_k+T_p)) + S(\hat{h}(\xi(t_k+T_p))) - S(0) \\
=&\int_{t_k}^{t_k+T_p} \ell(\overline{e}(\tau), \overline{\xi}(\tau), \overline{\omega}(\tau))d\tau + V_f(\overline{\xi}(t_k+T_p)) + C \\
=&J(\xi(t_k), \overline{e}(\cdot), \overline{\xi}(\cdot), \overline{\omega}(\cdot)) + C,
\end{aligned}$$

where C is a constant which equals to $S(\zeta(t_k)) - \ell_s(0,\omega_s)\cdot T_p - S(0)$. As disscused previously, the constraints (3.32b)-(3.32e) are equivalent to (3.18b)-(3.18f). Hence, OCP (3.32) and OCP (3.18) share identical solutions.

Lemma 6: Given $\forall\omega \in \Omega$, the pair $(\tilde{V}_f(\cdot), L(\cdot,\cdot))$ satisfies

$$\frac{\tilde{V}_f}{\partial\xi} f_\xi(\xi,\omega) + L(\xi,\omega) \leq 0 \quad \forall\xi \in \Xi_f,$$

if and only if $(V_f(\cdot), \ell(\cdot,\cdot,\cdot))$ satisfies the following condition

$$\frac{\partial V_f}{\partial\xi} f_\xi(\xi,\omega) + \ell(e,\xi,\omega) - \ell_s(0,\omega_s) \leq 0 \quad \forall\xi \in \Xi_f.$$

Proof. We firstly calculate the time derivative of the storage function $S : \Gamma \to \mathbb{R}$ in (3.27). Since $S(\zeta) = S(\hat{h}(\xi))$, we have

$$\dot{S} = \frac{\partial S}{\partial\zeta} f_\zeta(\xi,\omega) = \frac{\partial S}{\partial\hat{h}} \frac{\partial\hat{h}}{\partial\xi} f_\xi(\xi,\omega).$$

Using definitions of the rotated stage cost (3.29) and the rotated terminal cost (3.30),

we have

$$\begin{aligned}
&\frac{\partial V_f}{\partial \xi} f_\xi(\xi,\omega) + \ell(e,\xi,\omega) - \ell_s(0,\omega_s) \\
=&\frac{\partial V_f}{\partial \xi} f_\xi(\xi,\omega) + \frac{\partial S}{\partial \zeta} f_\zeta(\xi,\omega) - \frac{\partial S}{\partial \zeta} f_\zeta(\xi,\omega) + \ell(e,\xi,\omega) - \ell_s(0,\omega_s) \\
=&\frac{\partial V_f}{\partial \xi} f_\xi(\xi,\omega) + \frac{\partial S}{\partial \hat{h}} \frac{\partial \hat{h}}{\partial \xi} f_\xi(\xi,\omega) - \frac{\partial S}{\partial \zeta} f_\zeta(\xi,\omega) + \tilde{\ell}(\xi,\omega) - \ell_s(0,\omega_s) \\
=&\frac{\tilde{V}_f}{\partial \xi} f_\xi(\xi,\omega) + L(\xi,\omega).
\end{aligned}$$

Since the constraints of these two inequalities are consistent, Q.E.D..

Theorem 2 (Convergence of EMPC for output path-following problems)**.** *Given system* (3.13) *and sampling period* $\delta \geq 0$*, assume Assumptions* $6-11$ *hold. Suppose the following conditions hold:*

i. The optimization problems (3.18) *and* (3.19) *have feasible solutions at the initial time* t_0*.*

ii. A terminal region Ξ_f *and a terminal cost function* $V_f : \Xi_f \to \mathbb{R}$ *exist such that for all* $\xi(t) \in \Xi_f$ *there exists a scalar* $\delta^+ \geq \delta > 0$ *and a control signal* $\omega_f(\cdot) \in \mathcal{PC}(\Omega)$ *such that for all* $\tau \in [t, t+\delta^+]$

$$\begin{aligned}
&\frac{\partial V_f}{\partial \xi} f_\xi(\xi(\tau,\xi(t)|\omega_f(\cdot)),\omega_f(\tau)) \\
&+ \ell(e(\tau,e(t)|\omega_f(\cdot)),\xi(\tau,\xi(t)|\omega_f(\cdot)),\omega_f(\tau)) - \ell_s(0,\omega_s) \leq 0,
\end{aligned} \tag{3.33}$$

and the closed loop trajectory always stays in terminal region, i.e., $\xi(\tau,\xi(t)|\omega_f(\cdot)) \in \Xi_f$*.*

Then, the optimization problem (3.18) *is feasible for all sampling time* $t_k = t_0 + k\delta$*,* $k \in \mathbb{N}$ *and the closed-loop system resulting from EMPFC strategy based on* (3.18) *is asymptotically convergent to the output reference path* $\mathcal{P}$ (3.14) *in the sense that* $\lim_{t\to\infty} ||e(t)|| = 0$*, and the system moves along* $\mathcal{P}$ *in forward direction and finally converges to its optimal steady set, i.e.,* $\dot{\theta}(t) \geq 0$ *and* $\lim_{t\to\infty} \theta(t) - \theta_s = 0$*.*

Proof. We firstly show that Theorem 2 is equivalent to a rotated theorem. Lemma 6 shows the stability condition (3.33) is equivalent to the following inequality using

rotated stage cost (3.29) and rotated terminal cost (3.30)

$$\frac{\partial \widetilde{V}_f}{\partial \xi} f_\xi(\xi(\tau, \xi(t)|\omega_f(\cdot)), \omega_f(\tau)) + L(e(\tau, e(t)|\omega_f(\cdot)), \xi(\tau, \xi(t)|\omega_f(\cdot)), \omega_f(\tau)) \leq 0. \quad (3.34)$$

From Lemma 4, we know that Assumption 11 (strict dissipativity) ensures the rotated stage cost (3.29) is lower bounded by a class κ function $\beta(||\zeta||)$ over $\xi \times \omega$. Together with Lemma 5 and condition (3.34), Theorem 2 is equivalent to the following rotated theorem:

Given system (3.13) *and sampling period* $\delta \geq 0$, *assume Assumptions* $6 - 10$ *hold. Moreover, the rotated stage cost* (3.29) *is lower bounded by a class* κ *function* $\beta(||\zeta||)$ *over* $\xi \times \omega$. *Suppose the following conditions hold:*

i. The optimization problems (3.32) *and* (3.19) *have feasible solutions at the initial time* t_0.

ii. A terminal region Ξ_f *and a terminal cost function* $V_f : \Xi_f \to \mathbb{R}$ *exist such that for all* $\xi(t) \in \Xi_f$ *there exists a scalar* $\delta^+ \geq \delta > 0$ *and a control signal* $\omega_f(\cdot) \in \mathcal{PC}(\Omega)$ *such that for all* $\tau \in [t, t + \delta^+]$

$$\frac{\partial \widetilde{V}_f}{\partial \xi} f_\xi(\xi(\tau, \xi(t)|\omega_f(\cdot)), \omega_f(\tau)) + L(e(\tau, e(t)|\omega_f(\cdot)), \xi(\tau, \xi(t)|\omega_f(\cdot)), \omega_f(\tau)) \leq 0,$$

and the closed-loop trajectory always stays in terminal region, i.e., $\xi(\tau, \xi(t)|\omega_f(\cdot)) \in \Xi_f$.

Then, the optimization problem (3.32) *is feasible for all sampling time* $t_k = t_0 + k\delta$, $k \in \mathbb{N}$ *and the closed-loop system based on* (3.32) *is asymptotically convergent to the output reference path* $\mathcal{P}$ (3.14) *in the sense that* $\lim_{t\to\infty} ||e(t)|| = 0$, *and the system moves along* $\mathcal{P}$ *in forward direction and finally converges to its optimal steady set, i.e.,* $\dot{\theta}(t) \geq 0$ *and* $\lim_{t\to\infty} \theta(t) - \theta_s = 0$.

For this rotated theorem, the proofs can be obtained by a reformulation of continuous-time NMPC for set-point stabilization problems (e.g., [54]). The reformulation is directly achieved by constructing the augmented error system (3.21).

Following along lines of [54], the upper bound of the piecewise "MPC value function" can be obtained by

$$V^\delta(t, \xi(t)) \leq V^\delta(t_0, \xi(t_0)) - \int_{t_0}^{t} \beta_\zeta(||\zeta(\tau) - \zeta_s||) d\tau,$$

where $V^{\delta}(\cdot,\cdot)$ is the remainder of the value function for each sampling period $t \in [t_k, t_{k+1})$ (see [54] for detailed definition). Here, we only require the rotated stage cost (3.29) to be lower bounded by a class κ function of the augmented error vector ζ, not the state vector ξ. Hence, the application of Barbalat's Lemma only leads to the convergence of ζ to ζ_s, i.e., $\lim_{t\to\infty} \zeta(t) - \zeta_s = 0$. Furthermore, (3.26) ensures that the economic stage cost is chosen such that the optimal steady state $(\zeta_s, \omega_s) = ([\mathbf{0}^{1\times n_y}, \theta_s, \mathbf{0}^{1\times \hat{r}}]^{\mathrm{T}}, \omega_s)$. It then follows that $\lim_{t\to\infty} ||e(t)|| = 0$ and $\lim_{t\to\infty} \theta(t) - \theta_s = 0$. Finally, with the choice of state constraints Ξ (3.20) and $\Xi_f \subset \Xi$, the forward motion of the closed-loop system $\dot{\theta}(t) \geq 0$ can be guaranteed.

3.2.4 An Illustrating Example: Path-following Control of a Robot

In this section, we consider a fully actuated robot with 2-DoF. We firstly propose an economic stage cost function and show the corresponding optimal steady state is in the form of (3.26). Then, the assumption of dissipativity is satisfied by introducing the storage function $S(\zeta)$ in a quadratic form. Finally, the design of the terminal region and terminal cost is given. Using the proposed EMPFC scheme, the robot can economically converge to the reference path and finally stay at its optimal steady state on the reference path. Simulation results are given to show the effectiveness of the proposed control scheme.

The system dynamics is

$$\begin{aligned} \begin{bmatrix} \dot{x_1} \\ \dot{x_2} \end{bmatrix} &= \begin{bmatrix} \dot{x_2} \\ B^{-1}(x_1)(u - C(x_1, x_2)x_2 - g(x_1)) \end{bmatrix} \\ y &= x_1 \\ y_{ca} &= h_{ca}(x_1), \end{aligned} \tag{3.35}$$

where $x_1 = (q_1, q_2)^{\mathrm{T}} \in \mathbb{R}^2$ and $x_2 = (\dot{q}_1, \dot{q}_2)^{\mathrm{T}} \in \mathbb{R}^2$ are the vector of joint angles and joint velocities, respectively; $B : \mathbb{R}^2 \to \mathbb{R}^{2\times 2}$ describes the inertia of the robot; $C : \mathbb{R}^4 \to \mathbb{R}^{2\times 2}$ describes the centrifugal and Coriolis forces; $g : \mathbb{R}^2 \to \mathbb{R}^2$ represents the effect of gravity; the output $y = x_1$ is defined in the space of joint angles x_1 and the output $y_{ca} = h_{ca}(x_1)$ is the position of the end effector in Cartesian coordinates. For all $x_1 \in \mathbb{R}^2$, the matrix B is invertible, and C and g are bounded. The terms

B, C, g, h_{ca} are listed as follows

$$
\begin{aligned}
B(q) &= \begin{bmatrix} b_1 + b_2\cos(q_2) & b_3 + b_4\cos(q_2) \\ b_3 + b_4\cos(q_2) & b_5 \end{bmatrix} \\
C(q,\dot{q}) &= -c_1\sin(q_2)\begin{bmatrix} \dot{q_1} & \dot{q_1}+\dot{q_2} \\ -\dot{q_1} & 0 \end{bmatrix} \\
g(q) &= \begin{bmatrix} g_1\cos(q_1) + g_2\cos(q_1+q_2) \\ g_2\cos(q_1+q_2) \end{bmatrix} \\
h_{ca}(q) &= \begin{bmatrix} l_1\cos(q_1) + l_2\cos(q_1+q_2) \\ l_1\sin(q_1) + l_2\sin(q_1+q_2) \end{bmatrix}.
\end{aligned}
$$

The state and input constraints of (3.35) are

$$
\begin{aligned}
\mathcal{U} &= \{u \in \mathbb{R}^2 \mid \|u\|_\infty \le \bar{u}\} \\
\mathcal{X} &= \{x = (x_1, x_2)^{\mathrm{T}} \in \mathbb{R}^4 \mid \|x_2\|_\infty \le \bar{\dot{q}}\},
\end{aligned}
\tag{3.36}
$$

where $\bar{u} = 4000$ [Nm] and $\bar{\dot{q}} = 1.5\pi$ [rad/s].

Table 3.1 shows the system parameters. The details of this model can be found in [59].

Table 3.1:
System parameters of the robot (3.35).

b_1	200.0	[kg m^2/rad]	b_2	50.0	[kg m^2/rad]
b_3	23.5	[kg m^2/rad]	b_4	25.0	[kg m^2/rad]
b_5	122.5	[kg m^2/rad]	c_1	-25.0	[Nms^{-2}]
g_1	784.8	[Nm]	g_2	245.3	[Nm]
l_1	0.5	[m]	l_2	0.5	[m]

For the reference path, we refer to [58]. The reference path is given by

$$
\mathcal{P} = \left\{ \bar{p} \in \mathbb{R}^2 | \bar{p} = p(\theta) = \begin{bmatrix} \theta - \frac{\pi}{3} \\ \omega_1 \sin(\omega_2 \sin(\theta - \frac{\pi}{3})) \end{bmatrix}, \theta \in [\theta_0, 0] \right\}, \tag{3.37}
$$

where $\theta_0 = -5.3$, $\omega_1 = 5$, $\omega_2 = 0.6$. Then the output error $e = y - p(\theta)$.

Similarly to (3.21), the augmented error system can be represented in the form of

$$\dot{\zeta} = \begin{bmatrix} \dot{\zeta}_e \\ \dot{\zeta}_z \end{bmatrix} = \left[\begin{array}{c|c} A_e & \mathbf{0}^{4\times 2} \\ \hline \mathbf{0}^{2\times 4} & A_z \end{array}\right] \begin{bmatrix} \zeta_e \\ \zeta_z \end{bmatrix} + \left[\begin{array}{c|c} B_e & \mathbf{0}^{4\times 1} \\ \hline \mathbf{0}^{2\times 2} & B_z \end{array}\right] \begin{bmatrix} u_{FL} - \ddot{p}(z_1) \\ v \end{bmatrix}, \tag{3.38}$$

where $\zeta_e = (e^{\mathrm{T}}, \dot{e}^{\mathrm{T}})^{\mathrm{T}} \in \mathbb{R}^4$, $\zeta_z = (z_1, z_2)^{\mathrm{T}} = (\theta, \dot{\theta})^{\mathrm{T}} \in \mathbb{R}^2$, v is the virtual input of the path evolution dynamics, $u_{FL} \in \mathbb{R}^2$ is the input after feedback linearization of (3.35), that is $u_{FL} = B^{-1}(x_1)(u - C(x_1, x_2)x_2 - g(x_1))$, and $\ddot{p}(z_1) = \frac{\partial^2 p}{\partial^2 z_1} z_2^2 + \frac{\partial p}{\partial z_1} v$ is the second derivative of $p(\cdot)$ with respect to time. Here, the feedback linearization of (3.35) leads to $\dot{x_2} = u_{FL}$. The system matrices of (3.38) are listed as follows

$$A_e = \left[\begin{array}{c|c} \mathbf{0}^{2\times 2} & \mathbf{I}^{2\times 2} \\ \hline \mathbf{0}^{2\times 2} & \mathbf{0}^{2\times 2} \end{array}\right], \; A_z = \begin{bmatrix} 0 & 1 \\ 0 & 0 \end{bmatrix}, \; B_e = \begin{bmatrix} 0 & 0 & 1 & 0 \\ 0 & 0 & 0 & 1 \end{bmatrix}^{\mathrm{T}}, \; B_z = \begin{bmatrix} 0 \\ 1 \end{bmatrix}.$$

It is easy to compute the vector relative degree of (3.35) $\hat{r} = 2$ [58]. Since we apply a piecewise continuous input v, it is unnecessary to choose a path dynamics as described in (3.15). Here, we choose an integrator chain of length two as the path dynamics, i.e., the ζ_z-dynamics in (3.38). The constraints for the path dynamics are $\mathcal{Z} = \{(z_1, z_2) | z_1 \in [-5.3, 0], z_2 \in [0, 6]\}$ and $\mathcal{V} = \{v | v \in [-50, 50]\}$.

Economic stage cost function

The economic stage cost function is consisted of two parts as follows:

$$\ell(\zeta, \omega) = ||(e, \dot{e}, z_1, z_2)||_Q^2 + ||(u - \tilde{u}, v)||_R^2 + \beta z_1 z_2^2, \tag{3.39}$$

where $\omega = (u^{\mathrm{T}}, v)^{\mathrm{T}}$, $Q = \mathrm{diag}([10^5, 10^5, 10, 10, 5, 0.8])$, $R = \mathrm{diag}([10^{-6}, 10^{-6}, 10^{-4}])$, $\beta = 3$, and $\tilde{u} = [229.5, -162.9]^{\mathrm{T}} = g(p(0))$ is the torque required to keep the manipulator staying at its finial position $p(0)$ (also the optimal steady state). Here, the first two terms penalize the deviation of the system to its optimal steady state, and contribute to convergence of the system. The third term, i.e., $\beta z_1 z_2^2$, accounts for the economic performance. This term evaluates the forward speed of two joints on the reference path, but the value of this term is decreasing to zero as the system approaches to the optimal steady state.

Optimal steady state

We show that the optimal steady state of (3.38) with respect to (3.39) is in the form of (3.26).

By solving the following optimization problem

$$\begin{aligned}
\min_{\zeta,\omega} \quad & \ell(\zeta,\omega) \\
s.t. \quad & \dot{\zeta} = 0 \\
& \begin{bmatrix}\zeta_1 \\ \zeta_2\end{bmatrix} = x_1 - p(z_1), \quad \begin{bmatrix}\zeta_3 \\ \zeta_4\end{bmatrix} = x_2 - \frac{\partial p}{\partial z_1} z_2 \\
& \zeta_5 = z_1, \quad \zeta_6 = z_2 \\
& x \in \mathcal{X}, \quad z \in \mathcal{Z}, \quad \omega \in (\mathcal{U} \times \mathcal{V}),
\end{aligned}$$

the optimal steady state can be obtained, that is

$$(\zeta_s, \omega_s) = (\mathbf{0}^{6\times 1}, [\tilde{u}^{\mathrm{T}}, 0]^{\mathrm{T}}). \tag{3.40}$$

Obviously, (3.39) is not positive definite with respect to (ζ_s, ω_s). We want to show that the system can economically converge to its optimal steady state with choice of (3.39) and appropriately designed terminal region and terminal cost, which will be discussed later.

Checking dissipativity

Then we show that (3.38) and (3.39) satisfy the dissipativity assumption with respect to pair (ζ_s, ω_s).

Consider a storage function in quadratic form: $S(\zeta) = \lambda_1\zeta_1^2 + \lambda_2\zeta_2^2 + \lambda_3\zeta_3^2 + \lambda_4\zeta_4^2 + \lambda_5\zeta_5^2 + \lambda_6\zeta_6^2$. Combining (3.38)-(3.40), the rotated stage cost is given by

$$\begin{aligned}
L(\zeta,\omega) =& \ell(\zeta,\omega) - \frac{\partial S}{\partial \zeta}\dot{\zeta} - \ell(\zeta_s,\omega_s) \\
=& ||(e, \dot{e}, z_1, z_2)||_Q^2 + ||(u - \tilde{u}, v)||_R^2 + \beta z_1 z_2^2 - 2\lambda_1\zeta_1\zeta_3 - 2\lambda_2\zeta_2\zeta_4 \\
& - [2\lambda_3\zeta_3, 2\lambda_4\zeta_4]\left(B^{-1}(x_1)(u - C(x_1,x_2)x_2 - g(x_1)) - \frac{\partial^2 p}{\partial^2 \zeta_5}\zeta_6^2 - \frac{\partial p}{\partial \zeta_5} v\right) \\
& - 2\lambda_5\zeta_5\zeta_6 - 2\lambda_6\zeta_6 v - 0.
\end{aligned}$$

Clearly, $x_1 = \begin{bmatrix}\zeta_1 \\ \zeta_2\end{bmatrix} + p(\zeta_5)$ and $x_2 = \begin{bmatrix}\zeta_3 \\ \zeta_4\end{bmatrix} + \frac{\partial p}{\partial \zeta_5}\zeta_6$.

Then, the dissipativity condition can be verified by solving the following optimization problem (cf. Remark 2)

$$\begin{aligned} \max_{\lambda \in \mathbb{R}^6} \min_{\zeta,\omega} \quad & L(\zeta, \omega) \\ s.t. \quad & \left\| \begin{bmatrix}\zeta_3 \\ \zeta_4\end{bmatrix} + \frac{\partial p}{\partial \zeta_5}\zeta_6 \right\|_\infty \leq \frac{3}{2}\pi \\ & \begin{bmatrix}\zeta_5 \\ \zeta_6\end{bmatrix} \in \mathcal{Z}, \quad \omega \in (\mathcal{U} \times \mathcal{V}). \end{aligned} \tag{3.41}$$

Note that the solution of (3.41) is not unique. For each optimal λ^*, there exists the same minimizer of $L(\zeta, \omega)$, that is (ζ_s, ω_s).

Now, we give a candidate λ to examine the strict dissipativity of the system. For $\lambda = [0.9, 1.25, 0, 0, 8.2, 0]^{\mathrm{T}}$, there exists a unique minimizer of $L(\zeta, \omega)$, equals (ζ_s, ω_s), and $L(\zeta_s, \omega_s) = 0$. Then, it directly follows that (3.38) and (3.39) are strictly dissipative with respect to (ζ_s, ω_s).

Design of terminal region and terminal cost

Then, we are ready to apply Theorem 2 to design the terminal region and terminal cost such that the condition in (3.33) is satisfied. The design procedure can be referred to [58] and we show that the obtained terminal region and terminal cost also satisfy the stability condition in (3.33) using an economic stage cost function (3.39).

In (3.38), the dynamics of ζ_z can be handled independently since it is not influenced by the dynamics of ζ_e. Hence, we firstly design the terminal region $\mathcal{Z}_f$ for the path evolution dynamics.

Consider a state feedback controller

$$v_f = K_z \zeta_z, \tag{3.42}$$

where $K_z = (k_1, k_2)$. The closed-loop system is asymptotically stable if all the eigenvalues of $A_z + B_z K_z$ have negative real parts. Furthermore, to ensure the closed-loop solution stays in $\mathcal{Z} = \{(z_1, z_2) | z_1 \in [-5.3, 0], z_2 \in [0, 6]\}$, $A_z + B_z K_z$ should also have real eigenvalues to avoid the system oscillating around the origin. Therefore, K_z should be chosen such that $A_z + B_z K_z$ has two negative and real eigenvalues. This

can be achieved by choosing k_1 and k_2 satisfying

$$k_1 \leq 0, \quad k_2 \leq 0, \quad k_2^2 + 4k_1 > 0.$$

Besides, we need to ensure that $\mathcal{Z}_f$ is positively invariant under the control law $v_f = K_z\zeta_z$. To this end, for all states ζ_z initiated at the boundary of $\mathcal{Z}_f$, the closed-loop solution should points inside of $\mathcal{Z}_f$. In order to simplify the design of $\mathcal{Z}_f$, we further bound z_2 from above so that $z_2 \in [0, \bar{\dot{\theta}}]$. Then, we obtain (see [58] for a detailed explanation)

$$k_1\theta_0 + k_2\bar{\dot{\theta}} < 0, \quad z_2 \leq \frac{k_2 - \sqrt{k_2^2 + 4k_1}}{2} z_1. \tag{3.43}$$

We set $\bar{\dot{\theta}} = 0.4$, and consequently a possible feedback gain could be $K_z = (-0.1, -1.33)$. Together with (3.43), the terminal region for ζ_z is given by

$$\mathcal{Z}_f = \{(z_1, z_2) | z_1 \in [-5.3, 0], z_2 \in [0, 0.4], z_2 \leq -1.25 z_1\}. \tag{3.44}$$

It can be easily verified for all $\zeta_z \in \mathcal{Z}_f$, $v_f = K_z\zeta_z \in \mathcal{V} = \{v | v \in [-50, 50]\}$.

For the ζ_e-part of the augmented error system in (3.38), we consider the linearized input

$$u_{FL} = -K_e\zeta_e + \ddot{p}(z_1) = -K_e\zeta_e + \frac{\partial^2 p}{\partial^2 z_1} z_2^2 + \frac{\partial p}{\partial z_1} v. \tag{3.45}$$

The application of (3.45) to (3.38) leads to a closed-loop system governed by $\dot{\zeta}_e = (A_e - B_eK_e)\zeta_e$. By substituting $u_{FL} = B^{-1}(x_1)(u - C(x_1, x_2)x_2 - g(x_1))$ to (3.45), we obtain the terminal control law for ζ_e-dynamics

$$u_f = C(x_1, x_2)x_2 + g(x_1) + B(x_1)(-K_e\zeta_e + \ddot{p}(z_1)). \tag{3.46}$$

We want to find a terminal region $\mathcal{E}_f$ such that $\forall x \in \mathcal{X}$, $\zeta_z \in \mathcal{Z}_f$ and $\zeta_e \in \mathcal{E}_f$, $u_f \in \mathcal{U}$. Here, we refer to [58] to find the normed upper bound of (3.46) and ensure $u_f \in \mathcal{U}$ by restricting ζ_e inside a level set of a Lyapunov function $V(\zeta_e)$. For all $x \in \mathcal{X}$, we have

$$||B(x_1)|| \leq \bar{B} = 266.4, \quad ||C(x_1, x_2)|| \leq \bar{C} = 269.6, \quad ||g(x_1)|| \leq \bar{g} = 1059.0. \tag{3.47}$$

Note that the reference path $\mathcal{P}$ is sufficiently smooth and $\mathcal{Z}_f$ is compact. With the application of $v_f = K_z\zeta_z$, for all $\zeta_z \in \mathcal{Z}_f$, we have

$$||\ddot{p}(z_1)|| = \left\| \frac{\partial^2 p}{\partial^2 z_1} z_2^2 + \frac{\partial p}{\partial z_1} v_f \right\| \leq \left\| \frac{\partial^2 p}{\partial^2 z_1} \right\| \bar{\dot{\theta}}^2 + \left\| \frac{\partial p}{\partial z_1} \right\| \left\| k_2 \bar{\dot{\theta}} \right\| = \bar{\ddot{p}} = 1.47. \tag{3.48}$$

In order to compute the normed upper bound of (3.46), we introduce the tightened constraints transformed from (3.36):

$$\begin{aligned} \bar{\mathcal{U}} &= \{u \in \mathbb{R}^2 \mid \|u\| \leq \bar{u}\} \subset \mathcal{U} \\ \bar{\mathcal{X}} &= \{x = (x_1, x_2)^{\mathrm{T}} \in \mathbb{R}^4 \mid \|x_2\| \leq \bar{\dot{q}}\} \subset \mathcal{X}, \end{aligned}$$

Then, it follows that $\forall x \in \bar{\mathcal{X}} \subset \mathcal{X}$ and $\zeta_z \in \mathcal{Z}_f$

$$\begin{aligned} & \|u_f\| \leq \bar{C}\bar{\dot{q}} + \bar{g} + \bar{B}(\|K_e\| \|\zeta_e\| + \bar{\ddot{p}}) \\ \Rightarrow \quad & \|\zeta_e\| \geq \frac{\|u_f\| - \bar{C}\bar{\dot{q}} - \bar{g} - \bar{B}\bar{\ddot{p}}}{\bar{B}\|K_e\|}. \end{aligned}$$

Thus, if the following inequality holds

$$\|\zeta_e\| \leq \frac{\bar{u} - \bar{C}\bar{\dot{q}} - \bar{g} - \bar{B}\bar{\ddot{p}}}{\bar{B}\|K_e\|}, \tag{3.49}$$

then $\forall (x, \zeta_z)^{\mathrm{T}} \in \bar{\mathcal{X}} \times \mathcal{Z}_f$, $\|u_f\| \leq \bar{u}$, i.e., $u_f \in \bar{\mathcal{U}} \subset \mathcal{U}$.

Next step is to find a sub-level set of $V(\zeta_e)$ such that (3.49) holds. Since the pair (A_e, B_e) is stabilizable, the stabilizing feedback gain K_e and the corresponding Lyapunov function $V(\zeta_e)$ can be obtained by LQR method with $Q = \mathbf{I}^{4\times4}$, $R = \mathbf{I}^{2\times2}$

$$\begin{aligned} K_e &= \begin{bmatrix} 1 & 0 & 1.732 & 0 \\ 0 & 1 & 0 & 1.732 \end{bmatrix} \\ V(\zeta_e) = \zeta_e^{\mathrm{T}} P_e \zeta_e &= \zeta_e^{\mathrm{T}} \begin{bmatrix} 1.732 & 0 & 1 & 0 \\ 0 & 1.732 & 0 & 1 \\ 1 & 0 & 1.732 & 0 \\ 0 & 1 & 0 & 1.732 \end{bmatrix} \zeta_e. \end{aligned}$$

Considering that

$$V(\zeta_e) = \zeta_e^{\mathrm{T}} P_e \zeta_e \geq \lambda_{\min}(P_e) \|\zeta_e\|^2,$$

where $\lambda_{\min}(P_e)$ is the smallest eigenvalue of P_e, it follows that

$$\|\zeta_e\| \leq \frac{\bar{u} - \bar{C}\bar{\dot{q}} - \bar{g} - \bar{B}\bar{\ddot{p}}}{\bar{B}\,\|K_e\|} \quad \forall \zeta_e \in \left\{ \zeta_e \in \mathbb{R}^4 | \zeta_e^{\mathrm{T}} P_e \zeta_e \leq \left(\frac{\bar{u} - \bar{C}\bar{\dot{q}} - \bar{g} - \bar{B}\bar{\ddot{p}}}{\bar{B}\,\|K_e\|} \right)^2 \lambda_{\min}(P_e) \right\}.$$

From (3.47)-(3.48), we have $\left(\frac{\bar{u} - \bar{C}\bar{\dot{q}} - \bar{g} - \bar{B}\bar{\ddot{p}}}{\bar{B}\|K_e\|} \right)^2 \lambda_{\min}(P_e) = 2.4^2 \times 0.732 = 4.21$.
Together with (3.44), the overall terminal region mapping to (x, z) coordinates is given by

$$\Xi_f = \{(x, z) \in \mathbb{R}^6 | \zeta_e^{\mathrm{T}} P_e \zeta_e \leq 4.21, z \in \mathcal{Z}_f\} \subset \mathcal{X} \times \mathcal{Z}, \tag{3.50}$$

where $\zeta_e = \begin{bmatrix} x_1 - p(z_1) \\ x_2 - \frac{\partial p}{\partial z_1} z_2 \end{bmatrix}$.

Finally, we show that with the choice of (3.50), and the terminal control law (3.42) and (3.46), the stability condition (3.33) of Theorem 2 is satisfied, even with terminal cost function $V_f(\zeta) = 0$.

Along the closed-loop solution in the terminal region Ξ_f under the control laws (3.42) and (3.46), we have the following bounds

$$\|\zeta_z\| = \left\|(z_1, z_2)^{\mathrm{T}}\right\| \leq \alpha_z e^{-\beta_z t}, \quad \|v_f\| \leq \|K_z\|\,\alpha_z e^{-\beta_z t} \tag{3.51}$$

$$\|\zeta_e\| = \left\|(e^{\mathrm{T}}, \dot{e}^{\mathrm{T}})^{\mathrm{T}}\right\| \leq \alpha_e e^{-\beta_e t} \tag{3.52}$$

$$\|u_f - \tilde{u}\| \leq \alpha_u e^{-\beta_u t}, \tag{3.53}$$

where α_z, α_e, α_u, β_z, β_e and β_u are all positive scalers. For the linearized augmented system (3.38), it is easy to see that the closed-loop system controlled by (3.42) and (3.46), is exponentially stable. Thus, (3.51) and (3.52) can be obtained directly. The explanation of upper bound for $\|u_f - \tilde{u}\|$ is more complicated. From (3.46), we have

$$\|u_f - \tilde{u}\| \leq \|C(x_1, x_2)x_2\| + \|B(x_1)(-K_e\zeta_e + \ddot{p}(z_1))\| + \|g(x_1) - g(p(0))\|.$$

The main idea is to find the exponential bounds of each term using the exponential bounds of x_1, x_2 and $\ddot{p}(z_1)$. For the detailed derivation of (3.53), we refer to [58].

From (3.40), (3.51)-(3.53) and $\beta z_1 z_2^2 \leq 0$, we can directly obtain the upper bound of $\ell(\zeta, \omega)$ (3.39) on Ξ_f along the closed-loop trajectories under control laws (3.42) and

(3.46)

$$\ell(\zeta(t),\omega(t)) - \ell(\zeta_s,\omega_s) \leq \alpha_\ell e^{-\beta_\ell t}, \quad a_\ell \geq 0, \quad \beta_\ell \geq 0. \tag{3.54}$$

Then, with a choice of a purely time dependent terminal cost $V_f(t) = \frac{\alpha_\ell}{\beta_\ell} e^{-\beta_\ell t}$, the stability condition (3.33) of Theorem 2 is satisfied. Such a terminal cost function is not influenced by the inputs computed by the OCPs (3.18), hence can be dropped during the optimization. This implies that $V_f(\zeta) = 0$ is an appropriate choice. Compared to the similar example in [58], we do not require that $\ell(\zeta,\omega)$ is positive definite with respect to (ζ_s,ω_s) and the economic performance can be enhanced while the convergence to the optimal steady state on the reference path is guaranteed.

Remark 5. *It is worth noting that* (3.54) *is satisfied no matter how large the value of* β *is. However, the value of* β *is actually restricted, since it influences the optimal steady state and the dissipativity property. In other words, as long as* (3.40) *is satisfied and a storage function can be found to examine the dissipativity, the terminal region* (3.50) *and the terminal cost* $V_f(\zeta) = 0$ *can be employed to ensure the asymptotic convergence of the closed-loop system.*

Remark 6. *If we consider the energy consumption of the manipulator as the economic performance, the economic term could be* $\beta||u||^2$*, then the overall economic stage cost becomes*

$$\ell(e,\xi,\omega) = ||(e,\dot{e},z_1,z_2)||_Q^2 + ||(u-\tilde{u},v)||_R^2 + \beta||u||^2, \quad \beta > 0.$$

In this case, even the absolute value of β *is very small, the optimal steady state* (ζ_s,ω_s) *is no longer at the origin of the augmented error system* (3.21)*. However, we can still examine the dissipativity property by constructing a rotated stage cost in the form of* (3.29)*, lower bounded by a class* κ *function* $\beta_\zeta(||\zeta-\zeta_s||)$*. Following along the lines of the aforementioned discussion, we can design the corresponding terminal region and the terminal cost to guarantee the stability and feasibility of the proposed EMPFC.*

Simulation results

We firstly give simulation results without consideration of economic performance, i.e., we set $\beta = 0$ in (3.39). Figure 3.3 shows the system evolution with initial condition $x(0) = [-6.35, -3.09, 0, 0]^{\mathrm{T}}$. Specifically, Figure 3.3(a) shows the evolution

of joint positions $x_1(t)$ and the reference positions $p(z_1(t))$. Figure 3.3(b) illustrates the evolution of joint velocities $x_2(t)$ and the reference velocities $\frac{\partial p}{\partial z_1}(t)z_2(t)$. We can see the joint positions and velocities achieve fast convergence to their reference, respectively. Figure 3.3(c) records the evolution of input $u(t)$. As expected, they are all within the corresponding ranges of permitted values ($||u||_\infty \leq 4000$). Figure 3.3(d) shows the evolution of virtual state $z_1(t)$, $z_2(t)$ and the virtual input $v(t)$. It can be observed that the path evolution variable $z_1(t)$ converges to the optimal position $\theta_s = 0$ and the speed $z_2(t) \geq 0$ for all $t \geq 0$.

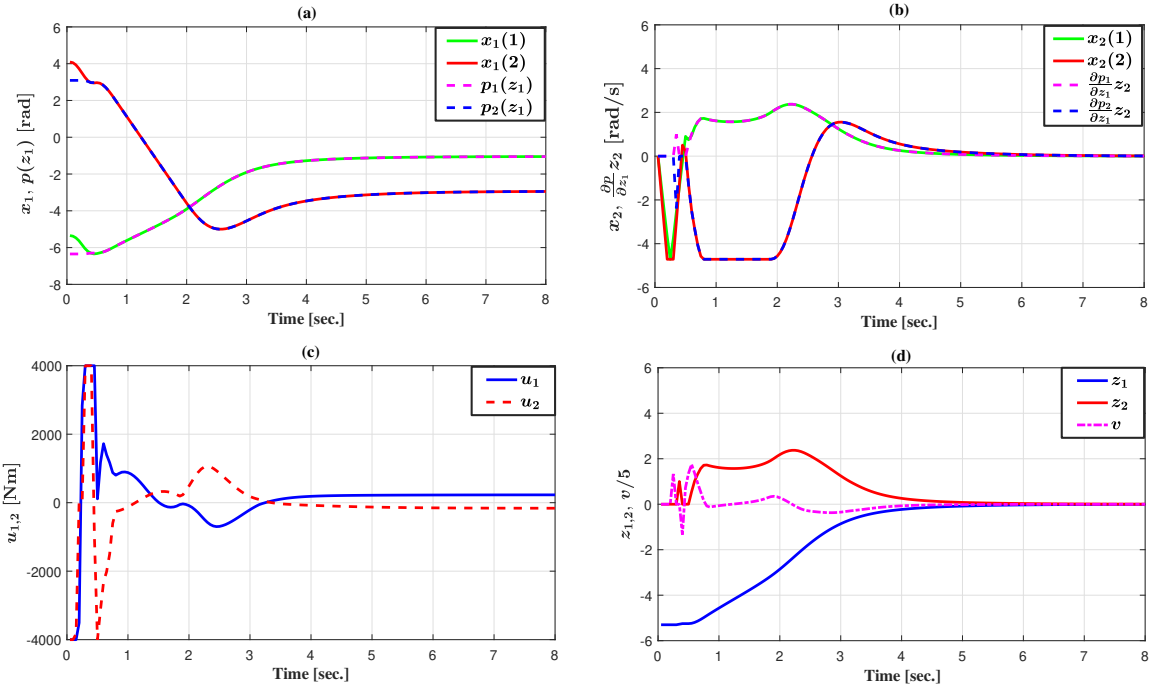

Figure 3.3: Closed-loop system evolution ($\beta = 0$).

The simulation results with economic consideration ($\beta = 3$) are shown in Figure 3.4 in a similar fashion. The initial condition is $x(0) = [-6.35, -3.09, 0, 0]^{\mathrm{T}}$. From Figure 3.3(a) and Figure 3.3(b), we can see that the joint positions and velocities can also converge to their reference in a short time, respectively. Compared to the results with $\beta = 0$, the forward speed on the reference path is much larger and it takes 43.6% less time for the system to arrive at its optimal steady state along the reference path (in Figure 3.3(d) the reaching time is around 5.5s, while in Figure 3.4(d) it is around 3.1s).

Figure 3.5 and Figure 3.6 illustrate the path-following results with different initial conditions in output space and in cartesian coordinates (defined by (3.35)), re-

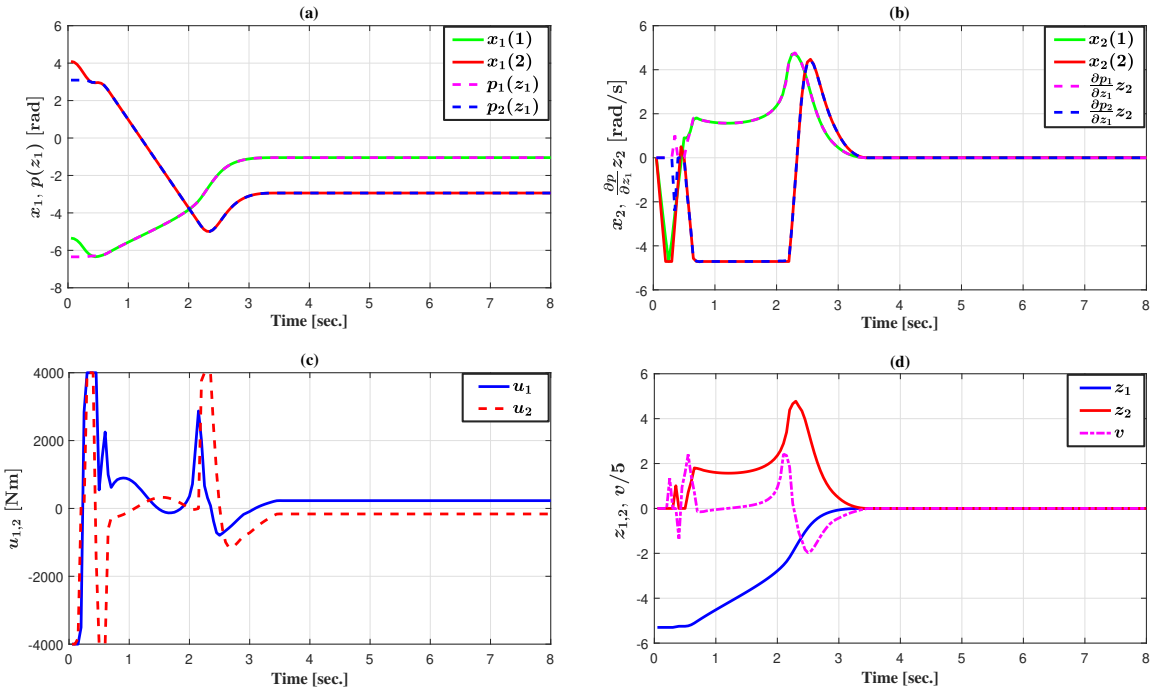

Figure 3.4: Closed-loop system evolution ($\beta = 3$).

spectively. It can be observed that all the closed-loop trajectories converge to their reference paths and finally reach the optimal steady state.

This illustrating example of the fully actuated robot suggests that the design of a suitable economic stage cost function plays a key role in guaranteeing the stability of EMPFC. First of all, the optimal steady state with respect to this cost function should be in form of (3.26). Furthermore, this cost function should be chosen such that the strict dissipativity assumption (3.27) is satisfied. Finally, the conditions of Theorem 2 can be used to design the corresponding terminal region and terminal cost. If all these conditions are satisfied, the closed-loop system under EMPFC is asymptotically convergent to the optimal operation on the reference path, while the economic performance is enhanced.

3.3 Conclusion

In this chapter, we study the constrained output path-following problem from an EMPC perspective. To begin with, a sampled-data EMPC framework for set-point stabilization problems is studied. An extended definition of dissipativity is introduced for continuous-time systems, followed by giving sufficient stability conditions. Then,

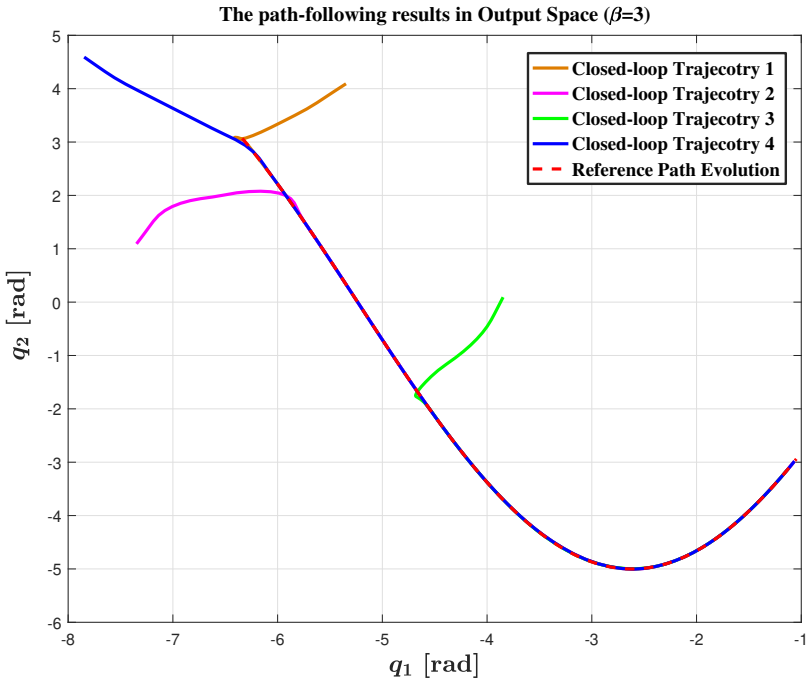

Figure 3.5: The path-following results with different initial positions (in output space, $\beta = 3$).

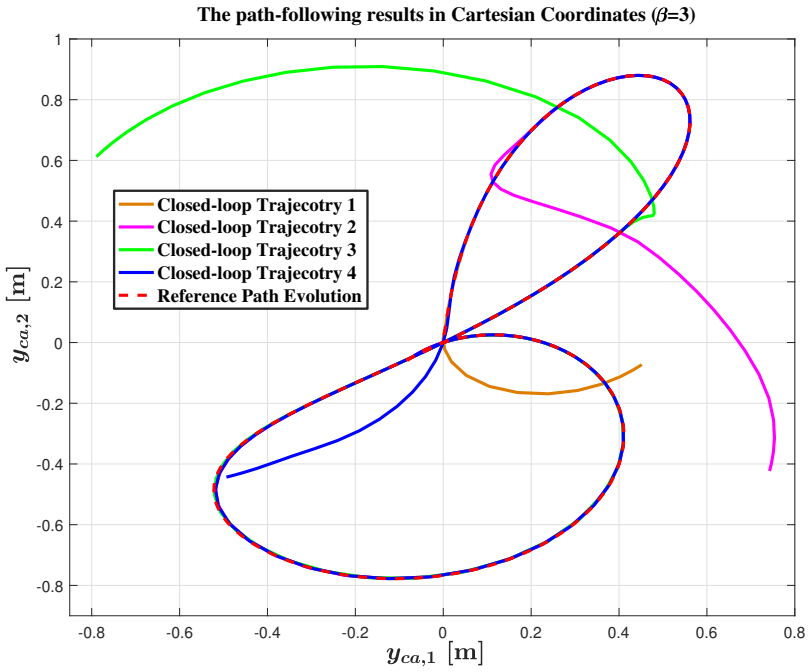

Figure 3.6: The path-following results with different initial positions (in cartesian coordinates, $\beta = 3$).

we propose the EMPFC scheme for output path-following problems. In order to enhance the economic performance with guaranteed convergence to an output reference path, we define an optimal steady state set which actually achieves a relaxation of the optimal operation. New dissipativity assumption is defined for output path-following problems. Sufficient conditions that guarantee the convergence of the system to the optimal operation on the reference path are derived. Finally, an example of a 2-DoF robot shows that, the proposed EMPFC scheme achieves better economic performance while the system can follow along the reference path in forward direction and finally converges to its optimal steady state.

Chapter 4

Economic Model Predictive Path-following Control for Power Kites

4.1 Introduction

4.1.1 Research Background and Contributions

Exploiting high altitude wind energy using power kites is an emerging topic in the field of renewable energy [3]. The claimed advantages of power kites over traditional wind power technologies are the lower construction costs, less land occupation and more importantly, the possibility of efficiently harvesting wind energy at high altitudes, where more dense and steady wind power exists [60, 61].

As discussed in Chapter 2, a challenging issue for power kites to really foster its industrial development is the controller design due to the fast and highly nonlinear dynamics. Model predictive control (MPC) has been successfully implemented for controlling power kites because it can optimize system performance and well respect system constraints. In [32–34], standard (tracking) MPC is employed for kites to track a time-dependent reference path. However, trajectory tracking may not be appropriate for kite control due to varying wind speed and limited controllability of the kite speed. In [8, 9, 35], economic model predictive control (EMPC) has also been employed for kite controller design. These EMPC schemes are designed by using pure economic cost functions associated with the generated power. Compared to [32–34], these EMPCs adapt to a wider range of wind speed and intuitively result in better

economic performance since the closed-loop trajectories are not limited to be periodic. However, in these EMPC schemes, there is no closed-form expression of the reference path. Therefore, the shape of closed-loop trajectories can not be adjusted directly and it is difficult to analyze the stability.

As a novel contribution, in this chapter, we tackle output path-following problems for kites from an EMPC perspective. The unknown wind conditions, limited controllability of the kite speed, and the objective of maximizing generated power motivate us to employ the EMPFC scheme. In order to enhance economic performance under unknown wind conditions, additional degrees of freedom are added to the predefined optimal operation. In other words, the reference path is relaxed in an output space and its speed assignment is not known a priori. We show the effectiveness of the proposed control scheme in two aspects. For a static reference path, the economic performance is enhanced while the kite is stabilized in the neighborhood of the reference path. For a dynamic reference path, the economic performance can be further improved since parameters for the reference path are treated as additional optimization variables. Therefore, an integration of path optimization and path-following is accomplished.

The closed-loop stability of EMPFC has been studied in Chapter 3 using assumptions of dissipativity and the existence of a local controller ensuring that the augmented cost function is always decreasing along the corresponding closed-loop trajectory. However, for the underactuated kite system, it is generally very hard to find an appropriate economic cost satisfying these conditions. In fact, rigorous asymptotic stability is not necessarily required for this application of kite control. Alternatively, we use terminal constraints to ensure that the system economically converges to the neighborhood of the output reference path. Inspired by [62], an economic cost with a logistic cost function is adopted to achieve a trade-off between the economic performance and the convergent performance. The economic performance enhancement by using the newly proposed economic cost function is reported in simulation results, for both cases (static and dynamic reference path). The robustness of the proposed control scheme is shown in the simulation results under considerable wind turbulence.

4.2 Chapter Organization

The remaining part of this chapter is organized as follows. In Section 4.2, the proposed EMPFC scheme is applied to solve the output path-following problem for power kites using a static reference path. Simulation results are given to show the economic performance enhancement and the robustness of the EMPFC method. In Section 4.2, we extend the EMPFC scheme to the case of using a dynamic reference path. Finally, Section 4.4 gives conclusion of this chapter.

4.3 EMPFC with a Static Reference Path

4.3.1 Augmented Kite System

In Chapter 2, we obtain the kite model (during the traction phase) as follows:

$$\begin{aligned}\dot{x}(t) = &\begin{bmatrix} \dot{\theta} \\ \dot{\phi} \\ \dot{r} \\ \frac{\vec{F}_{\{L\}\theta}}{rm} - \dot{\phi}^2\sin(\theta)\cos(\theta) - 2\frac{\dot{r}}{r}\dot{\theta} \\ \frac{\vec{F}_{\{L\}\phi}}{rm\cos(\theta)} + 2\dot{\theta}\dot{\phi}\tan(\theta) - 2\frac{\dot{r}}{r}\dot{\phi} \\ -\frac{\vec{F}_{\{L\}r}}{m} + r\dot{\theta}^2 + r\dot{\phi}^2\cos^2(\theta) \end{bmatrix} \\ =&f(x(t), u(t), \vec{v}_w(t), \dot{r}_{ref}(t)),\end{aligned} \tag{4.1}$$

where $x = [\theta, \phi, r, \dot{\theta}, \dot{\phi}, \dot{r}]^{\mathrm{T}}$ is the state vector, $u = \psi$ is the control input, $\vec{v}_w$ is the absolute wind speed vector at the kite's position and $\dot{r}_{ref}$ is the reference reeling out speed of cables. We assume the state constraints to be $\mathcal{X} \subseteq \mathbb{R}^6$ and the input signal is a piecewise continuous and right continuous function with values in the compact set $\mathcal{U} \subset \mathbb{R}$, i.e., input signal $u(\cdot) \in \mathcal{PC}(\mathcal{U})$.

For simplicity, we assume a constant $\dot{r}_{ref}$ during the kite's traction and $\vec{v}_w$ is a function of the altitude of the kite, i.e., $\vec{v}_w(t) = \vec{v}_w(r(t)\sin\theta(t))$. Then, the kite model can be expressed by

$$\dot{x}(t) = \tilde{f}(x(t), u(t)). \tag{4.2}$$

The output of the kite system is simply defined in (θ, ϕ) space, i.e.,

$$h(x) = \begin{bmatrix} \theta \\ \phi \end{bmatrix}. \tag{4.3}$$

First of all, we obtain an admissible reference path in the output space. Note that this reference path might not be optimal with respect to the generated power, but it is an admissible figure-eight path with high wind power generation. Then we use a lemniscate curve to approximate this reference path since a reference path with closed-form expression is required to formulate the path-following problem.

The static reference path can be described as follows:

$$\mathcal{P} = \{\bar{p} \in \mathbb{R}^{n_y} | \bar{p} = p(z), z \in [z_0, +\infty)\}, \tag{4.4}$$

where z is the path evolution vector, the function $p : \mathbb{R} \to \mathbb{R}^{n_y}$ is continuously differentiable, and $n_y = 2$ is the dimension of the output space of the system (4.1). The time evolution of $z(t)$ is not known a priori, hence the forward speed on the reference path is an additional degree of freedom.

Here, we assume an admissible reference path $\mathcal{P}$. Firstly, it satisfies assumption 10 in Section 3.2.3, i.e., the reference path in (4.4) is contained in the interior of the state constraints $\mathcal{X}$ under output mapping $h : \mathbb{R}^6 \to \mathbb{R}^2$, that is $\mathcal{P} \subseteq int(h(\mathcal{X}))$. In addition, the curvature of reference path $\mathcal{P}$ is limited such that it can be followed respecting the input constraints under the given wind condition.

The virtual dynamics of the path evolution variable is described by a single integrator

$$\dot{z} = v, \tag{4.5}$$

where v is the virtual input to control the forward speed.

Combining equation (4.2)-(4.5), we obtain the augmented kite system:

$$\begin{aligned} \dot{\xi} &= \begin{bmatrix} \dot{x} \\ \dot{z} \end{bmatrix} = \begin{bmatrix} \tilde{f}(x, u) \\ v \end{bmatrix} = f_\xi(\xi, \omega) \\ e &= h(x) - p(z) = \tilde{h}(\xi), \end{aligned} \tag{4.6}$$

where $\xi = [\theta, \phi, r, \dot{\theta}, \dot{\phi}, \dot{r}, z]^{\mathrm{T}}$ is the augmented state vector, $\omega = [\psi, v]^{\mathrm{T}}$ is the input for

the augmented system, and $\tilde{h} : \mathbb{R}^7 \to \mathbb{R}^2$. The output error $e \in \mathbb{R}^2$ can be interpreted as the output of the augmented system.

The state constraint for the augmented system is given by $\xi \in \Xi = \mathcal{X} \times [z_0, +\infty)$. Then the output constraint can be defined by $\mathcal{E} := \{\tilde{h}(\xi) | \xi \in \Xi\}$. In order to ensure the forward motion along $\mathcal{P}$, the input ω is additionally confined such that $\omega(\cdot) \in \mathcal{PC}(\Omega)$, where $\Omega = \mathcal{U} \times [0, +\infty)$.

4.3.2 The EMPFC Formulation

The employed EMPFC scheme is based on what we proposed in section 3.2.2. The cost function to be minimized at each sampling time is

$$J(\xi(t_k), \overline{e}(\cdot), \overline{\xi}(\cdot)) = \int_{t_k}^{t_k+T_p} \ell(\overline{e}(\tau), \overline{\xi}(\tau)) d\tau + V_f(\overline{e}(t_k + T_p)), \tag{4.7}$$

where $\ell : \mathcal{E} \times \Xi \to \mathbb{R}$ is a general economic cost; $V_f : \mathcal{E}_f \to \mathbb{R}$ is the terminal cost and $\mathcal{E}_f \subset \mathcal{E}$ is the terminal region; $\overline{e}$ and $\overline{\xi}$ indicate the predicted values which are not necessarily same as the system real evolutions; $T_p = N \cdot \delta$ is the prediction horizon. In order to account for the economic performance in state space, the augmented state vector ξ is considered in the economic stage cost $\ell(\cdot, \cdot)$.

Consider a constant sampling period δ, at each sampling time $t_k = t_0 + k \cdot \delta$, $k \in \mathbb{N}$, the following OCP is solved repeatedly

$$\begin{aligned}
\min_{\overline{\omega}(\cdot) \in \mathcal{PC}(\Omega)} \quad & J(\xi(t_k), \overline{e}(\cdot), \overline{\xi}(\cdot)) && \text{(4.8a)} \\
s.t. \quad & \dot{\overline{\xi}}(\tau) = f_\xi(\overline{\xi}(\tau), \overline{\omega}(\tau)), \quad \overline{\xi}(t_k) = \xi(t_k) && \text{(4.8b)} \\
& \overline{e}(\tau) = \tilde{h}(\overline{\xi}(\tau)) && \text{(4.8c)} \\
& \overline{\xi}(\tau) \in \Xi && \text{(4.8d)} \\
& \overline{\omega}(\tau) \in \Omega && \text{(4.8e)} \\
& \overline{e}(t_k + T_p) \in \mathcal{E}_f \subset \mathcal{E}. && \text{(4.8f)}
\end{aligned}$$

At each sampling time t_k, we do the prediction of the system behavior over the horizon $[t_k, t_k + T_p]$ and the optimal solution of the optimization problem (4.8) is denoted by $\bar{\omega}^*(\cdot, \xi(t_k))$ over the time span $[t_k, t_k + T_p]$. Then, only the first sampling period of the optimal input profile $\bar{\omega}^*(\cdot, \xi(t_k))$ is applied to the augmented system

(4.6), i.e., the closed-loop control signal $\omega^*(\cdot)$ is

$$\omega^*(t) = \overline{\omega}^*(t, \xi(t_k)), \quad t \in [t_k, t_k + \delta], \tag{4.9}$$

where $\bar{\omega}^*(\cdot, \xi(t_k))$ over the time span $(t_k + \delta, t_k + T_p]$ is discarded. At next sampling time t_{k+1}, the new states vector is available and this procedure is repeated.

At the first sampling time t_0, the initial condition for the virtual dynamics can be obtained by

$$\overline{z}(t_0) = \underset{z \in [z_0, +\infty]}{\arg\min} ||h(x(t_0)) - p(z)|| \tag{4.10}$$

At the following sampling time $t_k = t_0 + k \cdot \delta$, $k \in \mathbb{Z}^+$, the initial state for the virtual dynamics $z(t_k)$ is exactly the predicted value at time t_k from the last open loop OCP, since there is no model mismatch or disturbance in the virtual system (4.5).

Unlike the standard MPC, the stage cost function in (4.7) is a general economic cost, i.e., $\ell(\cdot, \cdot)$ is not necessary to be positive definite with respect to the output error e. This function should be appropriately chosen so that the trade-off between the economic performance and the stability can be accomplished.

4.3.3 Economic Cost with a Logistic Function

We give a candidate economic cost with a logistic function to assign appropriate weights to two objectives, i.e., the path convergence and the economic performance. The economic performance is chosen as the generated power in the form of

$$h_g(\xi) = -F_{trac}(x, v_w, \dot{r}_{ref})\dot{r}. \tag{4.11}$$

Here, F_{trac} from (2.13) is the traction force on cables to compensate other forces and regulate the reeling out speed $\dot{r}$ to the desired value $\dot{r}_{ref}$. We add the minus sign in order to maximize the term $F_{trac} \cdot \dot{r}$ by solving the minimization problem.

Then, the economic stage cost function in (4.7) is given by

$$\ell(e, \xi) = \alpha(\epsilon)||e||_Q^2 + (1 - \alpha(\epsilon))\eta h_g(\xi), \tag{4.12}$$

where $Q > 0$ is the weighting matrix, $\alpha(\cdot)$ is the designed function to assign weights to

two objectives, and $\eta \geq 0$ is a tunning term to make two objectives have comparable values. Note that we do not consider the input ω in (4.12), because it is hard to predefine the reference input along output reference path $\mathcal{P}$. Here, $\alpha(\cdot)$ is obtained according to the logistic function

$$\alpha(\epsilon) = \frac{1}{1 + \exp(-\beta\epsilon)}, \tag{4.13}$$

where $\epsilon = ||e||_Q^2$ and $\beta \geq 0$ is the tuning parameter to control the change rate of the function. Note that the logistic function (4.13) is smooth and monotonic, and $\alpha(\epsilon) \in [0.5, 1)$ for $\forall \epsilon \geq 0$. Since the objective is to enhance the economic performance in the neighborhood of reference path, i.e., the path convergence is a prior objective, it turns out that (4.13) is an appropriate choice.

Choosing an appropriate economic cost accomplishing the trade-off between the economic performance and the convergent performance, is generally not an easy task. It is worth noting that if the system and the economic cost are satisfied with the dissipative property [44] and the convergence conditions in Theorem 2, both transient performance and zero-error performance with respect to the economic criteria can be improved with guaranteed stability. However, both the assumption of dissipativity and the convergence conditions are hard to be verified due to the high nonlinearity and underactuation of the kite system. Here, we give a heuristic economic cost (4.12) aiming to improve the performance when the system is stabilized in the neighborhood of the reference path, and show the economic performance enhancement in the simulation results.

4.3.4 Simulation Results

In this section, we present simulation results of the kite to follow a static reference path using EMPFC. The numerical implementation of our continuous EMPFC scheme is based on sampled-data manner. The OCP (4.8) in the sampled-data setting is solved by using the sequential quadratic programming algorithm [63] of Matlab function *fmincon*.

Parameter Selection

1. Model Parameters
   $m = 50$ [kg], $A = 100$ [m^2], $d_c = 0.025$ [m], $\rho_c = 970$ [kg/m^3], $\rho = 1.2$ [kg/m^3],

$g = 9.8$ [N/kg], $C_L = 1.2$, $C_D = 0.15$, $C_{D,c} = 1$, $\dot{r}_{ref} = 2$ [m/s], the local controller gain $K = -3.33$.
Nominal wind shear model along x axis: $v_x = (0.015(r\sin(\theta) - 100) + 12)$ [m/s].
State constraints: $\theta \in [0.03\pi, 0.5\pi)$, $\phi \in (-0.5\pi, 0.5\pi)$.
Input constraints: $\Omega = \{(u, v)|u \in [-0.07, 0.07], v \in [0, 1.6\pi]\}$.

2. Reference Path
The static reference path $\mathcal{P}$ (4.4) is defined by

$$p(z) = \begin{pmatrix} \arcsin\left(\frac{a_1 \sin(2z)}{R}\right) + \theta_a \\ \arcsin\left(\frac{a_2 \cos(z)}{R}\right) \end{pmatrix}, \tag{4.14}$$

where θ_a is the average θ angle of the reference path, a_1, a_2 and R affect the shape and size of the figure-eight reference path. $\theta_a = 0.45$ [rad], $a_1 = 15$, $a_2 = 21$ and $R = 500$.

3. EMPFC setup
$\delta = 0.1$[sec], N=10, $Q = \text{diag}([2, 1])$, $\eta = 10^{-7}$.
The terminal penalty $V_f(e) = ||e||^2_{Q_f}$, where $Q_f = \text{diag}([0.2, 0.1])$.
The terminal constraint $\mathcal{E}_f = \{e|e^T P e \leq 0.01\}$, where $P = \text{diag}([1, 1])$.
Initial state $\xi_0 = [0.2\pi; 0; 500; -0.08; -0.08; 0; 0.5\pi]^{\mathrm{T}}$.

EMPFC with a Static Reference Path

For a static reference path, we give the kite path-following results with different β values. We find that the closed-loop trajectories converge to the reference path with a large value of β ($\beta \geq 400$). When $\beta \leq 400$, the kite can still be stabilized in the neighborhood of the reference path and the economic performance is improved.

Figure 4.1 shows the closed-loop trajectory with $\beta = 400$. As seen, the closed-loop trajectory converges to the reference path successfully with a large initial error. Figure 4.2 records the closed-loop system evolution with $\beta = 400$. Specifically, Figure 4.2(a) records the path-following error; Figure 4.2(b) and Figure 4.2(c) show the evolution for control inputs. As expected, they are all within the corresponding ranges of permitted values (Input constraints: $\Omega = \{(u, v)|u \in [-0.07, 0.07], v \in [0, 1.6\pi]\}$). Figure 4.2(d) records the generated power [kW].

Figure 4.3 shows the closed-loop trajectories with different β values. It can be observed that when the kite is far away from the reference path, these trajectories

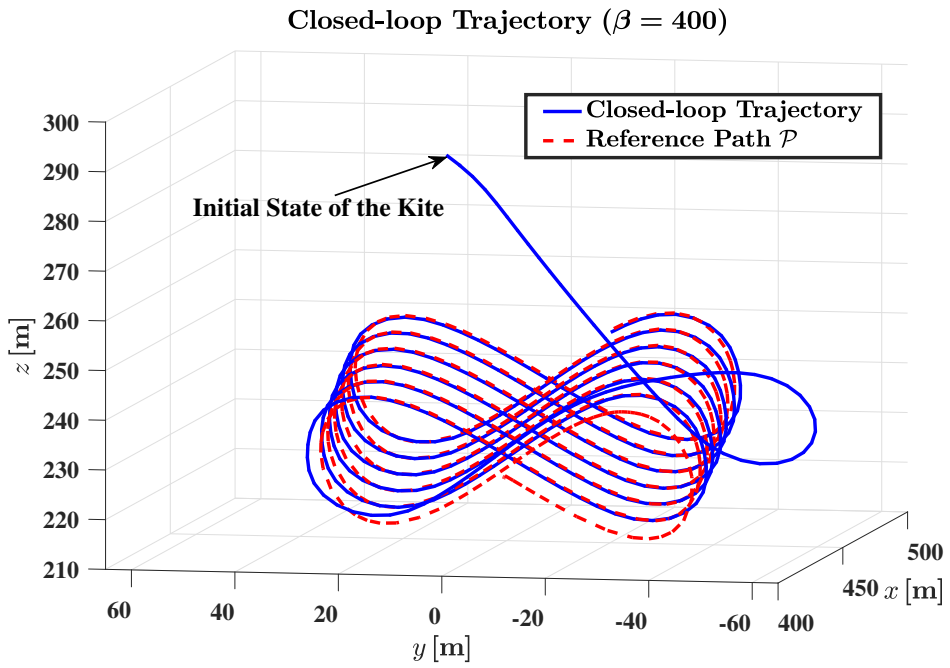

Figure 4.1: Comparison between the closed-loop trajectory ($\beta = 400$, solid) and the static reference path $\mathcal{P}$ (dashed).

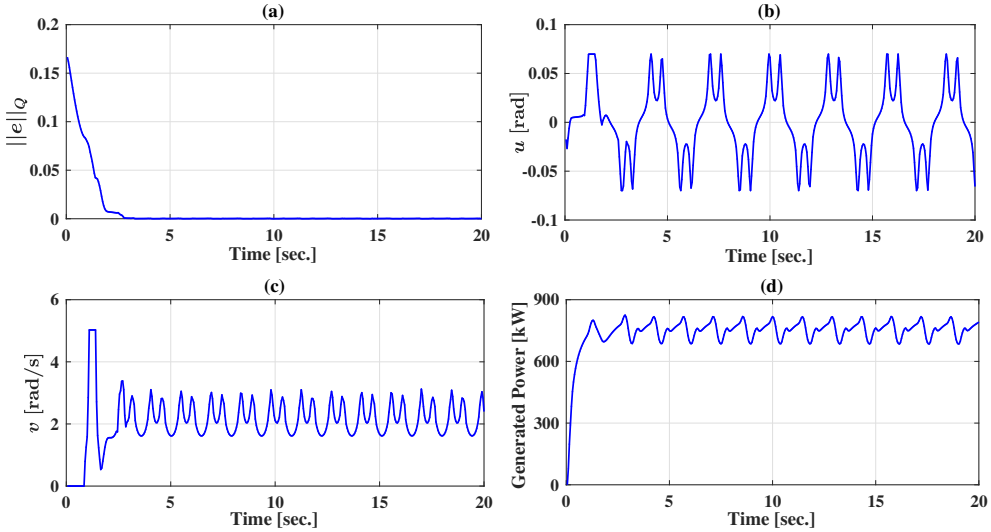

Figure 4.2: Closed-loop system evolution ($\beta = 400$).

with different β values are almost same. This is because when the output error $||e||_Q^2$ is large, the economic cost (4.12) is dominated by the output error. Hence, all of these trajectories have fast convergence rate to the reference path which is a desirable property. When the kite reaches the neighborhood of the reference path, the

closed-loop behaviors start to be different since (4.12) is dominated by the economic performance in this case. In other words, the main control objective is switched to enhance the economic performance when the system is operated near the reference path.

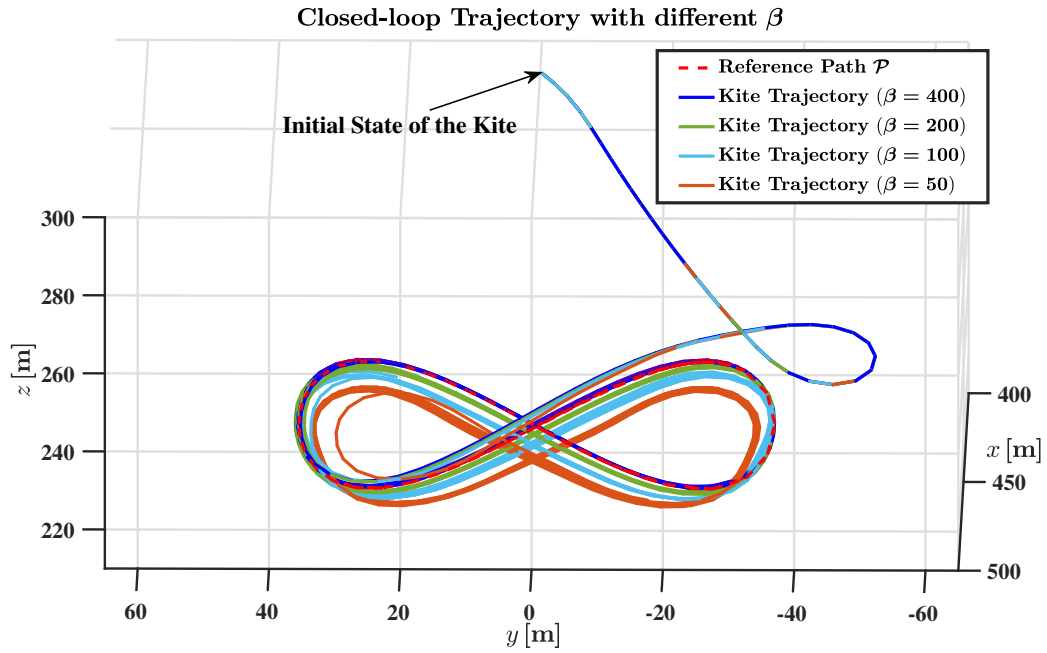

Figure 4.3: Closed-loop trajectory with different β values.

Table 4.1 shows the average error $||e||_Q$ and the average generated power $|h_g(\xi)|$ for the closed-loop trajectories with different β values. As we can see, as the value of β decreases, the convergence performance gets worse but the economic performance is enhanced. Hence, β plays an important role in guaranteeing convergence. In fact, if the value of β is infinitely large, the economic cost (4.12) becomes positive definite and the assumption of dissipativity is satisfied. To some extent, this explains that the closed trajectory converges to the reference path with a large value of β, as shown in Figure 4.3.

Robustness Test

For real implementation of power kite systems, wind turbulence should be taken into consideration. In this section, we present the simulation results with considerable wind turbulence, with maximum absolute value 4.5 m/s, 33% of the nominal wind speed at the altitude of 200 m. Sinusoidal wind turbulence $\vec{v}_{t,x}$ and $\vec{v}_{t,y}$ are introduced

Table 4.1:
Mean value of path-following error $||e||_Q$
and generated power $|h_g(\xi)|$ with different β values.

β	Mean value of $||e||_Q$	Mean value of $|h_g(\xi)|$
400	1.55×10^{-4}	745 [kW]
200	2.64×10^{-3}	750 [kW]
100	6.25×10^{-3}	758 [kW]
50	1.12×10^{-2}	768 [kW]

along x and y axes, respectively:

$$\begin{aligned} \vec{v}_{t,x} &= 2\sin(\omega_0 t) \quad [\text{m/s}] \\ \vec{v}_{t,y} &= 4\cos(\omega_0 t) \quad [\text{m/s}], \end{aligned} \tag{4.15}$$

where $\omega_0 = 0.2\pi$ [rad/s]. In order to obtain a better convergent performance, we choose a conservative value of β, $\beta = 400$.

Figure 4.4 illustrates the closed-loop trajectory under the wind turbulence (4.15) with $\beta = 400$. Figure 4.5 records the corresponding closed-loop system evolutions. Specifically, Figure 4.5(a) records the path-following error; Figure 4.5(b) and Figure 4.5(c) show the evolution for control inputs. Figure 4.5(d) records the generated power [kW]. From Figure 4.4 and Figure 4.5(a), it can be observed that the closed-loop trajectory still achieves good convergent performance with respect to the reference path, even under a considerable wind turbulence.

4.4 EMPFC with a Dynamic Reference Path

The static reference path $\mathcal{P}$ may not be optimal with respect to the economic performance under the varying wind condition. Hence, it is possible to further enhance the economic performance using a dynamic reference path $\mathcal{P}_\mu$. In this section, we propose EMPFC for path-following control of kites using a dynamic reference path. A new augmented system is constructed and the path parameter μ is treated as the additional optimization variable.

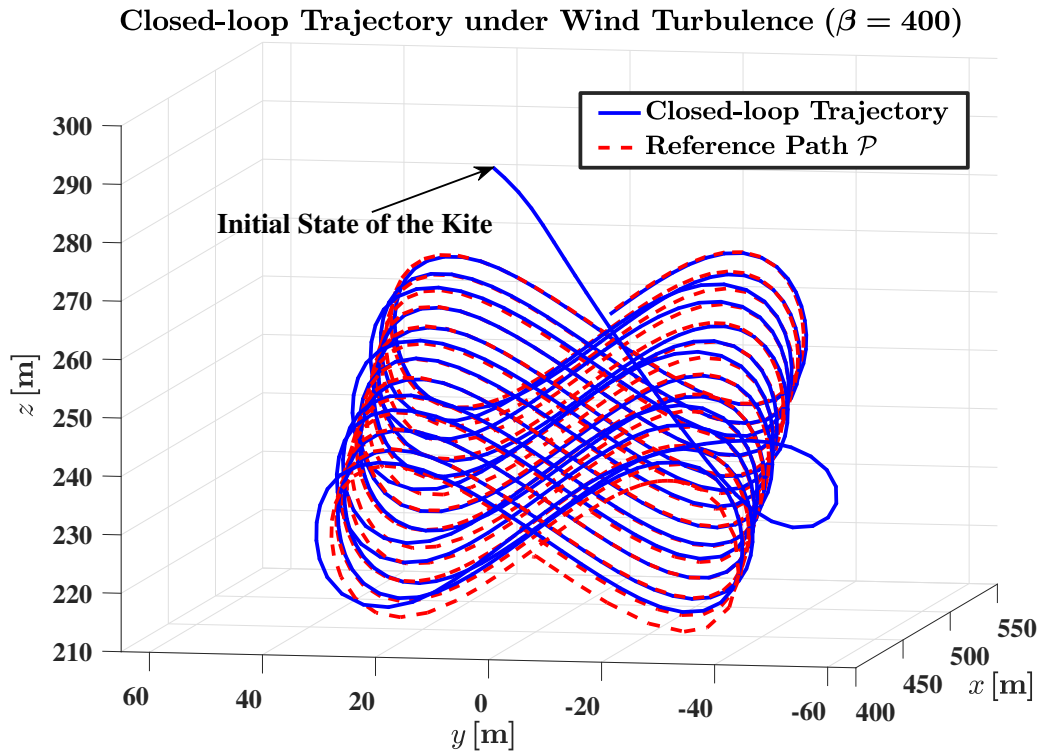

Figure 4.4: The closed-loop trajectory under wind turbulence ($\beta = 400$, solid) and the static reference path $\mathcal{P}$ (dashed).

4.4.1 Augmented Kite System with Dynamic Reference Path

By adding additional variable μ to the static reference path (3.14), the dynamic reference path is defined by

$$\mathcal{P}_\mu = \{\bar{p}_\mu \in \mathbb{R}^{n_y} | \bar{p}_\mu = p_\mu(z, \mu), z \in [z_0, +\infty), \mu \in \mathcal{M}\}, \tag{4.16}$$

where $\mu \in \mathcal{M}$ is a path parameter vector associated with the closed-form of the reference path, influencing its shape, size, average position, etc; the constraint $\mathcal{M} \subseteq \mathbb{R}^{n_\mu}$ is a compact set; the function $p_\mu : \mathbb{R}^{n_\mu+1} \to \mathbb{R}^{n_y}$ is continuously differentiable. Generally, the path parameter vector μ affects the economic performance when the system follows along $\mathcal{P}_\mu$.

Then, the output error e_μ for the dynamic reference path is further defined as

$$e_\mu(t) = h(x(t)) - p_\mu(z(t), \mu(t)). \tag{4.17}$$

Combining (4.2), (4.3), (4.5), (4.17) and the virtual dynamics of the path pa-

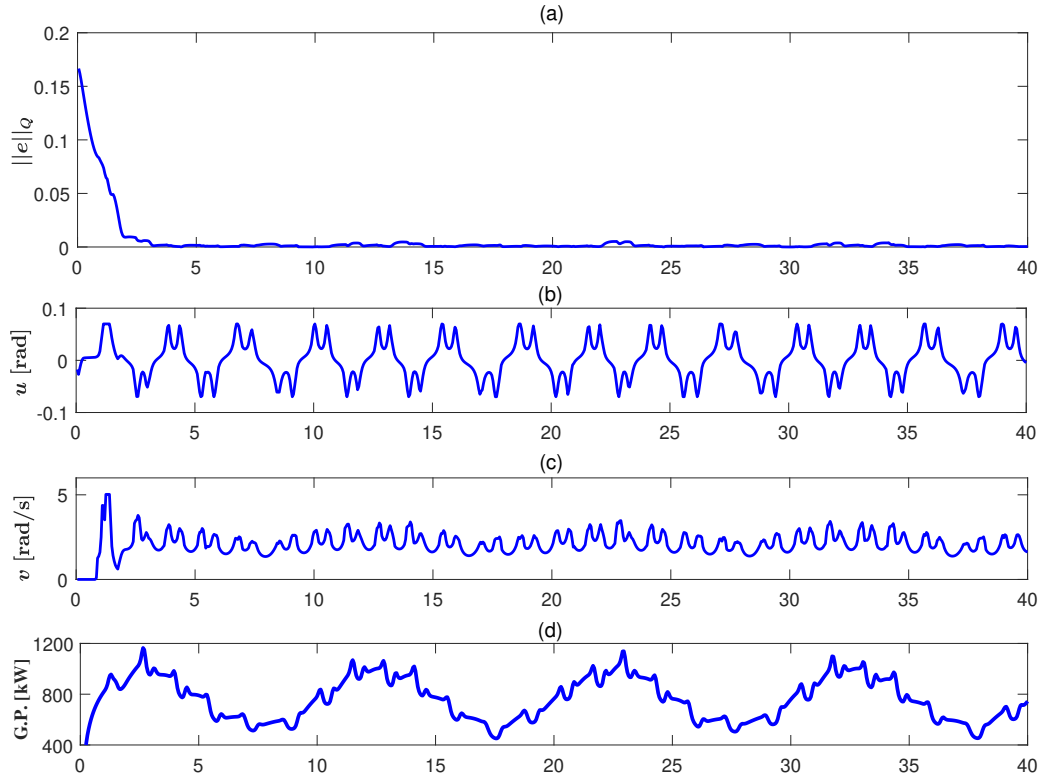

Figure 4.5: Closed-loop system evolutions under wind turbulence ($\beta = 400$).

rameter vector, the augmented kite system with a dynamic reference path is defined by

$$\begin{aligned} \dot{\xi}_\mu &= \begin{bmatrix} \dot{x} \\ \dot{z} \\ \dot{\mu} \end{bmatrix} = \begin{bmatrix} \tilde{f}(x,u) \\ v \\ v_\mu \end{bmatrix} = f_{\xi_\mu}(\xi_\mu, \omega_\mu) \\ e_\mu &= h(x) - p_\mu(z,\mu) = \tilde{h}_\mu(\xi_\mu), \end{aligned} \tag{4.18}$$

where $v_\mu \in \mathcal{V}_\mu$ controls the change rate of path parameter vector μ, and $\mathcal{V}_\mu \subset \mathbb{R}^{n_\mu}$ is a compact set; $\xi_\mu = [\theta, \phi, r, \dot{\theta}, \dot{\phi}, \dot{r}, z, \mu]^{\mathrm{T}}$ is the augmented state vector; $\omega_\mu = [\psi, v, v_\mu]^{\mathrm{T}}$ is the input for the augmented system; $\tilde{h}_\mu : \mathbb{R}^{7+n_\mu} \to \mathbb{R}^2$ denotes the output mapping for the augmented system.

The state constraint for (4.18) is given by $\xi_\mu \in \Xi_\mu = \mathcal{X} \times [z_0, +\infty) \times \mathcal{M}$. Then the output constraint can be defined by $\mathcal{E}_\mu := \{\tilde{h}_\mu(\xi_\mu) | \xi_\mu \in \Xi_\mu\}$. The input ω_μ is additionally confined such that $\omega_\mu(\cdot) \in \mathcal{PC}(\Omega_\mu)$, where $\Omega_\mu = \mathcal{U} \times [0, +\infty) \times \mathcal{V}_\mu$.

Compared to (4.6), (4.18) additionally involves the dynamics of the path parame-

ter vector μ. This allows us to formulate the path-following problem using a dynamic reference path $\mathcal{P}_\mu$ and analyze the relationship between μ and the system performance.

4.4.2 The EMPFC Formulation with a Dynamic Reference Path

We use the newly constructed augmented system (4.18) to formulate the OCPs. Similarly to Section 4.2, the cost function to be minimized at each sampling time is

$$J(\xi_\mu(t_k), \overline{e}_\mu(\cdot), \overline{\xi}_\mu(\cdot)) = \int_{t_k}^{t_k+T_p} \ell(\overline{e}_\mu(\tau), \overline{\xi}_\mu(\tau))d\tau + V_f(\overline{e}_\mu(t_k+T_p)), \tag{4.19}$$

where $\ell : \mathcal{E}_\mu \times \Xi_\mu \to \mathbb{R}$ is a general economic cost, $V_f : \mathcal{E}'_f \to \mathbb{R}$ is the terminal cost, and $\mathcal{E}'_f \subset \mathcal{E}_\mu$ is the terminal region.

At each sampling time $t_k = t_0 + k \cdot \delta$, $k \in \mathbb{N}$, the following OCP is solved repeatedly

$$\begin{aligned}
\min_{\overline{\omega}_\mu(\cdot) \in \mathcal{PC}(\Omega_\mu)} \quad & J(\xi_\mu(t_k), \overline{e}_\mu(\cdot), \overline{\xi}_\mu(\cdot)) && \text{(4.20a)}\\
s.t. \quad & \dot{\overline{\xi}}_\mu(\tau) = f_{\xi_\mu}(\overline{\xi}_\mu(\tau), \overline{\omega}_\mu(\tau)), \quad \overline{\xi}_\mu(t_k) = \xi_\mu(t_k) && \text{(4.20b)}\\
& \overline{e}_\mu(\tau) = \tilde{h}_\mu(\overline{\xi}_\mu(\tau)) && \text{(4.20c)}\\
& \overline{\xi}_\mu(\tau) \in \Xi_\mu && \text{(4.20d)}\\
& \overline{\omega}_\mu(\tau) \in \Omega_\mu && \text{(4.20e)}\\
& \overline{e}_\mu(t_k+T_p) \in \mathcal{E}_f \subset \mathcal{E}_\mu. && \text{(4.20f)}
\end{aligned}$$

Compared to OCP (4.8), (4.20) additionally solves the optimal solutions of the path parameter vector μ.

Here, the economic stage cost function in (4.19) is chosen in the same form of (4.12), i.e.,

$$\ell(e_\mu, \xi_\mu) = \alpha(\epsilon)||e_\mu||_Q^2 + (1-\alpha(\epsilon))\eta h_g(\xi_\mu), \tag{4.21}$$

where $h_g(\cdot)$ and $\alpha(\cdot)$ is from (4.11) and (4.12), respectively. We assume that there exists an unique $\mu_s \in \mathcal{M}$, such that $\mathcal{P}_{\mu_s}$ is optimal with respect to $h_g(\cdot)$, and $\mathcal{P}_{\mu_s}$ can be followed with the given input constraints $u(\cdot) \in \mathcal{PC}(\mathcal{U})$.

Our first priority is forcing the kite system to fly in the desired flight pattern

(figure-eight shape). This can be realized by penalizing the newly defined output error (4.17) since for all $\mu \in \mathcal{M}$, $\mathcal{P}_\mu$ is always a lemniscate curve in figure-eight shape. After the kite reaches the neighborhood of $\mathcal{P}_\mu$, i.e., $||e_\mu||_Q^2$ is small, the path evolution variable z and the path parameter vector μ can be further optimized according the predefined economic performance $h_g(\xi_\mu)$.

We find that the economic cost defined by (4.21) is very suitable to realize the above objective. When the system is far away from $\mathcal{P}_\mu$, i.e., $||e_\mu||_Q^2$ is large, the economic cost function is dominated by path-following error and the system is forced into the neighborhood of $\mathcal{P}_\mu$ under the EMPFC strategy. Besides, the terminal constraints (4.20f) are added to ensure the priority of the path convergence. When the kite reaches the neighborhood of $\mathcal{P}_\mu$, i.e., $||e_\mu||_Q^2$ is small, (4.21) is dominated by the economic performance $h_g(\xi_\mu)$. Then, the path evolution variable z and the path parameter vector μ are optimized with respect to $h_g(\xi_\mu)$. Meanwhile, the output of the system $h(x)$ is driven into the neighborhood of the dynamic reference path $\mathcal{P}_\mu$ since (4.21) gives first priority to path convergence. Furthermore, if (4.21) is appropriately tuned, the path convergence can be achieved in the sense that $\lim_{t\to\infty} ||h(x(t)) - p_\mu(z(t), \mu(t))|| = 0$. This can be shown in the following simulation results when a large value of β is chosen.

4.4.3 Simulation Results

In this section, we present simulation results of the kite to follow a dynamic reference path using EMPFC. We choose the variable μ to represent θ_a (the average θ angle of the reference path) which is a significant parameter influencing the generated power when the kite is forced to follow a certain path. For comparison between the simulation results using $\mathcal{P}_\mu$ and $\mathcal{P}$ (4.14), the initial value $\mu_0 = \theta_a = 0.45$ [rad].

Parameter Selection

1. Model Parameters
   $m = 50$ [kg], $A = 100$ [m^2], $d_c = 0.025$ [m], $\rho_c = 970$ [kg/m^3], $\rho = 1.2$ [kg/m^3], $g = 9.8$ [N/kg], $C_L = 1.2$, $C_D = 0.15$, $C_{D,c} = 1$, $\dot{r}_{ref} = 2$ [m/s], the local controller gain $K = -3.33$.
   Nominal wind shear model along x axis: $v_x = (0.015(r\sin(\theta) - 100) + 12)$ [m/s].
   State constraints: $\theta \in [0.03\pi, 0.5\pi)$, $\phi \in (-0.5\pi, 0.5\pi)$, $\mu \in [0.05\pi, 0.4\pi]$.
   Input constraints: $\Omega_\mu = \{(u, v, v_\mu) | u \in [-0.07, 0.07], v \in [0, 1.6\pi], v_\mu \in [-0.03, 0.03]\}$.

2. Reference Path
   The dynamic reference path $\mathcal{P}_\mu$ is given by

$$p_\mu(z,\mu) = \begin{pmatrix} \arcsin\left(\frac{a_1 \sin(2z)}{R}\right) + \mu \\ \arcsin\left(\frac{a_2 \cos(z)}{R}\right) \end{pmatrix},$$

   where $a_1 = 15$, $a_2 = 21$ and $R = 500$.

3. EMPFC setup
   $\delta = 0.1$[sec], N=10, $Q = \text{diag}([2, 1])$, $\eta = 10^{-7}$.
   The terminal penalty $V_f(e_\mu) = ||e_\mu||^2_{Q_f}$, where $Q_f = \text{diag}([0.2, 0.1])$.
   The terminal constraint $\mathcal{E}_f = \{e_\mu | e_\mu^T P e_\mu \leq 0.01\}$, where $P = \text{diag}([1, 1])$.
   Initial state $\xi_{\mu 0} = [0.2\pi; 0; 500; -0.08; -0.08; 0; 0.5\pi; 0.45]^{\mathrm{T}}$.

EMPFC with a dynamic Reference Path

The economic performance enhancement and the convergence of μ to its optimal value μ_s can be shown in the following simulation results.

Figure 4.6 shows the closed-loop trajectory using $\mathcal{P}_\mu$ as reference path. To guarantee the convergence, β is chosen to be 400, which is a conservative value. Figure 4.7 records the corresponding closed-loop system evolutions. Specifically, Figure 4.7(a) records the path-following error; Figure 4.7(b) and Figure 4.7(c) show the evolutions for control inputs; Figure 4.7(d) records the generated power [kW], whose mean value keeps increasing until μ reaches its optimal value (0.286 rad); Figure 4.7(e) records the evolution of μ. As we can see, it converges to its optimal value at around 28 s; The average generated power reaches its maximum (885 [kW]), which is increased about 18.8% compared to the results of using a static reference path $\mathcal{P}$ (as shown in Table 4.1).

4.5 Conclusion

In this chapter, we investigate the output path-following problem for power kites using the proposed EMFPC scheme. Due to the unknown wind condition and wind turbulence, it is hard or even impossible to predefine the optimal operation for the kite system. Alternatively, we formulate the output path-following problem to involve additional degrees of freedom in the zero-error manifold (i.e., the space where the

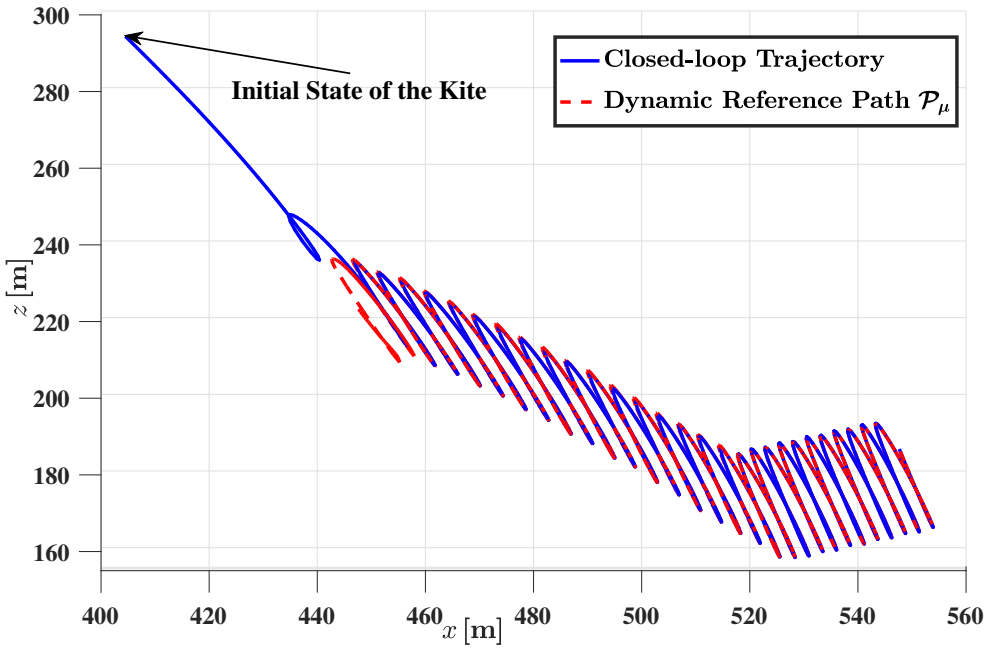

Figure 4.6: Right side view of closed-loop trajectory ($\beta = 400$) vs. dynamic reference path $\mathcal{P}_\mu$.

output error is zero). Thus, a relaxation of the optimal operation is accomplished. We show the effectiveness of the proposed control scheme in two aspects. For a static reference path, the generated power is increased while the kite is stabilized in the neighborhood of the reference path. For a dynamic reference path, the economic performance can be further enhanced since parameters for the reference path are treated as additional optimization variables. The proposed EMPFC achieves the integration of path optimization and path-following, resulting in a better economic performance for the closed-loop system. Simulation results are given to show the effectiveness of the proposed control scheme.

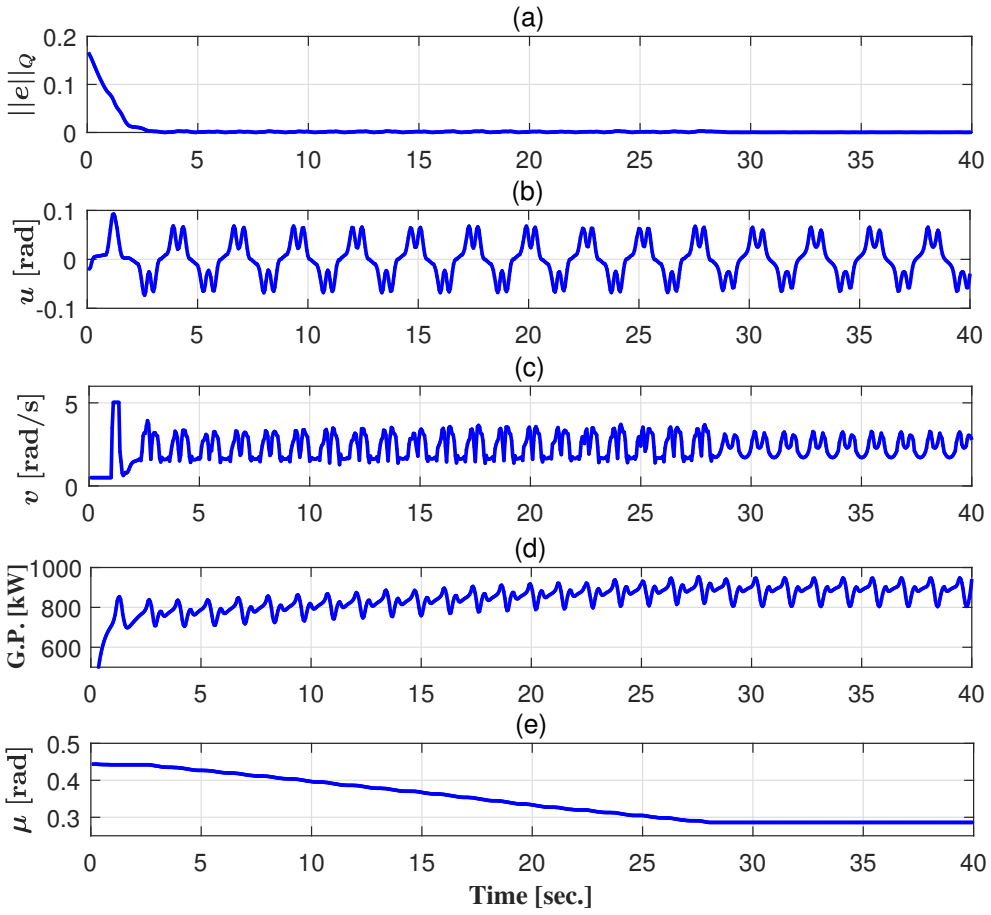

Figure 4.7: Closed-loop system evolution with dynamic reference path $\mathcal{P}_\mu$ ($\beta = 400$).

Chapter 5

Conclusions and Future Work

5.1 Conclusions

This thesis aims to tackle output path-following problems with enhanced economic performance. A novel economic model predictive path-following control (EMPFC) framework is developed. Sufficient conditions that guarantee the recursive feasibility and closed-loop stability of the EMPFC is derived, followed by an illustrating example of a 2-DoF robot. Then, the proposed EMPFC scheme is applied to a challenging nonlinear kite model and the economic performance enhancement is shown in the simulations.

Chapter 2 introduces a point-mass kite model considering the effect of cables (gravity and aerodynamic forces). The definition of three different coordinates and the detailed derivation of each force acting on the kite are given. Additionally, the applied wind speed profile along z-axis is introduced.

Chapter 3 provides the stability analysis of EMPFC. First of all, a sampled-data EMPC scheme for set-point stabilization problems is studied. An extended definition of dissipativity is introduced for continuous-time systems, followed by giving sufficient stability conditions. Then, we propose the EMPFC scheme for output path-following problems. In order to enhance the economic performance with guaranteed convergence to an output reference path, we define an optimal steady state set which actually achieves a relaxation of the optimal operation. New dissipativity assumption is defined for output path-following problems. Sufficient conditions that guarantee the convergence of the system to the optimal operation on the reference path are derived. Finally, an example of a 2-DoF robot shows that, the proposed EMPFC scheme

achieves better economic performance while the system can follow the reference path in forward direction and finally converge to its optimal steady state.

In **Chapter 4**, we apply the proposed EMPFC scheme to a challenging nonlinear kite model. In order to enhance the economic performance under varying wind condition, we formulate the output path-following problem to involve additional degrees of freedom in the zero-error manifold (i.e., the space where the output error is zero). The effectiveness of the proposed control scheme is shown in two aspects. For a static reference path, the generated power is increased while the kite is stabilized in the neighborhood of the reference path. For a dynamic reference path, the economic performance can be further enhanced since parameters for the reference path are treated as additional optimization variables. The proposed EMPFC achieves the integration of path optimization and path-following, resulting in a better economic performance for the closed-loop system. Simulation results are given to show the effectiveness of the proposed control scheme.

5.2 Future Work

Reducing the computational burden. We discuss the EMPFC scheme for output path-following problems from theoretical and practical perspective in Chapter 3-4, respectively. The main focus is to design the EMPFC scheme to guarantee the convergence of the closed-loop system to the reference path, while enhancing the economic performance. However, since virtual path dynamics is additionally involved in the optimization problem, the computational complexity increases exponentially with the problem size. For real implementation of the MPC, the heavy computational burden must be taken into consideration, especially for the application of fast dynamics like power kites. Hence, it is practically desirable to study an efficient implementation of EMPFC that performs within the permitted sampling period, which is usually less than 0.1 [sec.] in the applications of motion control.

Lyapunov-based economic model predictive control (LEMPC). Chapter 3 studies the stability of EMPFC using assumptions of dissipativity and the existence of a desirable local controller. However, these assumptions are generally difficult to be verified. Especially, there is no general approach to find an appropriate storage function to examine the dissipativity. Moreover, the assumption of dissipativity may be too conservative since it requires the corresponding rotated stage cost function to be positive definite over the whole set of the state and input constraints. In contrast,

Lyapunov-based economic model predictive control (LEMPC) takes advantage of a two-mode control strategy and the stability is enforced by introducing Lyapunov-based constraints (e.g., [64]). In LEMPC, we only require the existence of a Lyapunov-based controller locally and no dissipativity assumption is needed. Thus, there is much less restriction of the chosen economic stage cost function and it is of great interest to investigate our proposed EMPFC using Lyapunov techniques.

Realizing a full-cycle power generation using EMPFC. In Chapter 4, we only discuss the path-following control for the kite's traction phase (where the cables are reeling out under high traction force). In order to achieve a full-cycle power generation, retraction phase should also be taken into consideration. From traction phase to retraction phase, not only the kite model is changed, but also the control objective is totally different. In traction phase, we aim to stabilize the kite on the reference path and maximize the generated power. In retraction phase, the kite is switched to a gliding flight pattern (thus the model is changed) and the objective is to reel back the kite with minimum energy consumption. Therefore, it is necessary to design a new EMPFC scheme considering the switched kite model and time-varying economic cost during the full-cycle kite power generation.

Bibliography

[1] U.S. Energy Information Administration (EIA), *International Energy Outlook 2016*. available online: https://www.eia.gov/outlooks/ieo/pdf/0484(2016).pdf.

[2] R. Schmehl, *Airborne Wind Energy: Advances in Technology Development and Research*. Springer, 2018.

[3] A. Cherubini, A. Papini, R. Vertechy, and M. Fontana, "Airborne wind energy systems: A review of the technologies," *Renewable and Sustainable Energy Reviews*, vol. 51, pp. 1461–1476, 2015.

[4] A. U. Zgraggen, *Automatic power cycles for airborne wind energy generators*. PhD thesis, ETH Zurich, Switzerland, 2014.

[5] M. Zanon, S. Gros, J. Andersson, and M. Diehl, "Airborne wind energy based on dual airfoils," *IEEE Transactions on Control Systems Technology*, vol. 21, no. 4, pp. 1215–1222, 2013.

[6] Guangdong High Altitude Wind Power Technology. Guangdong, China. [Online]. Available: `http://www.gdgkfn.com/`.

[7] L. Fagiano, *Control of tethered airfoils for high-altitude wind energy generation*. PhD thesis, Politecnico di Torino, Torino, Italy, 2009.

[8] M. Canale, L. Fagiano, and M. Milanese, "Power kites for wind energy generation," *IEEE Control Systems Magazine*, vol. 27, no. 6, pp. 25–38, 2007.

[9] M. Canale, L. Fagiano, and M. Milanese, "High altitude wind energy generation using controlled power kites," *IEEE Transactions on Control Systems Technology*, vol. 18, no. 2, pp. 279–293, 2010.

[10] International Energy Agency (IEA), *World Energy Outlook 2015*. Paris, France: IEA Publications, 2015.

[11] International Energy Agency (IEA), *World Energy Outlook 2008*. Paris, France: IEA Publications, 2008.

[12] C. L. Archer and M. Z. Jacobson, "Evaluation of global wind power," *Journal of Geophysical Research: Atmospheres*, vol. 110, no. D12, 2005.

[13] G. M. Masters, *Renewable and Efficient Electric Power Systems*. John Wiley & Sons, 2013.

[14] C. L. Archer and K. Caldeira, "Global assessment of high-altitude wind power," *Energies*, vol. 2, no. 2, pp. 307–319, 2009.

[15] R. Ruiterkamp and S. Sieberling, "Description and preliminary test results of a six degrees of freedom rigid wing pumping system," in *Airborne Wind Energy*, pp. 443–458, Springer, 2013.

[16] L. Fagiano, E. Nguyen-Van, F. Rager, S. Schnez, and C. Ohler, "A small-scale prototype to study the takeoff of tethered rigid aircrafts for airborne wind energy," *IEEE/ASME Transactions on Mechatronics*, vol. 22, no. 4, pp. 1869–1880, 2017.

[17] L. Fagiano and S. Schnez, "On the take-off of airborne wind energy systems based on rigid wings," *Renewable Energy*, vol. 107, pp. 473–488, 2017.

[18] M. Erhard and H. Strauch, "Control of towing kites for seagoing vessels," *IEEE Transactions on Control Systems Technology*, vol. 21, no. 5, pp. 1629–1640, 2013.

[19] R. van der Vlugt, J. Peschel, and R. Schmehl, "Design and experimental characterization of a pumping kite power system," in *Airborne Wind Energy*, pp. 403–425, Springer, 2013.

[20] L. Fagiano, A. U. Zgraggen, M. Morari, and M. Khammash, "Automatic crosswind flight of tethered wings for airborne wind energy: Modeling, control design, and experimental results," *IEEE Transactions on Control Systems Technology*, vol. 22, no. 4, pp. 1433–1447, 2014.

[21] C. Vermillion, B. Glass, and A. Rein, "Lighter-than-air wind energy systems," in *Airborne Wind Energy*, pp. 501–514, Springer, 2013.

[22] P. R. Payne and C. McCutchen, "Self-erecting windmill," Oct. 26 1976. US Patent 3,987,987.

[23] B. Houska and M. Diehl, "Optimal control for power generating kites," in *Proceedings 9th European Control Conference*, Kos, Greece, 2007, pp. 3560–3567.

[24] M. L. Loyd, "Crosswind kite power (for large-scale wind power production)," *Journal of Energy*, vol. 4, no. 3, pp. 106–111, 1980.

[25] Makani Power Inc. California, USA. (Sept. 2013). [Online]. Available: `https://x.company/makani/`.

[26] B. Lansdorp and W. Ockels, "Comparison of concepts for high-altitude wind energy generation with ground based generator," in *Proceedings of International Renewable Energy Equipment & Technology Exhibition and Conference*, pp. 409–417, Beijing, China, 2005.

[27] J. Zhang, N. Zou, and W.-L. Zhou, "System and method for umbrella power generation," Mar. 26 2013. US Patent 8,405,244.

[28] U. Fechner and R. Schmehl, "Model-based efficiency analysis of wind power conversion by a pumping kite power system," in *Airborne Wind Energy*, pp. 249–269, Springer, 2013.

[29] A. U. Zgraggen, L. Fagiano, and M. Morari, "Automatic retraction and full-cycle operation for a class of airborne wind energy generators," *IEEE Transactions on Control Systems Technology*, vol. 24, no. 2, pp. 594–608, 2016.

[30] M. Diehl, *Real-time optimization for large scale nonlinear processes*. PhD thesis, Interdisciplinary Inst. for Scientific Comput. (IWR), Heidelberg University, Heidelberg, Germany, 2001.

[31] B. Houska, "Robustness and stability optimization of open-loop controlled power generating kites," Master's thesis, Heidelberg University, Heidelberg, Germany, 2007.

[32] A. Ilzhöfer, B. Houska, and M. Diehl, "Nonlinear MPC of kites under varying wind conditions for a new class of large-scale wind power generators," *International Journal of Robust and Nonlinear Control*, vol. 17, no. 17, pp. 1590–1599, 2007.

[33] M. Diehl, L. Magni, and G. De Nicolao, "Efficient NMPC of unstable periodic systems using approximate infinite horizon closed loop costing," *Annual Reviews in Control*, vol. 28, no. 1, pp. 37–45, 2004.

[34] S. Gros, M. Zanon, and M. Diehl, "Control of airborne wind energy systems based on nonlinear model predictive control & moving horizon estimation," in *Proceedings 12th European Control Conference*, Zurich, Switzerland, 2013, pp. 1017–1022.

[35] S. Lucia and S. Engell, "Control of towing kites under uncertainty using robust economic nonlinear model predictive control," in *Proceedings European Control Conference*, Strasbourg, France, 2014, pp. 1158–1163.

[36] J. H. Baayen and W. J. Ockels, "Tracking control with adaption of kites," *IET Control Theory & Applications*, vol. 6, no. 2, pp. 182–191, 2012.

[37] A. U. Zgraggen, L. Fagiano, and M. Morari, "Automatic retraction phase of airborne wind energy systems," in *Proceedings 19th IFAC World Congress on Automatic Control*, Cape Town, South Africa, 2014, pp. 5826–5831.

[38] A. U. Zgraggen, L. Fagiano, and M. Morari, "Real-time optimization and adaptation of the crosswind flight of tethered wings for airborne wind energy," *IEEE Transactions on Control Systems Technology*, vol. 23, no. 2, pp. 434–448, 2015.

[39] B. Houska and M. Diehl, "Robustness and stability optimization of power generating kite systems in a periodic pumping mode," in *Proceedings IEEE International Conference Control Application*, Yokohama, Japan, Sep. 2010, pp. 2172–2177.

[40] C. Novara, L. Fagiano, and M. Milanese, "Direct data-driven inverse control of a power kite for high altitude wind energy conversion," in *Proceedings IEEE International Conference Control Application*, Denver, CO, USA, Sep. 2011, pp. 240–245.

[41] O. Ravn, N. Poulsen, L. Hansen, *et al.*, "Neural networks for modelling and control of dynamic systems," 2000.

[42] L. Fagiano, E. Nguyen-Van, F. Rager, S. Schnez, and C. Ohler, "Autonomous takeoff and flight of a tethered aircraft for airborne wind energy," *IEEE Transactions on Control Systems Technology*, vol. 26, no. 1, pp. 151–166, 2018.

[43] M. Diehl, R. Amrit, and J. B. Rawlings, "A Lyapunov function for economic optimizing model predictive control," *IEEE Transactions on Automatic Control*, vol. 56, no. 3, pp. 703–707, 2011.

[44] D. Angeli, R. Amrit, and J. B. Rawlings, "On average performance and stability of economic model predictive control," *IEEE Transactions on Automatic Control*, vol. 57, no. 7, pp. 1615–1626, 2012.

[45] L. Grüne, "Economic receding horizon control without terminal constraints," *Automatica*, vol. 49, no. 3, pp. 725–734, 2013.

[46] J. Köhler, M. A. Müller, and F. Allgöwer, "Nonlinear reference tracking: An economic model predictive control perspective," *IEEE Transactions on Automatic Control*, 2018.

[47] H. Bosch, "Finite element analysis of a kite for power generation," Master's thesis, Delft University of Technology, Delft, Netherlands, 2012.

[48] P. Williams, B. Lansdorp, R. Ruiterkamp, and W. Ockels, "Modeling, simulation, and testing of surf kites for power generation," in *Proceedings AIAA Modeling and Simulation Technologies Conference and Exhibit*, Honolulu, HI, USA, 2008.

[49] B. Houska, *A 9 DOF Kite Model*. Internal Paper, University of Heidelberg.

[50] S. de Groot, "Modelling the dynamics of an arc-shaped kite for control law design," Master's thesis, Delft University of Technology, Delft, Netherlands, 2010.

[51] M. Ray, A. Rogers, and J. McGowan, "Analysis of wind shear models and trends in different terrains," *University of Massachusetts, Department of Mechanical and Industrial Engineering, Renewable Energy Research Laboratory*, 2006.

[52] J. F. Manwell, J. G. McGowan, and A. L. Rogers, *Wind Energy Explained: Theory, Design and Application*. John Wiley & Sons, 2010.

[53] H. Chen and F. Allgöwer, "A quasi-infinite horizon nonlinear model predictive control scheme with guaranteed stability," *Automatica*, vol. 34, no. 10, pp. 1205–1217, 1998.

[54] F. A. Fontes, "A general framework to design stabilizing nonlinear model predictive controllers," *Systems & Control Letters*, vol. 42, no. 2, pp. 127–143, 2001.

[55] T. Faulwasser, *Optimization-based solutions to constrained trajectory-tracking and path-following problems*. Contributions in Systems Theory and Automatic Control. 3, Aachen: Shaker Verlag, 2013.

[56] D. A. Carlson, A. B. Haurie, and A. Leizarowitz, *Infinite horizon optimal control: deterministic and stochastic systems*. Springer Science & Business Media, 2012.

[57] R. Amrit, J. B. Rawlings, and D. Angeli, "Economic optimization using model predictive control with a terminal cost," *Annual Reviews in Control*, vol. 35, no. 2, pp. 178–186, 2011.

[58] T. Faulwasser and R. Findeisen, "Nonlinear model predictive control for constrained output path following," *IEEE Transactions on Automatic Control*, vol. 61, no. 4, pp. 1026–1039, 2016.

[59] B. Siciliano, L. Sciavicco, L. Villani, and G. Oriolo, *Robotics: Modelling, Planning and Control*. Springer Science & Business Media, 2010.

[60] M. Diehl, "Airborne wind energy: Basic concepts and physical foundations," in *Airborne Wind Energy*, pp. 3–22, Springer, 2013.

[61] L. Fagiano and M. Milanese, "Airborne wind energy: An overview," in *Proceedings American Control Conference*, Montreal, Canada, 2012, pp. 3132–3143.

[62] C. Shen, Y. Shi, and B. Buckham, "Path-following control of an AUV: A multiobjective model predictive control approach," *IEEE Transactions on Control Systems Technology*, no. 99, pp. 1–9, 2018.

[63] S. Boyd and L. Vandenberghe, *Convex Optimization*. Cambridge University Press, 2004.

[64] M. Heidarinejad, J. Liu, and P. D. Christofides, "Economic model predictive control of nonlinear process systems using Lyapunov techniques," *AIChE Journal*, vol. 58, no. 3, pp. 855–870, 2012.